AN EXAMINATION OF VEGETATION MODELING-RELATED ISSUES AND THE VARIATION AND CLIMATE SENSITIVITY OF VEGETATION AND HYDROLOGY IN CHINA

by

GUOPING TANG

A DISSERTATION

Presented to the Department of Geography
and the Graduate School of the University of Oregon
in partial fulfillment of the requirements
for the degree of
Doctor of Philosophy

September 2008

University of Oregon Graduate School

Confirmation of Approval and Acceptance of Dissertation prepared by:

Guoping Tang

Title:

"AN EXAMINATION OF VEGETATION MODELING-RELATED ISSUES AND THE VARIATION AND CLIMATE SENSITIVITY OF VEGETATION AND HYDROLOGY IN CHINA"

This dissertation has been accepted and approved in partial fulfillment of the requirements for the Doctor of Philosophy degree in the Department of Geography by:

Patrick Bartlein, Chairperson, Geography
W. Andrew Marcus, Member, Geography
Amy Lobben, Member, Geography
Sarah Shafer, Member, Not from U of O
Michelle Wood, Outside Member, Biology

and Richard Linton, Vice President for Research and Graduate Studies/Dean of the Graduate School for the University of Oregon.

September 6, 2008

Original approval signatures are on file with the Graduate School and the University of Oregon Libraries.

© 2008 Guoping Tang

An Abstract of the Dissertation of

Guoping Tang for the degree of Doctor of Philosophy

in the Department of Geography to be taken September 2008

Title: AN EXAMINATION OF VEGETATION MODELING-RELATED ISSUES AND THE VARIATION AND CLIMATE SENSITIVITY OF VEGETATION AND HYDROLOGY IN CHINA

Approved: _____
Dr. Patrick J. Bartlein

This dissertation examined a number of general vegetation-modeling issues, and the sensitivity of terrestrial net primary productivity (NPP), soil moisture and actual evapotranspiration (ET) to climatic variations in China. The specific issues addressed included: (1) the sensitivity of the performance of an equilibrium vegetation model to the choice of monthly-mean climatologies, observed validation data sets, and three map-comparison approaches; and (2) the limitations of existing map-comparison approaches in vegetation modeling; and the variation and climate sensitivity of (3) terrestrial NPP and (4) soil moisture and actual ET in China.

To address the first issue, BIOME4 (Kaplan *et al.*, 2002), a typical example of an equilibrium vegetation model, was used along with a set of 19 different monthly-mean climatologies, three validation data sets, and several map-comparison methods. To address the second issue, the "opposite and identity" (OI) index (Tang, 2008) was

developed for evaluating the correspondence of two simulation results. To examine the third issue, a set of historical NPP dynamics were derived from normalized-difference vegetation index data by modifying the CASA (Potter *et al.*, 1999) approach and then were linked to the variation of temperature and precipitation to analyze the climatic effects on terrestrial NPP in China. To examine the fourth issue, a stand-alone water balance model, LH (LPJ-hydrology), was developed by modifying the LPJ dynamic global vegetation model (Sitch *et al.*, 2003), and applying it to a China case study.

The results of these analyses indicate that (1) the 30-year mean-climatology preceding the observed data produces the most accurate vegetation simulations; (2) the OI index is a useful tool to compare two simulation results or to evaluate simulation results against observed spatiotemporal data; (3) climate and land-use change jointly controlled NPP dynamics in the eastern monsoon zone of China. In contrast, NPP dynamics in the north-west arid zone and in the Tibet Plateau frigid zone depended more on climatic variation; and (4) the spatial patterns of soil moisture and ET in China were correlated with the variation of temperature and precipitation. However, the strength of such relationship varies spatially.

This dissertation includes my published and coauthored materials.

CURRICULUM VITAE

NAME OF AUTHOR: Guoping Tang

GRADUATE AND UNDERGRADUATE SCHOOLS ATTENDED:

University of Oregon, Eugene, Oregon
Beijing Normal University, Beijing, China
Hunan Normal University, Changsha, China

DEGREES AWARDED:

Doctor of Philosophy in Geography, 2008, University of Oregon
Master of Science in Environmental Geography, 1998, Beijing Normal University, Beijing, China
Bachelor of Science in Geography, 1993, Hunan Normal University, Changsha, China

AREAS OF SPECIAL INTEREST:

Dynamic vegetation modeling
Climate impacts assessment
Spatial data analysis and visualization

PROFESSIONAL EXPERIENCE:

Research Assistant, Department of Geography, University of Oregon, Eugene, 2007-2008

Graduate Teaching Assistant, Department of Geography, University of Oregon, Eugene, 2001-2007

Research Assistant, Institute of Geographical Sciences and Natural Resources Research, the Chinese Academy of Sciences, Beijing, China, 1998-2001

GRANTS, AWARDS AND HONORS:

Department of Geography Summer Research Award, 2005, 2007

GIS Graduate Teaching Fellowship, the Social Sciences Instructional Lab, University of Oregon, 2005-2006

PUBLICATIONS:

Tang GP. 2008. A new metric for evaluating the correspondence of spatial patterns in vegetation models. *Global Ecology and Biogeography*, 17, 465-478.

Long HL, Tang GP, Li XB, Heilig CK. 2006. Socio-economic driving forces of land-use change in Kunshan, the Yangtze River Delta Economic Area of China. *Journal of Environmental Management*, 83, 352-364.

ACKNOWLEDGMENTS

I gratefully thank Dr. Patrick J. Bartlein for his contribution to this dissertation and for his thoughtful guidance, instruction and financial aid over the course of my Ph.D. study. I sincerely thank Dr. Sarah L. Shafer for her guidance on and contribution to the preparation of Chapter III and for her friendship and kindness. I thank Dr. Daniel Gavin for proofreading Chapter V. I thank Jennifer Marlon for proofreading Chapter IV. I express my appreciation to my dissertation committee members: Dr. Patrick J. Bartlein, Dr. W. Andrew Marcus, Dr. Amy K. Lobben, Dr. Sarah L. Shafer and Dr. A. Michelle Wood for their comments and suggestion on this dissertation. I give my thanks to my peers in the Department of Geography at the University of Oregon for their friendship over the years.

The dissertation was supported by U.S. National Science Foundation grant numbers ATM 9532074, ATM 9910638 and ATM 0602409 to Dr. Patrick J. Bartlein, and by the Department of Geography. I greatly thank the developers of the LPJ dynamic global vegetation model (Sitch *et al.*, 2003; Gerten *et al.*, 2004) and the coupled biogeography and biogeochemistry vegetation model BIOME4 (Kaplan *et al.*, 2002) for distributing model codes.

For Lixia Li and Zimu Tang

TABLE OF CONTENTS

LIST OF FIGURES

LIST OF TABLES

CHAPTER I

INTRODUCTION

The development and application of simulation models is motivated as an important approach for studying various interactions or couplings in soil-vegetation-atmosphere systems that govern exchanges of energy, water and momentum because (i) direct or indirect experimental measurements of key variables in soil-vegetation-atmosphere systems, such as terrestrial net primary productivity (NPP), soil moisture and evapotranspiration (ET), are often expensive and difficult at the regional scale; (ii) model simulation can provide finer spatiotemporal resolution of ecological and hydrological variables than can experimental approaches; and (iii) models can mathematically express some of the mechanistic processes that govern terrestrial vegetation and hydrology, such as plant photosynthesis and the surface water and energy balance. However, the sensitivity of model simulations (e.g. to input climate data) and the limitations of existing approaches for comparing and evaluating model simulations (e.g. the sensitivity of the Pearson correlation coefficient to influential data and outliers) may greatly affect accuracy assessments of model results.

Terrestrial NPP, soil moisture and ET are three key components of soil-vegetation-atmosphere systems and affect many important processes, such as the cycle of carbon, water and energy, in soil-vegetation-atmosphere systems. Over the past decades, attempts have been made to capture the dynamics of terrestrial NPP, soil moisture and actual ET at the land surface (e.g. Brogaard *et al.* 2005; Zhao & Zhou, 2006; Gao *et al.*, 2007). However, because the spatiotemporal variations of these ecological and hydrological variables are very complex and depend on multiple factors, and because changes in these variables have important effects on vegetation and crop productivity, and on the sustainable utilization of water resources, examination of their responses to

external controls, especially climate variation, is important for understanding terrestrial ecosystems and for managing agricultural systems and water resource.

The goals of this dissertation are (1) to review the approaches, issues and challenges in vegetation modeling, (2) to examine the sensitivity of vegetation model simulations to different input climate data, to the selection of observed validation data, and to the choice of map comparison approaches used to compare simulated and observed vegetation, (3) to develop a cell-by-cell-based continuous-data comparison approach for evaluating the agreement between two sets of simulated time-series data, (4) to investigate the variation and climate sensitivity of terrestrial NPP in China over the years 1982-2000, and (5) to develop a stand-alone hydrologic model to examine the variation and climate sensitivity of soil moisture and actual ET in China, including their response to atmospheric CO_2 concentrations.

Toward these goals, the dissertation is organized into five major chapters, each of which has been written as a stand-alone article. Chapter II aims (1) to review the approaches for simulating the responses of terrestrial vegetation to climate change at the regional to global scales, (2) to analyze potential issues in vegetation modeling, and (3) to propose the strategies to address the existing issues. The author hopes that this literature synthesis can provide researchers with useful information on using and developing vegetation models in related research.

Chapter III examines the sensitivity of vegetation model simulations to different input monthly-mean climatologies and their associated CO_2 concentration, to the choice of observed data for evaluating model results, and to the methods used to compare simulated and observed vegetation. The equilibrium vegetation model BIOME4 (Kaplan *et al.*, 2002) was used as a typical example of vegetation models to simulate vegetation for Asia under 19 different monthly-mean climatologies that are derived from the CRU TS 2.0 data set (Mitchell *et al.*, 2004). Three map comparison approaches were used to quantify the agreement between the BIOME4-simulated vegetation under each of the monthly-mean climatologies and the observed vegetation from three different land- and

tree-cover data sets. This study is intended to provide model users with assistance in designing experimental protocols for simulating vegetation.

Chapter IV presents a new metric for quantifying the agreement between two sets of simulated time-series data. The study first introduced the geometry and definition of the new continuous-data comparison approach, the "opposite and identity" (OI) index (Tang, 2008). Then, a comparison between the OI index and the Pearson correlation coefficient was made to highlight the similarity and dissimilarity of the two concepts. Finally, a case study was given to demonstrate the application and reliability of the OI index in evaluating the agreement between two sets of simulated NPP dynamics for Asia from 1982 to 2000. Chapter IV not only presents researchers with a useful tool for model comparison and evaluation research, but also demonstrates that the OI index can in some cases quantify the agreement between two sets of simulated NPP dynamics for Asia more robustly than the Pearson correlation coefficient.

Chapter V examines the variation of terrestrial NPP in China over the years 1982-2000, and the sensitivity of NPP to the temperature and precipitation variations over the same period. To do this, the study first derived a set of NPP data from satellite-based normalized-difference vegetation index (NDVI) data using a modification of the CASA approach (Potter & Klosster, 1999). Then, another set of terrestrial NPP data at the same temporal and spatial scale was simulated by LPJ, a dynamic global vegetation model (Sitch *et al.*, 2003), and compared with the NDVI-derived NPP data. Finally, the NDVI-derived NPP dynamics were linked to the variations of temperature and precipitation to analyze the climatic sensitivity of NPP in three climatic zones of China, i.e. the eastern monsoon zone, the north-west arid zone and the Tibetan Plateau frigid zone. With this analysis, Chapter V provides researchers with new insights into the climatic sensitivity of NPP variations in China.

Chapter VI develops a stand-alone hydrologic model and employs it to examine the climatic sensitivity of soil moisture and actual (as opposed to potential) ET in China. This study first introduced the development of the LH (LPJ-hydrology) model in which vegetation is prescribed as opposed to simulated, and which uses as input climate and

soils data, as well as atmospheric CO_2 levels. Then, a series of simulations were run using observed climate and CO_2 data. Both observed and simulated (using different approaches) data for runoff, soil moisture and ET at different spatial scales were used to evaluate the LH simulations. Finally, the model results for five regions in China were used to examine the climatic controls on soil moisture and ET. Chapter VI presents not only a useful tool in hydrological modeling but also new insights into the climatic sensitivity of soil moisture and actual ET in China.

Chapter VII summarizes the major conclusions from this dissertation. Of the five major chapters, Chapter II, V and VI are coauthored with Patrick J. Bartlein (University of Oregon), and are intended for submission to the journals *Progress in Physical Geography, Climatic Change* and *Journal of Hydrology*, respectively. Chapter III is coauthored with Sarah L. Shafer (U.S. Geological Survey), Patrick J. Bartlein, and Justin O. Holman (TerraSeer, Inc.), and was submitted to the journal *Ecological Modelling*. Chapter IV was published in "*Global Ecology and Biogeography*" (Tang, 2008).

CHAPTER II

SIMULATING THE CLIMATIC EFFECTS ON VEGETATION: APPROACHES, ISSUES AND CHALLENGES

The Chapter is coauthored with Patrick J. Bartlein. G. Tang prepared the initial draft of the manuscript and Patrick J. Bartlein edited the manuscript.

Introduction

The terrestrial biosphere and the atmosphere interact with each other through a variety of mechanisms that include the carbon, nitrogen and water cycles. Through these mechanisms, natural and human-induced climate change produces changes in terrestrial vegetation. Over the past decades, studies have confirmed climate-induced effects on vegetation, such as shifts in the environmental function of forests (e.g. Hollister *et al.* 2005) and the changes of carbon cycles (e.g. Berthelot *et al.*, 2005). Moreover, additional studies have revealed that climate-induced changes in vegetation are ongoing (e.g. Hinzman *et al.* 2005). Given that terrestrial vegetation is very important to human society and that it has a limited capacity to adapt to rapid climate change (IPCC, 2001), simulating climatic effects on terrestrial vegetation becomes a paramount practical issue.

Terrestrial vegetation responds to climate change at different spatiotemporal scales. At the global scale, species evolution and migration due to climate change may take years to millennia. At the regional scale, changes in succession, competition and reproduction of vegetation require years to centuries. At the local scale, changes in the physiological processes of plants such as respiration rate take hours to seasons. From a biogeographical perspective, climate change can shift the distribution, structure and composition of terrestrial vegetation (Jackson & Overpeck, 2000; Koca *et al.*, 2006). From a biophysical and biogeochemical perspective, climate change can trigger changes in the canopy height, biomass, and leaf area index (LAI) of vegetation as well as the

cycling of carbon and nitrogen in terrestrial vegetation. Climate change can also shift the regime of wildfires, thus further affecting terrestrial vegetation.

Because the mechanisms that trigger changes in vegetation are very complex, vegetation modeling has been viewed as a major tool for investigating the effects of climate change on vegetation (Bolliger *et al.*, 2000; Schumacher *et al.*, 2004). Vegetation models, either static-equilibrium or dynamic-transient, have utility in examining the climatic effects on vegetation because: (i) vegetation models can incorporate explicit representations of some of the mechanistic processes of vegetation, such as tree establishment, growth and death, and therefore are able to capture the response of vegetation to climate change (Cramer, 2002); (ii) vegetation models can be applied at large spatial scales, which enables researchers to study the broad spatial patterns of vegetation (Prentice *et al.*, 1996); (iii) vegetation models can be updated or revised when new knowledge and techniques become available; and (iv) vegetation modeling is often time-saving and less expensive compared to field observations.

Although vegetation models of differing sophistication have been developed to study climatic effects on terrestrial vegetation, the uncertainty of model results is still a key issue of concern to researchers. To improve model-based research, it is necessary to assess the major methods and issues in vegetation modeling and to propose strategies for promoting the quality of model results. However, few syntheses of the relevant literature have been done. The goals of this study are: (i) to summarize the vegetation modeling approaches for studying climatic effects on vegetation; (ii) to analyze the major issues that lead to uncertainties in model results; and (iii) to identify the challenges that arise in improving future model-related research.

Simulating the climatic effects on terrestrial vegetation: approaches

Static-equilibrium vegetation models

Simulating the climate-induced biogeographical dynamics of vegetation was a main task for earlier generations of vegetation models. Correlations of control variables (such as climatic factors) and response variables (such as vegetation-type, biome, or

species distributions) have played a crucial role in predicting the response of vegetation to climate change (Burke *et al.*, 1997). For example, the Holdridge diagram (Holdridge, 1947) used three bioclimatic variables, i.e. the bio-temperature, mean annual precipitation and a ratio of potential evapotranspiration to mean annual precipitation, to express the relation of macroclimate pattern and life zones on the earth. Using the Holdridge classification schemes to estimate climatic effects on vegetation assumes that the distribution of vegetation is solely correlated to climate, and the climate-induced shift of vegetation occurs as a fixed unit (as opposed to individualistic responses of the component species in a vegetation type). Later, the Box model (Box, 1981) was developed to organize plant species on the Earth into characteristic plant functional types (PFTs) based on their physiognomic and morphological traits and their relation to macroclimate. The geographic space of a PFT is then defined by its climatic limits, and a particular, usually global, climatic data set.

Like the Holdridge classification scheme and the Box model, statistical approaches such as climate responses surface (e.g. Huntley *et al.*, 1995), regression models (e.g. Smith & Shugart, 1993; Calef *et al.*, 2005) and probabilistic models (e.g. Siegel *et al.*, 1995) were used to predict the climate-induced changes in the distribution and habitat of natural vegetation. These approaches still assumed that the macroclimate is the major factor determining the features of vegetation distribution at regional or global scales. For example, climate-pollen response surfaces (e.g. Overpeck *et al.*, 1991) have been coupled with climate-model output to project climatic effects on the distribution of terrestrial vegetation. Similarly, probabilistic models or presence-absence response surfaces (e.g. Siegel *et al.*, 1995; Shafer *et al.*, 2001) utilized species or ecosystem distributions and climate data to estimate the probability of occurrence of those ecosystems or species under given climatic conditions.

Because vegetation models built on statistical relations between vegetation distribution and macroclimate can not determine or distinguish the particular mechanisms that may drive the spatial shift of vegetation (Neilson *et al.*, 1992), researchers have constructed rule- and the ecophysiology-based models. Rule-based models such as the

CCVM (Lenihan & Neilson, 1993) used a set of rules (expressed as climate limits, much like the Box model) to specify the distribution of vegetation. For example, minimum temperature and evapotranspiration were used to constrain the distribution of different life forms. Ecophysiology-based models such as BIOME (Prentice *et al.*, 1992) aimed at understanding the fundamental aspects of structure in terrestrial ecosystems. In these models, terrestrial vegetation was grouped into several different PFTs based on a set of climatic tolerances. Differing from simple bioclimatic classification schemes, the climate limits of each PFT in ecophysiology-based models are expressed in terms of fundamental phenological constraints rather than observed correlations between the macroclimate and vegetation distribution.

The current equilibrium vegetation models incorporate more mechanistic processes of plants, and consider more the interactions between the biosphere and the atmosphere. For example, BIOME4 (Kaplan *et al.*, 2002, 2003) is a typical example of equilibrium vegetation models. Like the ecophysiology-based models, BIOME4 still simulates the distribution of vegetation in the form of PFTs but with significant improvements, including improved parameterization of the PFTs. In BIOME4, each PFT is assigned a set of bioclimatic limits, which determine whether it will be simulated to exist in a grid cell. Moreover, BIOME4 contains a coupled carbon and water flux scheme, which determines the seasonal maximum LAI based on a daily time-step simulation of the soil water balance and monthly calculations of canopy conductance, photosynthesis and respiration (Haxeltine & Prentice, 1996; Kaplan et al., 2002). Compared to the rule- and ecophysiology-based models, current equilibrium vegetation models can more accurately simulate the distribution and the biogeochemical dynamics of terrestrial vegetation under climatic change.

Dynamic-transient vegetation models

In fact, vegetation is far from an equilibrium system. In 1926, Cooper (1926) viewed vegetation dynamics as a "flowing stream". Because static vegetation models can not capture nonlinear or threshold effects along the trajectory of vegetation change, including interannual variations, dynamic vegetation models were developed to

complement static vegetation models, to simulate vegetation dynamics such as the succession of plants through time, and to estimate the variability of the terrestrial carbon and nitrogen and their responses to episodic events such as drought and fire (Tian *et al*, 1998; Bachelet *et al*., 2001). To some degree, dynamic vegetation models fall into four subcategories: (1) models simulating the species composition and distribution of vegetation, (2) models focusing on the biogeochemical processes of vegetation, (3) models addressing the physiological processes of vegetation, and (4) coupled dynamic multifunctional models that incorporate all or some of the ecological, biogeochemical, and physiological variations. Dynamic models often have an ability to predict the responses of vegetation to climate change at time scales ranging from days to centuries, and at spatial scales ranging from local to global (Woodward & Lomas, 2004).

Dynamic models can be constructed by coupling static models with smaller scale ecosystems or species models. Because both ecosystems and species models are capable of simulating vegetation and species change by considering the differential birth, growth, and death of individual trees as a function of species' response to climatic factors, light and nutrients, the resulting dynamic models are therefore able to simulate transient changes in vegetation distribution. For example, Steffen *et al*. (1996) developed a dynamic global vegetation model (DGVM) to simulate the transient changes in vegetation distribution over a decadal time scale. The structure of this DGVM is based on a linkage between an equilibrium global vegetation model and smaller scale ecosystem dynamic modules that simulate the rate of vegetation change.

Physiological models simulate the physiological processes of vegetation such as stomatal resistance and plant transpiration. In these models, the transpiration rates of plants are linked to their photosynthesis via stomatal conductance or leaf area (Running *et al*., 1989). When physiological models are linked to other models such as demographic vegetation model or ecosystem model, they have an ability to simulate the succession, competition and other ecological processes of plants under climate change. For example, small-scale ecosystem models have an ability to estimate the gas exchange processes such as photosynthesis, respiration and evapotranspiration (e.g. Kergoat *et al*. 2002).

Biogeochemical models aim to predict the carbon and nitrogen cycle in terrestrial vegetation. For example, a set of carbon cycle models (e.g. King et al., 1997; Ito & Oikawa; 2002) were used to examine the carbon dynamics in terrestrial ecosystems under climatic change. In such models, terrestrial carbon storage is divided into different compartments such as foliage, stem, root, litter, and mineral soil. The division of carbon into different compartments allows researchers to understand the carbon fluxes in the biosphere. These models estimates NPP and net ecosystem production (NEP) by explicitly calculating such carbon fluxes as gross primary production (GPP), plant respiration and soil decomposition on a monthly time-step. These fluxes are regulated by a multitude of environmental factors at the physiological scale. In addition, empirical models based on the normalized difference vegetation index (NDVI) and climate variables can be used to analyze the response of terrestrial productivity to climate change (e.g. Potter *et al.*, 1999; Zhang *et al.*, 2003).

Current dynamic vegetation models are mostly multifunctional and combine process-based, large-scale representations of terrestrial vegetation dynamics and the exchanges of carbon and water between the biosphere and the atmosphere (For these reasons, they are referred to as DGVMs—dynamic global vegetation models). The Lund-Potsdam-Jena (LPJ) DGVM (Sitch et al., 2003) is such a typical example. In LPJ, the PFTs are differentiated by their physiological, morphological, phenological, bioclimatic and fire-response attributes. LPJ incorporates some of the principal processes of the biosphere that influence the global carbon cycle (e.g. photosynthesis, autotrophic and heterotrophic respiration of plants and in soils) and the latent, sensible and kinetic energy exchanges at the surface of soils and plants. LPJ also considers competitive processes between PFTs, such as light competition and sapling establishment. The carbon, water and nitrogen flows are simulated on a daily basis, while vegetation structure, PFT population densities and NPP of each PFT are updated monthly and annually. Most current dynamic models can be coupled with climate or other land-cover models and are able to simulate transient changes in vegetation distribution, structure and function, and

the terrestrial carbon and nitrogen cycle under climatic change (Cowling & Shin, 2006; Zaehle *et al.*, 2005).

Simulating the climatic effects on terrestrial vegetation: issues

The issues related to vegetation models

The structure of vegetation models affects model results. The bioclimatic classification models usually predict the distribution of high-level physiognomic units such as biomes and life zones at the broad spatial scale but ignore the individualistic response of species to climate change (Peng, 2000). Consequently, the equilibrium character of the bioclimatic relationships limits the applications of such models to long-term scenarios of changing climate (Kirilenko & Solomon, 1998). Static models may ignore migration or succession processes of terrestrial vegetation, which further limits their ability to simulate the transient dynamics of terrestrial vegetation (Prentice & Solomon, 1990). Likewise, if dynamic models do not stress the structure difference among different types of vegetation, their ability to simulate the categories and distribution of terrestrial vegetation is limited. In addition, the simulations of the biochemical dynamics such as the carbon and nitrogen cycle are mostly based on fixed vegetation types (Walker, 1994) and the simulations of natural disturbances (e.g. wildfire) or human disturbance (e.g. land use change) may not be adequate in both static and dynamic models (e.g. Thonicke *et al.* 2001).

Second, the assumptions and theoretical foundations of vegetation models affect model results. Static models mostly assume that climate is the primary factor for controlling vegetation dynamics. The resilience of terrestrial vegetation under external environmental alterations and other important factors such as human activities that affect the vegetation dynamic are ignored (Loehle & LeBlanc, 1996). However, other disturbances such as wildfire, grazing and deforestation can be the dominant factors controlling the distribution of terrestrial vegetation in a given area. Therefore, vegetation models that only take into account climatic factors may not accurately simulate the spatiotemporal dynamics of terrestrial vegetation under climate change (Camill, 2000),

largely because the implicit cause-effect relationship in vegetation models may be problematic (Scheffer *et al.*, 2005). In addition, the aggregation of all species into several PFTs that may encompass the full spectrum of migration rates hinders the accuracy of model results (Neilson *et al.*, 2005).

Third, the parameterization of physiological, biological and biogeochemical processes of terrestrial vegetation is still difficult because of our limited knowledge of plant physiology and biology, the limitation of sampling and the key processes which may be currently unknown (Grieb *et al.*, 1999; Mitchell & Csillag, 2001). For example, Arora & Boer (2005) pointed out that leaf phenology remains one of the most difficult processes to parameterize in vegetation models because of our incomplete understanding of leaf onset and senescence. In addition, information with considerable uncertainty may continue to be used to parameterize future vegetation models (Gifford, 1992, 2003). The selection and use of static parameters (e.g. leaf Nitrogen concentration) in vegetation model is likely to affect model results by overestimating the respiration of plants and subsequently underestimating the productivity estimates (Wythers *et al.* 2005).

The issues related to analytical data

The outputs from vegetation models are often hampered by considerable uncertainties associated with the input data used to run a model (Kickert *et al.* 1999). Problems with the input data include missing key components, errors associated with biased or incomplete observations, and the resolution of the data. For example, climate data from general circulation models (GCMs) may be biased because of the uncertainties in future greenhouse gases and aerosols emissions, radiative forcings, global and regional climate sensitivity (Forest *et al.*, 2002; Stott & Kettleborough, 2002), and the cycle of carbon (Lenton & Huntingford, 2003) specified in GCMs. In addition, the uncertainties related to future population growth, technological progress, economic activity, land use and cover changes, and the simplification of the complex physical processes that govern climate in GCMs can affect the accuracy and reliability of GCM data (Loehle & LeBlanc, 1996), which in turn affects vegetation modeling being run using such GCM data (Jones, 2000).

Satellite-based land- and tree-cover data are increasingly used to evaluate a model's ability to simulate terrestrial vegetation. However, human-induced errors in satellite-image processing such as image classification may bias the realistic distribution pattern of vegetation in an area (Campbell, 2002). Therefore, satellite-based land-cover data used to validate model results may greatly influence the accuracy assessment of model results. In addition, lack of data that would help to make vegetation models mechanistic and to provide evidence on what climate-induced impacts will occur is one of the critical gaps in developing dynamic models and in validating model results (Tian *et al.*, 1998). For example, Neilson *et al.* (2005) pointed out that theories about climate change and migration of vegetation are limited by inadequate data for key processes at the different spatiotemporal scales. The spatial resolution of input data affects model results. Turner *et al.* (1996) pointed out that the model simulations run by coarser input data is more likely to bias the resulting estimates of vegetation dynamic than those run by finer input data.

The issues related to analytical approaches

Categorical-data comparison approaches are used to assess the accuracy of model results through comparing simulated and observed distributions of vegetation type. Statistics, such as the Kappa statistic (Congalton & Green, 1999), Kappa-for-location (Pontius, 2000), and Fuzzy kappa (Hagen, 2003) have strengths and weaknesses in assessing a model's accuracy. For example, the Kappa statistic lacks the ability to measure error magnitude (Congaltong, 1991; Foody, 2002) and tends to underestimate the overall similarity between simulated and observed spatial pattern of terrestrial vegetation (Foody, 1992). The Fuzzy Kappa can underestimate a model's ability by overestimating the expected similarity between two compared data sets (Hagen, 2003). The receiver (or relative) operating characteristic (ROC) technique is sensitive to the number of vegetation types in the two data sets being compared (Fielding & Bell, 1997; Pontius & Schneider, 2001).

Continuous-data comparison approaches assess a model's ability to simulate the state of ecological variables that are numerical. Statistics, such as confidence levels

(Barrett *et al.*, 2001), correlation and regression coefficients, Kendall's tau and measures of absolute and relative error (Gordon *et al.*, 2004) are widely used in model comparison and evaluation research. However, they may be problematic in some cases. For example, the correlation coefficient cannot determine whether two patterns have the same amplitude of variation (Taylor, 2001). The correlation coefficient is sensitive to influential data and outliers from two compared simulations but insensitive in situations when the compared data differ by a constant factor (Murphy & Epstein, 1988; Storch & Zwiers, 1998). Similarly, root-mean-squared error is very sensitive to systematic errors because the penalty grows as the square of the error (Storch & Zwiers, 1998). In addition, most statistics assume that the data being compared are independent of one another. However, model results are often spatiotemporally auto-correlated.

The issues related to the spatiotemporal scaling

The spatiotemporal scaling in vegetation modeling may greatly affect the model results. For example, the mismatch between the coarser spatial resolution of GCM data and the relatively finer resolution of vegetation models has long been a concern in vegetation modeling (Adams, 2003). In addition, modeling interactions between land-use change and vegetation dynamic is still a challenge because vegetation models often rely on pixel sizes of a few kilometers or more but the land-use change frequently occurs on a much smaller scale (Peng, 2000), which makes the interactions among land-use drivers, topography and climate change difficult to simulate.

The 'scaling-up' approaches used in vegetation modeling to extrapolate information from individuals to ecosystems, or from sites to regions to the globe are often based on observations, experiments and modeling of individuals or sites. However, the basic assumptions of environmental homogeneity across different spatial scales are questionable (Tian *et al.*, 1998; Liu *et al.*, 2006). Likewise, the 'scaling-down' approaches that apply the relation of large-scale patterns of vegetation and climate to local and landscape scales may ignore the fact that other process rather than climate may play important roles in vegetation dynamics at local scales (Moorcroft *et al.*, 2001).

Simulating the climatic effects on terrestrial vegetation: challenges

To improve the model design and parameterization

Because vegetation modeling often involves a variety of processes of plants, such as water and carbon cycle among the soil-vegetation-atmosphere systems, and because the intent of a same vegetation model may vary in practical applications, establishing model with a clear structural hierarchy would allow researchers to easily alter and compare the individual equations and to select the level of model detail based on the availability of data or the particular research question being investigated (Homann *et al.*, 2000). Given that static models may ignore the biogeochemical processes of plants, it would be rewarding to couple them with biogeochemical models to address the effects of climate change on vegetation. Similarly, if dynamic models do not consider competition between plants and instead determine the existence and fractional coverage of vegetation based on inferred climate-vegetation relationships, then it would be desirable to include the mechanisms of competition for light and water among different PFTs (Daly *et al.*, 2000; Arora & Boer, 2006). In addition, both static and dynamic models need to incorporate the impacts of land-cover change on vegetation (Bond-Lamberty *et al.*, 2005) and the coupling of climate and carbon cycle models should be improved to better represent the photosynthesis process of plants (Matthews *et al.*, 2005).

Second, vegetation models should be developed to incorporate as many factors as possible that have a big role in shifting the vegetation's structure and function and the cycle of carbon and nitrogen in terrestrial ecosystems. Van *et al.* (2000) suggested that the ability of plant species to migrate is one of the critical issues for accurately assessing future responses of terrestrial vegetation to climate change. Given that natural disturbances (e.g. forest fire and insects) and human activities (e.g. land-use and grazing) are critical factors in determining the composition, structure and dynamics of most vegetation (Thonicke *et al.* 2001), new vegetation models should have an ability to simulate the role of these factors on vegetation dynamics (Peng, 2000). For example, better estimates of carbon sources and sinks require improved assessments of current and

future deforestation (Cramer *et al.*, 2004) and the role of land-cover changes in shifting the cycle of terrestrial carbon and nitrogen (Chen *et al.*, 2006).

Third, it is very important to determine which processes and parameters contribute most to the uncertainty of model results (Knorr & Heimann, 2001; Mitchell & Csillag, 2001). For example, Peters (2002) argued that our limited understanding of the key processes in many ecotones hinders the reliability of model results. The uncertainty in the simulation of PFT distributions and in the estimates of the carbon cycle mainly result from the uncertainty in parameters controlling the photosynthesis, evapotranspiration and root distribution of plants and the water balance (Hallgren & Pitman, 2000; Zaehle *et al.*, 2005). Therefore, efforts must be made to determine which parameters need further attention in observational work and in their representation in models (Matthews *et al.*, 2005). For those parameter uncertainties caused by limited sampling, much work on sampling and corresponding statistical analysis is needed (Higgings *et al.*, 2003).

To improve the quality of model-driven and validation data

The reliability of model results highly depends on the quality of climate data used to run a model (Kickert *et al.*, 1999). To accurately simulate the effects of climatic variations on vegetation requires input climate data to capture those aspects of climate that control ecological processes, including key spatial gradients and modes of temporal variability (Kittel *et al.*, 2004). Therefore, it is necessary to further the study of climate projection and the positive feedbacks between the terrestrial carbon cycle and climate (Matthews *et al.*, 2005; Meir *et al.*, 2006). Meanwhile, more efforts should be made on studying the frequency, intensity and magnitude of extreme weather events, and on how they affect terrestrial vegetation. In addition, because one of the major uncertainties in vegetation modeling is in understanding processes in soil-vegetation-atmosphere systems, continuous, long-term data are therefore needed to correctly model the balances of water, energy and CO_2 in these systems (Halldin *et al.*, 1999; Lundin *et al.*, 1999).

The quality of other data is also important for the accuracy and evaluation of model results (Pan *et al.*, 1996). Long time-series data or experiments allow researchers

to better understand the relative magnitudes of short- and long-term responses of vegetation under climate change (Hanson *et al.*, 2005). In addition, more and continuing field observations are needed at sites where studies already have been conducted in order to calibrate the model results (Higgins *et al.*, 2003). In order to make full use of vegetation models, it is necessary to establish the magnitude and sources of uncertainty associated with data, which will be useful for guiding field surveys and experiments (Grieb *et al.* 1999).

To improve the model evaluation and the uncertainty analysis

Vegetation models must be tested for their ability to reproduce features of real vegetation (Hickler *et al.*, 2004). Model evaluation allows researchers to determine the accuracy and applicability of a model (Bolliger *et al.*, 2000). However, because model evaluation is likely sensitive to the selection of the evaluation methods, the evaluation strategy needs to be prescribed to solve such sensitivity issues. In addition, model evaluation should be closely related to its intended purpose: description, understanding and prediction (Araujo & Guisan, 2006). Intercomparison of results from different models should be stressed because they are very important to improve our understanding of the model behavior, to assess the robustness of inferred mechanisms used to build a model, and to measure the stability of selected variables (Bolliger *et al.*, 2000; Knorr & Heimann, 2001).

The promotion of approaches for evaluating model results is important. The statistical confidence levels (Barrett *et al.*, 2001), Markov chain (Schulz *et al.*, 2001) and Monte Carlo-based uncertainty estimation (Paltoniemi *et al.*, 2006), Bayesian probabilities (Webster & Sokolov, 2000; Katz *et al.*, 2002), and statements of uncertainty such as probability density functions (Grieb *et al.*, 1999; Radtke *et al.*, 2001), allow us to weigh the analytical results and to estimate the predictive uncertainty of vegetation dynamics to climate change. Nevertheless, innovative methods for evaluating model results and for exploring parameter uncertainty in complex vegetation models are still needed. Different approaches for model evaluation and uncertainty analysis can

complement each other and thus provide more insights into the contribution of various factors to the uncertainty of model results (House *et al.*, 2003).

To strengthen the development of coupled dynamic vegetation models

Vegetation models are developed at different levels of biological organization: global, regional or landscape, community and individual plants (Dale & Rauscher, 1994). However, no model can address all aspects of vegetation dynamic at different spatial scales. Moreover, the biosphere and the atmosphere are a coupled system with biogeophysical and biogeochemical processes occurring across a range of timescales, ranging from short (i.e. seconds to hours) to intermediate (i.e. days to months) and to longer (e.g. seasons, years and decades) timescales (Foley *et al.*, 2000). On different timescales, the processes that control the exchange of matter and energy between the biosphere and the atmosphere are different. In order to consider the full range of coupled atmosphere-biosphere processes, vegetation models should include short, intermediate and long-term ecological phenomena occurring at different spatial scales, which necessitates coupling different vegetation models or coupling vegetation models with other land-use and climate models.

Scale is an important issue in simulating climatic effects on vegetation (Higgins & Vellinga, 2004) and has been a critical impediment to incorporate important fine-scale processes into large-scale vegetation models (Moorcroft *et al.*, 2001). Our knowledge of fine-scale physiological and ecological processes comes from a variety of measurements and experiments made at spatial resolutions considerably smaller than the large scale at which many vegetation models are defined. However, it is the interactions of factors and processes at different scales that determine the vegetation dynamics. Therefore, new vegetation models should have an ability to quantify the mechanisms from micro-level fast eco-physiological responses to macro-level slow acclimation in the pattern, structure and function of vegetation (Cao *et al.*, 2005). Integrating approaches of different vegetation models is therefore necessary because they can help us to understand the interconnections and interactions among different mechanisms at different scales. Given

that the role of local-scale effects is poorly explored, new integrated vegetation models need to stress fine-scale processes such as species dispersal (Del *et al.*, 2006).

Conclusion

Vegetation models have progressed from static-equilibrium to transient-dynamic models. The former simulates vegetation dynamic primarily as a function of the abiotic biophysical environment. Because the data used to infer the abiotic environment are from large spatial scales, these vegetation models are considered a top-down approach in vegetation modeling. In contrast, the latter simulates vegetation dynamics based on some mechanistic processes of terrestrial vegetation. Because local-scale or species-specific information are often used to describe the mechanistic processes of plants, these vegetation models are considered a bottom-up approach. In comparing the two, dynamic models are superior in simulating climatic effects on vegetation because they can include many mechanistic processes of plants and incorporate more non-climatic factors.

The factors that affect the accuracy of model results are multifold. First, the structure, assumptions and parameterization of a model each influence the model results. Static models often ignore some mechanistic processes of vegetation. In contrast, dynamic models may overlook the structural differences among PFTs. A model's assumption may overemphasize the roles of some factors but overlook other factors that are important in controlling vegetation dynamics. The parameterization of some key process of plants is a key issue in vegetation modeling; second, the quality of data used to run a model and to assess model results greatly affects the accuracy of model results; third, both categorical- and continuous-data comparison approaches have their own weakness and thus may bias the accuracy assessment of model results; and fourth, the mismatch of the spatiotemporal resolution of data used in vegetation modeling and the extrapolation of information from one scale to another greatly influence the accuracy of model results.

To address the major factors resulting in the uncertainty of model results, more attention should be put on: (i) establishing structural models with a good hierarchy that

can incorporate as many factors as possible in affecting the vegetation's structure, function and the cycle of carbon and nitrogen in terrestrial vegetation; (ii) improving the quality of model input and validation data, especially high quality input climate data and field observations needed to calibrate model results; (iii) strengthening the intercomparison between different model results, the validation of model results by multiple approaches and the development of new methods for evaluating model results; and (iv) promoting the coupling of different vegetation models or vegetation models with climate or land-cover models, which will greatly contribute to our understanding of the mechanisms from micro-level fast response to macro-level slow acclimation of vegetation to climate change.

Bridge

As mentioned above, the data used to run a model and to evaluate model results greatly affect the accuracy assessment of model results. To demonstrate these, Chapter III aims to examine how the accuracy assessment of vegetation model simulations is sensitive to different input climate data, to the selection of observed validation data and to the choice of map comparison approaches by taking the equilibrium vegetation model BIOME4 (Kaplan *et al.*, 2002) as a typical example.

CHAPTER III

EFFECTS OF EXPERIMENTAL PROTOCOL ON GLOBAL VEGETATION MODEL ACCURACY: A COMPARISON OF SIMULATED AND OBSERVED VEGETATION PATTERNS FOR ASIA

The Chapter is coauthored with Sarah L. Shafer, Patrick J. Bartlein, and Justin O. Holman. The overall research design was conceived by G. Tang, S. Shafer, and P. Bartlein, with input from J. Holman. J. Holman developed the Nomad index and contributed to the analysis of map-comparison methods. G. Tang prepared the initial draft of the manuscript, tables, and figures, with contributions from all authors.

Introduction

Over recent decades, many studies have examined the impacts of climate change on terrestrial vegetation dynamics (e.g. Prentice *et al.*, 1993; Harrison & Prentice, 2003) and the global carbon cycle (e.g. White *et al.*, 2000; Woodward & Lomas, 2004). To assist with these studies, a number of prognostic vegetation models have been developed and used to examine the interactions between environmental change and biological systems (Bolliger *et al.*, 2000). Vegetation models such as IBIS (Foley *et al.*, 1996), BIOME4 (Kaplan *et al.*, 2002), LPJ (Sitch *et al.*, 2003), CENTURY (Parton *et al.*, 1987) and BIOME-BGC (Running & Coughlan, 1988), have greatly improved our ability to understand the response of terrestrial vegetation to past and future environmental variation at global-to-regional scales. However, evaluations of the performance of model-based simulations are subject to a number of limitations, both inherent in the models themselves and in the input data used to run the models (Allen *et al.*, 2001; Barrett *et al.*, 2001). For example, many equilibrium vegetation models assume that climate is the primary factor controlling the dynamics of terrestrial vegetation, and so model-simulated

vegetation is highly dependent on the quality and characteristics of the specific input (or baseline) climatology data, including the number of years of climate data included in the climatology (Kickert *et al.*, 1999).

Remotely sensed global land- and tree-cover data sets, such as the Advanced Very High Resolution Radiometer (AVHRR) Pathfinder Land data, are frequently used to evaluate the ability of vegetation models to simulate global terrestrial vegetation because these data map the pattern of vegetation over large areas (Turner *et al.*, 1993; Gould, 2000). However, errors created in remotely sensed image processing steps, such as image classification and geo-registration, may misclassify the vegetation pattern in a given area (Campbell, 2002). In addition, remotely sensed image classifications developed for different purposes may put different emphases on the categories and characteristics of the post-classified data. For example, NOAA's 1992-93 AVHRR data have been used to produce both 1-km global land-cover characteristics data with 97 different land cover types (Loveland *et al.*, 2000) and continuous field tree-cover data with only three tree-cover classes (DeFries *et al.*, 2000; Hansen *et al.*, 2000). The accuracy assessment of simulated vegetation may vary significantly depending on the choice of the observed vegetation data set used to evaluate the simulated vegetation.

A number of quantitative map-comparison techniques have been used to assess the ability of vegetation models to simulate observed vegetation. These techniques, such as the Kappa statistic (Cohen, 1960; Congalton & Green, 1999), Tau (Ma & Redmond, 1994), Kappa-for-location (Pontius, 2000), and Fuzzy Kappa (Hagen, 2003) are used in raster-based categorical data comparison through pixel-to-pixel arithmetic. Each approach has its own strengths and weaknesses for evaluating a model's performance. For example, the Kappa statistic may greatly underestimate the similarity of two maps if they display a similar data pattern but that pattern is slightly offset from one map to the other (Foody, 1992, 2002). The assessed accuracy of simulated vegetation will vary depending on the choice of which quantitative techniques are used to compare maps of simulated and observed vegetation.

The goal of this study is to examine the effects of three elements of experimental protocols on the evaluation of global vegetation model accuracy: 1) the choice of the input climatology (and its associated atmospheric CO_2 concentration), 2) validation data selection, and 3) map-comparison method. We use vegetation simulated with the equilibrium model BIOME4 (Kaplan *et al.*, 2002; Kaplan *et al.*, 2003) as a typical example of the output from a vegetation model. The geographic focus of this study is most of Asia, ranging from 60.0°E to 150.0°E and from 8.0°N to 80.0°N. This region was chosen because it contains a diversity of terrestrial vegetation and climate zones, and few detailed studies assessing vegetation simulations have been done for this area (e.g. Song *et al.*, 2005). Methodologically, the well-known Kappa statistic, Fuzzy Kappa statistic (hereafter Fuzzy Kappa) and a newly developed method for map comparison, the Nomad index (Holman, 2004), are employed to quantify the agreement between BIOME4-simulated biomes and those derived from three global land- and tree-cover data sets. Through this analysis, we hope to improve our understanding of the model's behavior and provide model users with information to use in designing experimental protocols for vegetation model simulations.

Materials and Methods

The BIOME4 model and baseline climatology data sets

BIOME4 (version 2b1) is an equilibrium, coupled biogeography and biogeochemistry vegetation model that simulates global vegetation in the form of 13 plant functional types (PFTs) that are combined to form 27 biomes (Table 3.1; Kaplan *et al.*, 2002, 2003). The model also calculates a variety of other variables, such as net primary productivity and leaf area index for each PFT under a prescribed global atmospheric CO_2 concentration. BIOME4 has been employed in a number of studies of past, present and potential future vegetation patterns (e.g. Bigelow *et al.*, 2003; Diffenbaugh *et al.*, 2003; Song *et al.*, 2005).

The input variables required to run BIOME4 include monthly mean temperature (°C), monthly mean total precipitation (mm), monthly mean sunshine (%), soil water

holding capacity (mm) for each of two soil layers, a conductivity index of water movement through the soil column (mm/day), and atmospheric CO_2 concentration (ppm). We used the CRU TS 2.0 data set from the Climatic Research Unit (CRU), University of East Anglia (U.K.), to create the input climatologies for running BIOME4. The CRU TS 2.0 data set is supplied on a 0.5-degree global land grid at a monthly time-step for 1901-2000 and builds upon several previous CRU gridded data sets (New *et al.*, 1999; New *et al.*, 2000; Mitchell *et al.*, 2004). Soil data were obtained from the derived soil properties defined in the FAO digital soil map of the world (Food & Agriculture Organization, 1995). Annual atmospheric CO_2 values for 1901 to 1995 were provided by the Carbon Cycle Model Linkage Project (Kicklighter *et al.*, 1999).

Table 3.1 Original biome types simulated by BIOME4

Biome types simulated by BIOME4 (Kaplan et al.,2002; Kaplan et al., 2003)	
1) Tropical evergreen forest	15) Temperate sclerophyll woodland
2) Tropical semi-deciduous forest	16) Temperate broadleaved savanna
3) Tropical deciduous forest/woodland	17) Open conifer woodland
4) Temperate deciduous forest	18) Boreal parkland
5) Temperate conifer forest	19) Tropical grassland
6) Warm mixed forest	20) Temperate grassland
7) Cool mixed forest	21) Desert
8) Cool conifer forest	22) Steppe tundra
9) Cold mixed forest	23) Shrub tundra
10) Evergreen Taiga/montane forest	24) Dwarf shrub tundra
11) Deciduous taiga/montane forest	25) Prostrate shrub tundra
12) Tropical savanna	26) Cushion forb lichen moss tundra
13) Tropical xerophytic shrubland	27) Barren
14) Temperate xerophytic shrubland	

We designed 19 scenarios to analyze the sensitivity of BIOME4 simulations to different climatologies and their associated atmospheric CO_2 concentrations. The 19 monthly mean climatologies used to run BIOME4 are derived from the CRU TS 2.0 data set and each of them extends backward in time from December of 1992 for 2, 5, 10, 15, 20, 25, 30, 35, 40, 45, 50, 55, 60, 65, 70, 75, 80, 85 and 90 years respectively. The year 1992 was chosen as the common end point for the climatologies because all three

observed vegetation data sets used in this study were developed from remotely-sensed images taken over the period of April 1992 to March 1993. The associated atmospheric CO_2 concentrations for each BIOME4 simulation were developed by averaging annual CO_2 values for each of the 19 different climatology time periods. We also designed 8 scenarios to examine the sensitivity of BIOME4 simulations to different 30-year monthly mean climatologies (1963-1992, 1961-1990, 1951-1980, 1941-1970, 1931-1960, 1921-1950, 1911-1940 and 1901-1930) and their associated atmospheric CO_2 concentrations following the same approach.

Global land cover and forest cover data

We used one tree-cover and two global land cover data sets to investigate how the selection of observed vegetation data influences the accuracy assessment of the model-based simulations. The data sets include (i) the global potential natural vegetation (PNV) data (Ramankutty & Foley 1999), (ii) the 1-km global land cover characteristic (GLCC) data (version 2.0) (Loveland *et al.*, 2000), and (iii) the global AVHRR continuous field tree-cover data (DeFries *et al.*, 2000; Hansen *et al.*, 2000). Each observed vegetation data set was compared to each of the 19 BIOME4 simulations.

The gridded global PNV data describe the distribution of global potential natural vegetation patterns that would most likely exist in the absence of human activities (Ramankutty & Foley, 1999). For regions not dominated by human land use, the PNV vegetation types were based on the DISCover land cover data set derived from the International Geosphere-Biosphere Programme (IGBP) AVHRR data of 1992 to 1993 (Loveland *et al.*, 2000). For regions dominated by human land use, the vegetation types were based on the Haxeltine and Prentice (1996) potential natural vegetation data. The PNV data are classified into 15 biome types (Table 3.2) at a spatial resolution of 0.5°, which matches the resolution at which biomes were simulated by BIOME4 for this study. The GLCC data were generated from IGBP 1-km AVHRR 10-day composites from April 1992 through March 1993 (Eidenshink & Faundeen, 1994), and the data were classified into 97 global land cover types at a 30 arc-second spatial resolution. The GLCF data were obtained by combining the "Global maps of proportional cover for three vegetation

characteristics" data (DeFries *et al.*, 1998) with the "Global land cover classification" data (Hansen *et al.*, 2000). Both of these data sets were derived at a 1-km spatial resolution from NOAA's AVHRR data acquired in 1992-1993. The GLCF data used in this study are at a 30 arc-second spatial resolution and consist of continuous fields of vegetation characteristics divided into three classes: (i) percent tree cover with values ranging from 10 to 80 percent; (ii) percent tree cover less than 10 percent (coded as "255"); and (iii) non-vegetated areas (coded as "254") (DeFries *et al.*, 2000; Hansen *et al.*, 2000).

Table 3.2 Original biome types classified in the PNV data

Biome types classified in the PNV data (Ramankutty & Foley, 1999)	
1) Tropical evergreen forest/woodland	9) Savanna
2) Tropical deciduous forest/woodland	10) Grassland/steppe
3) Temperate broadleaf evergreen Forest/woodland	11) Dense shrubland
4) Temperate needleleaf evergreen forest/woodland	12) Open shrubland
5) Temperate deciduous forest/woodland	13) Tundra
6) Boreal evergreen forest/woodland	14) Desert
7) Boreal deciduous forest/woodland	15) Polar desert/rock/ice
8) Mixed forest	

Data processing

Unlike the global PNV data, which have the same spatial resolution (0.5°) as the CRU TS 2.0 data set, the global GLCC and GLCF data have a much finer spatial resolution. In order to compare the BIOME4-simulated biome types with the land cover classes in the GLCC data and the tree-cover classes in the GLCF data, we first reregistered the 30 arc-second GLCC and GLCF data into 0.5° gridded data using a nearest-neighbor algorithm we developed. For each 0.5° grid point we assigned the value of the geographically nearest point in the GLCC and GLCF data. We compared this nearest neighbor approach with reclassification using the modal land cover type in a 60 by 60 grid cell window, which produced similar results to those obtained using the nearest-neighbor method.

After regridding the GLCC and GLCF data, we reclassified the vegetation in each pair of data sets (BIOME4 vs. GLCC, BIOME4 vs. PNV, and BIOME4 vs. GLCF) into matching or comparable biome types. Given that BIOME4 produces 27 biome types and that there are 51 land cover classes in the GLCC data for Asia, we attempted to maximize the number of reclassified biome types. BIOME4 biomes that did not match a land cover type in the GLCC data were grouped with related BIOME4 biomes to produce a total of 16 reclassified (BIOME4) biomes (Table 3.3). In general, the BIOME4 biomes that were grouped in this manner consisted of small numbers of grid cells in our research area (e.g. tropical grassland simulated under the 1961-1990 30-year climatology consists of only three grid cells and was combined with tropical savanna).

The GLCC data were reclassified into the same 16 biome types (Table 3.3) by: (i) classifying the same or similar land cover types in each pair of compared data sets as the same biome types; (ii) classifying the land cover types located in one climate zone into the biomes shared by the same climate zone (e.g. temperate vegetation was grouped into temperate biome types rather than tropical biome types); and (iii) for a land cover type that could not be classified based on the steps described above, we first assigned it the value of its most-likely neighbor (i.e. the mode of land cover types in neighboring grid cells) in the source data and then reclassified it according to the steps outlined above. In practice, those land cover types hardest to classify, such as "heath scrub" (which consists of 23 grid cells in the GLCC data), are often clustered in specific areas and represented by relatively few grid cells. Thus, they do not have a large effect on the accuracy assessments of the BIOME4 simulations. In addition, given that BIOME4 simulates potential vegetation in the absence of human activity, we excluded from our analysis all grid cells in which the GLCC land cover types represent human activities (e.g. crops, urban).

Table 3.3 Reclassified BIOME4 biome types and GLCC land cover types

Reclassified biome types	BIOME4 biomes	GLCC land cover
1) Tropical evergreen forest	1	19,33,72
2) Tropical semi- and deciduous forest	2,3	5,29,34,90,96
3) Temperate deciduous/conifer forest	4,5	5,27
4) Warm mixed forest	6	24
5) Cool/cold mixed forest	7,9	23,24
6) Cool conifer forest	8	22,57
7) Evergreen taiga/montane forest	10	19,21,44,62
8) Deciduous taiga/montane forest	11	4,61
9) Tropical savanna and grassland	12,19	2,10,58,94
10) Tropical xerophytic shrubland	13	51,55,56
11) Temperate xerophytic shrubland	14	51
12) Temperate savanna and grassland	16,20	2,10,40,43,58,92
13) Barren and desert	21,27	8,50
14) Steppe tundra	22	11
15) Shrub tundra	23	63,64
16) Dwarf and prostrate shrub and moss tundra	24,25,26	9,69

The BIOME4 biomes with codes 15, 17, and 18 (Table 3.1) are not listed because they were not simulated to occur in the study region. The land-cover types with codes 2, 5, 10, 19, 24 and 51 are divided into their tropical (latitude $\leq 23.5^{o}$) and temperate (latitude $> 23.5^{o}$) subparts. The land-cover types with code 16, 17, 19, 40, 45, 60 and 91 are not listed because they are reassigned the value of their nearest neighbor in the source data. The human-related land-cover types with codes 1, 30, 31, 36, 37, 38, 55, 56, 57, 58 and 93, and inland water (code 14) are excluded in the comparison. The GLCC land cover types and codes are listed in the "Global Ecosystem Legend" (http://edcsns17.cr.usgs.gov/GLCC/globdoc2_0.html, owned by the U.S. Geological Survey's (USGS) National Center for Earth Resources Observation and Science).

There is good agreement between the BIOME4 biome categories and the PNV categories (Tables 3.1 and 3.2). We reclassified vegetation types from these two data sets into 6 biome types: forest cover, tropical/temperate savanna, grassland, tropical/temperate shrubland, tundra, and barren/desert (Table 3.4). In order to compare the BIOME4-simulated biomes with those classified in the GLCF data, we grouped the BIOME4-simulated biomes into three categories: forest biomes, grassland and savanna biomes, and desert biomes including barren areas (Table 3.5). As with the comparison of BIOME4 vs. GLCC, the comparison of BIOME4 vs. GLCF data also excluded all grid cells where the GLCC land cover types reflected human activities.

Table 3.4 Reclassified biome types and PNV types for comparison

Reclassified biome types	BIOME4 biome codes	PNV biome codes
1) Forest cover	1,2,3,4,5,6,7,8,9,10,11	1,2,3,4,5,6,7,8
2) Tropical/temperate savanna	12,16	9
3) Grassland	19,20	10
4) Tropical/temperate shrubland	13,14	11,12
5) Tundra	22,23,24,25,26	13
6) Barren and desert	21,27	14,15

Table 3.5 Reclassified biome types and tree-cover percentage classes for comparison

Reclassified biome types	BIOME4 biome codes	GLCF tree cover codes
1) Forest cover	1,2,3,4,5,6,7,8,9,10,11	10-80
2) Grassland/percent tree cover (<10%)	12,13,14,16, 19,20,22,23,24,25,26	255
3) Barren and desert	21,27	254

Map Comparison Methods

The Kappa statistic

The Kappa statistic (Cohen, 1960) has been widely used to quantitatively assess the accuracy of land cover classifications derived from remotely sensed data, such as AVHRR data (Roy & Joshi, 2002). It also has gained widespread use in global-change research (Diffenbaugh *et al.*, 2003; Prentice *et al.*, 1992). The advantage of the Kappa statistic is that it takes into account chance agreement, regardless of the number of categories in the maps being compared. In addition, it is easy to calculate and is an intuitive measure of agreement (Monserud & Leemans, 1992; Foody, 2002). For each pair of compared observed and simulated vegetation data sets, an error matrix, A, is constructed. Then, for each category i in the constructed error matrix A, the Kappa statistic is calculated by the following equation:

$$\kappa_i = (p_{ii} - p_{i.row}p_{col.i})/((p_{i.row} + p_{col.i})/2 - p_{i.row}p_{col.i}) \quad (1)$$

where $p_{i.row}$ is the row total for each category i; $p_{col.i}$ is the column total for each category i; and p_{ii} is the individual entry for the row and column on the main diagonal

of constructed error matrix A. The overall agreement between two compared maps is estimated by the formula:

$$\kappa = (p_0 - p_e)/(1 - p_e) \quad (2)$$

where $p_0 = \sum_{i=1}^{c} p_{ii}$; $p_e = \sum_{i=1}^{c} p_{i.row} p_{col.i}$; and c is the number of categories in each data set.

The Fuzzy Kappa statistic

Like the Kappa statistic, the Fuzzy Kappa statistic is also a cell-by-cell-based map comparison approach. However, the Fuzzy Kappa takes the neighborhood of a cell into account to express the similarity of that cell to its neighbor. In order to distinguish minor differences from major differences, the Fuzzy Kappa assesses two types of fuzziness: fuzziness of category and fuzziness of location. Category fuzziness refers to the ordinal similarity among all categories on a map. Location fuzziness refers to the fact that the spatial location of a category on a map is not always precise (Hagen, 2003; Hagen-Zanker *et al.*, 2005). For each cell, a local measure of similarity can be calculated based on a two-way comparison. An overall Fuzzy Kappa statistic can be obtained by averaging the similarity calculated for all grid cells, which yields a result between 0 (for total disagreement) and 1 (for identical maps). The formula for Fuzzy Kappa is identical in form to equation (2) but different in the calculation of the expected similarity (P_e), which is expressed by the formula:

$$P_e = \sum_{i=1}^{R} E(i) \times M(d_i) \quad (3)$$

where R is the number of the furthest ring (cells that are at the same distance from a central cell are said to form a neighborhood ring); M is the fuzzy membership function; d_i is the radius of ring i; and $E(i)$ refers to the probability of matching central cells and is calculated separately according to the Kappa statistic. In this study, we calculate location fuzziness using an exponential decay membership function with a halving distance of 0.5 and a neighborhood radius of 1 grid cell. Category fuzziness is not considered. A Fuzzy Kappa statistic for all individual categories in two maps can be calculated through the creation of "temporary category similarity matrices," in which all

categories are set equal to each other except for the category being considered (Hagen, 2003).

The Normalized Minimum Agreement Distance (Nomad) index

The Nomad index (Holman, 2004) was developed to better quantify the agreement of spatial patterns between maps and to overcome map coregistration issues (e.g. Costanza, 1989). For each category in two raster datasets, the calculation of the Nomad index follows three steps: (i) determine a set of grid-cell pairs (one grid cell in map A, one grid cell in map B) that minimizes the total distance between all possible pairs; (ii) calculate the average distance for this minimum distance-based set of pairs and the overall average grid-cell-to-cell-based distance of a category; and (iii) compare the average minimum distance with the overall average distance to quantify the level of map agreement (Holman, 2004). If the minimum distance between pairs for a category is less than the overall average distance of a category, then map agreement will be relatively high and vice versa. For each category, the values of the Nomad index range from near or below 0 for poor agreement to 1 for perfect agreement. The overall agreement is determined by calculating a frequency-weighted average of individual Nomad values.

The individual Nomad index $n(c)$ for category c in two maps is calculated according to the following equation:

$$n(c) = 1 - ((\sum d(c) / d_{avg}) / g_c) \tag{4}$$

where $d(c) = \min(\sum d_{ab})$, which stands for the minimum geometric distance for all possible grid-cell comparisons ab; d_{ab} is the distance from grid cell a in map A to its match b in map B; d_{avg} is the overall average distance of d_{ab}; and g_c is the number of grid cells in category c. The overall Nomad index (N) for two maps with k categories is expressed as the following equation:

$$N = [\sum n(c)] / k \quad c = 1, 2, \ldots, k \tag{5}$$

The rating system used in the accuracy assessment

For the Kappa statistic and Fuzzy Kappa, we used the accuracy rating system of Landis and Koch (1977) and Monserud and Leemans (1992) where values greater than

0.75 indicate very good-to-excellent agreement, values between 0.40 and 0.75 indicate fair-to-good agreement, and values of 0.40 or less indicate poor agreement. Values close to 0.0 suggest that the agreement is no better than would be expected by chance. For the Nomad index, Holman (2004) suggests values greater than 0.75 indicate very good-to-excellent agreement, values between 0.60 and 0.75 indicate fair-to-good agreement, and values less than 0.60 indicate poor agreement.

Results and Discussion

Effect of different input climatologies and their associated CO_2 concentrations on simulated vegetation

A number of patterns emerge when the BIOME4 vegetation simulated under each of the 19 different climatologies and their associated atmospheric CO_2 concentrations (hereafter "climatologies") is compared to each of the observed land cover data sets. First, the simulated vegetation accuracy differs from one biome to another under the same climatology. For example, the shrub tundra biome simulated using the 2-year climatology agrees well (Kappa statistic=0.46, Fuzzy Kappa=0.47 and Nomad index=0.62) with the GLCC data while other biomes from the same simulation, such as evergreen taiga montane forest (EvTMF), display relatively poor agreement (Kappa statistic=0.30, Fuzzy Kappa=0.30 and Nomad index=0.38). These differences in simulated accuracy may reflect differences in the model's ability to simulate particular vegetation types or they may indicate that the input data, in this case the 2-year climatology, fails to capture the long-term mean climate for certain regions.

Second, the simulated vegetation accuracy varies with the length of the climatology used to simulate the vegetation data. For example, under the "BIOME4 vs. GLCC" comparison, when the climatology length is less than 30 years the Kappa statistic, Fuzzy Kappa and the Nomad index values vary substantially from one simulation to the next for most biomes. In contrast, the three statistics tend to vary less from one simulation to the next when the climatology length is greater than 30 years (Figure 3.1). This consistency reflects the fact that climatological means spanning longer

time periods are less influenced by the addition of individual years than climatological means spanning shorter time periods.

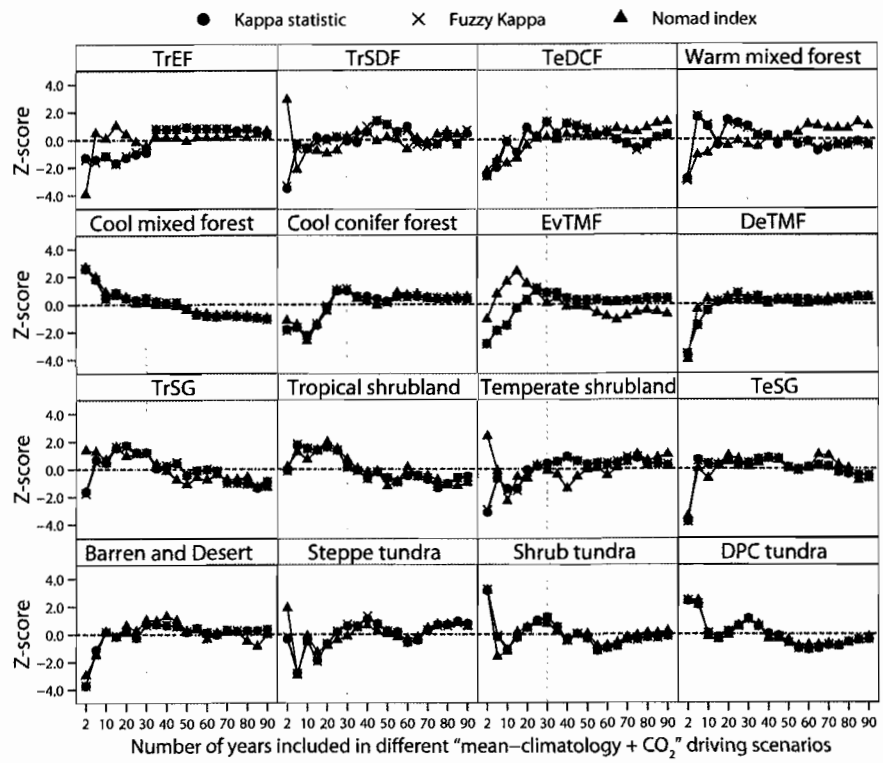

Figure 3.1 Sensitivity of BIOME4-simulated biomes to different input climatologies when compared to the GLCC data as illustrated by the variation of three standardized statistics. In general, the simulations under climatologies with a length less than 30 years vary more among simulations than those under the climatologies with a length greater than 30 years (TrEF = tropical evergreen forest, TrSDF = tropical semi- and deciduous forest, TeDCF =temperate deciduous/conifer forest, EvTMF = evergreen taiga/montane forest, DeTMF = deciduous taiga/montane forest, TrSG= tropical savanna and grassland, TeSG= temperate savanna and grassland, DPC tundra = dwarf and prostrate shrub and cushion forb lichen moss tundra).

Third, the vegetation simulations run with the 25-, 30- and 35-year climatologies produce simultaneously the highest overall Kappa statistic, Fuzzy Kappa and Nomad index when compared to the three observed data sets (Figure 3.2 & Table 3.6). This accuracy may reflect the general adaptation of regional-scale vegetation to the long-term mean climate of a region. It also indicates that climatologies including 25 or more years

are of sufficient duration to capture the the interannual and regional climate variations that affect a region's vegetation (Carter *et al.*, 2001). The overall accuracy of the simulated vegetation supports the continued use of 30-year climatological means, which have been a standard length for climatologies used in vegetation modeling studies.

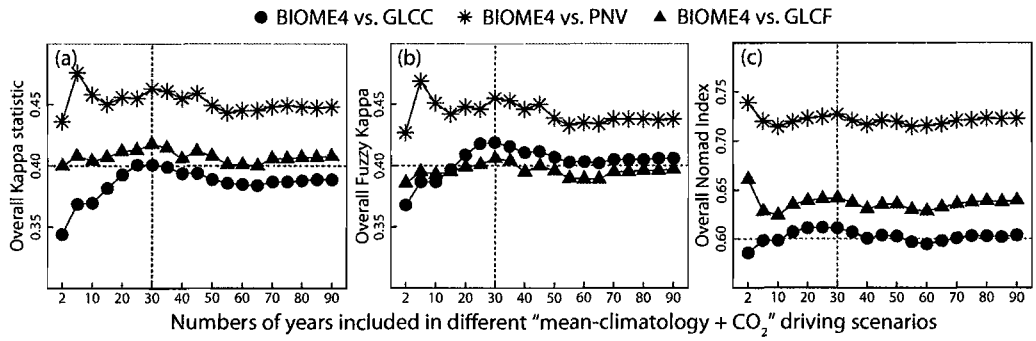

Figure 3.2 Sensitivity of BIOME4-simulated overall vegetation to different model-driving scenarios as illustrated by the variation of three overall statistics. Under all comparisons, the three overall statistics are simultaneously high under the 1963-1992 30-year climatology.

Table 3.6 The three scenarios with the highest overall statistics under all comparisons

Compared data	Statistic	Years included in 19 different "mean-climatology + CO_2" scenarios									
		2	5	10	15	20	25	30	35	40	Others
GLCC	κ						0.40	0.40	0.39		
PNV	κ		0.48					0.46	0.46		
GLCF	κ						0.41	0.42	0.41		
GLCC	*FK*						0.42	0.42	0.42		
PNV	*FK*		0.47					0.46	0.45		
GLCF	*FK*						0.40	0.41	0.40		
GLCC	*NI*					0.61	0.61	0.60			
PNV	*NI*	0.74					0.72	0.73			
GLCF	*NI*	0.66					0.64	0.64			
Total numbers		2	2	0	0	1	7	9	6	0	0

κ ----Kappa statistic; *FK* ----Fuzzy kappa; *NI* ----Nomad index.

For the simulations run using 30-year mean climatologies for different time periods, the vegetation simulated using the most recent 30-year climatologies (i.e. 1963-1992 or 1961-1990) produce the highest overall Kappa statistic, Fuzzy Kappa and Nomad

index under all three comparisons (Figure 3.3). These high values may reflect the influence of recent climate on the GLCC and GLCF observed vegetation data. In addition, the statistics show that the 1963-1992 30-year climatology can accurately simulate the greatest number of biomes (e.g. 9 out of 16 biomes under the "BIOME4 vs. GLCC" comparison) (Table 3.7).

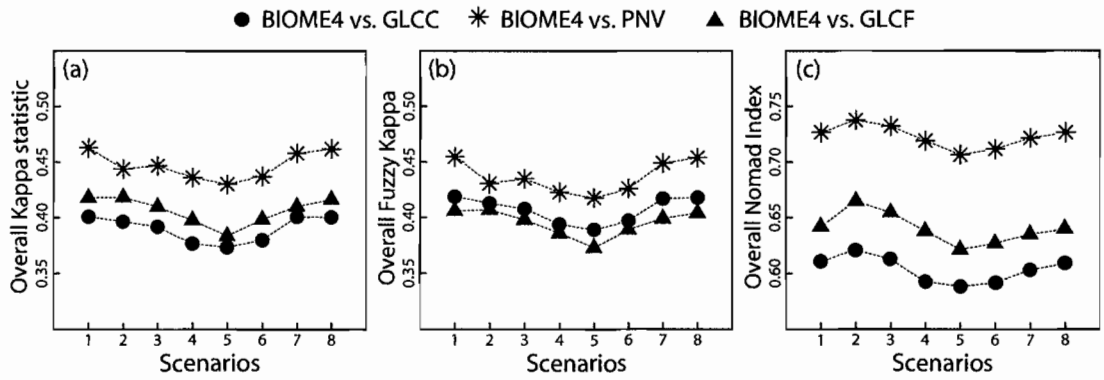

Figure 3.3 Sensitivity of the BIOME4 simulations to eight different 30-year climatologies: 1 (1963-92), 2 (1961-90), 3 (1951-80), 4 (1941-70), 5 (1931-60), 6 (1921-50), 7 (1911-40) and 8 (1901-30). The high values for the three statistics in the early part of the 20th century may reflect the relaxation of the CRU TS 2.0 monthly climate data for this period towards the 1961–1990 climatology values because of an insufficient number of Asian climate station records (see New *et al.*, 2000).

Although the 5-year climatology produces a high overall Kappa statistic and Fuzzy Kappa under the "BIOME4 vs. PNV" comparison, the values of these statistics are relatively low under the "BIOME4 vs. GLCC" and "BIOME4 vs. GLCF" comparisons (Table 3.6). Similarly, although the 2-year climatology produces a high Nomad index under the "BIOME4 vs. PNV" and "BIOME4 vs. GLCF" comparisons, it results in the lowest overall Kappa statistic and Fuzzy Kappa under all three comparisons (Figure 3.2). Compared to other climatologies, the simulations run using the 2- and 5-year climatologies have the greatest potential to incorrectly simulate the greatest number of individual biomes (Figure 3.4), largely because the climate data included in the 2- and 5-year climatologies may not reflect the long-term climate mean of a given area. Assuming that vegetation is responding to conditions that prevail over the long-term as opposed to

those of any given year, the accuracy of the vegetation simulated using a 30-year climatology should be better than that simulated using a 2- or 5-year climatology.

Table 3.7 Comparison of GLCC biomes with the BIOME4 biomes simulated under the 1963-1992 30-year mean climatology

Reclassified biome types	Kappa statistic	Fuzzy Kappa	Nomad index
1) Tropical evergreen forest	0.25	0.26	0.30
2) Tropical semi-deciduous and deciduous forest	0.45	0.48	0.61
3) Temperate deciduous/conifer forest	0.41	0.43	0.68
4) Warm mixed forest	0.51	0.54	0.76
5) Cool/cold mixed forest	0.16	0.17	0.35
6) Cool conifer forest	0.07	0.08	0.05
7) Evergreen taiga/montane forest	0.38	0.38	0.39
8) Deciduous taiga/montane forest	0.42	0.40	0.83
9) Tropical savanna and grassland	0.26	0.28	0.44
10) Tropical xerophytic shrubland	0.29	0.29	0.65
11) Temperate xerophytic shrubland	0.40	0.41	0.80
12) Temperate savanna and grassland	0.36	0.36	0.38
13) Barren and desert	0.55	0.56	0.89
14) Steppe tundra	0.50	0.54	0.84
15) Shrub tundra	0.42	0.42	0.56
16) Dwarf and prostrate shrub and moss tundra	0.48	0.50	0.58
Overall statistics	0.40	0.42	0.61

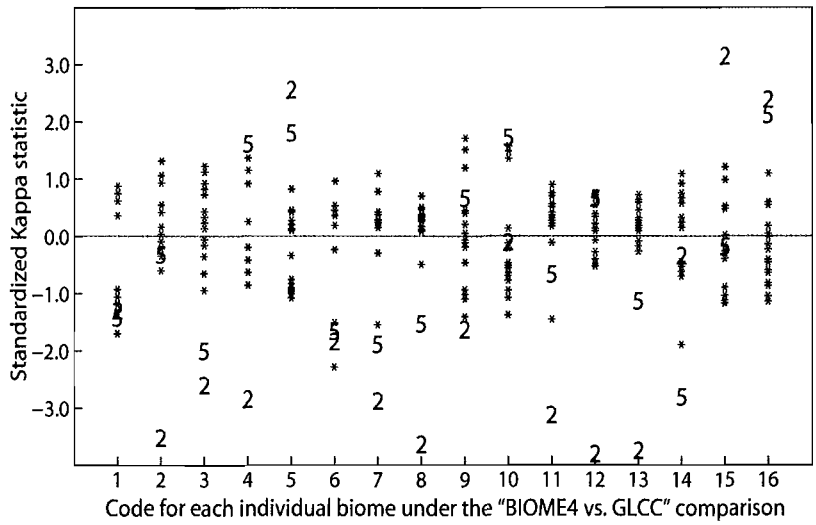

Figure 3.4 Standardized Kappa values (z-score) for the BIOME4 biomes simulated under the 19 climatologies as compared with the GLCC data (see Table 3.3). For each individual biome, the different simulations are indicated by asterisks ("*") except for those simulations using the 2- and 5-year climatologies, which are indicated by the numbers 2 and 5, respectively. For each biome, the 2- and 5-year climatologies tend to produce standardized Kappa values that are 1.0 or more standard deviation above or below the mean of all the Kappa values for that biome.

Effect of observed data choice on model accuracy assessment

The choice of what observed vegetation data to use in evaluating model results can significantly affect the assessment of a model's ability to simulate the overall vegetation pattern for a region. For example, when the BIOME4 simulations created with the most recent 30-year (1963-1992) climatology are compared with the PNV data, the Kappa statistic (κ=0.46) indicates that BIOME4 has a fair ability to simulate potential natural vegetation patterns in continental Asia (Table 3.8). However, BIOME4's ability to accurately simulate vegetation is weaker when compared to both the GLCF data (κ=0.42) and the GLCC data (κ=0.40). As illustrated in Figure 3.5, the "BIOME4 vs. PNV" case produces both a higher overall Kappa statistic, a higher overall Fuzzy Kappa and a higher overall Nomad index under all 19 scenarios than either the comparison of "BIOME4 vs. GLCC" or "BIOME4 vs. GLCF" does.

Table 3.8 Comparison of PNV biomes with the BIOME4 biomes simulated under the 1963-1992 30-year mean climatology

Reclassified biome types	Kappa statistic	Fuzzy Kappa	Nomad index
1) Forest cover	0.49	0.45	0.77
2) Tropical/temperate savanna	0.01	0.01	0.16
3) Grassland	0.32	0.31	0.41
4) Tropical/temperate shrubland	0.37	0.37	0.75
5) Tundra	0.65	0.65	0.78
6) Barren and desert	0.57	0.58	0.84
Overall statistics	0.46	0.46	0.73

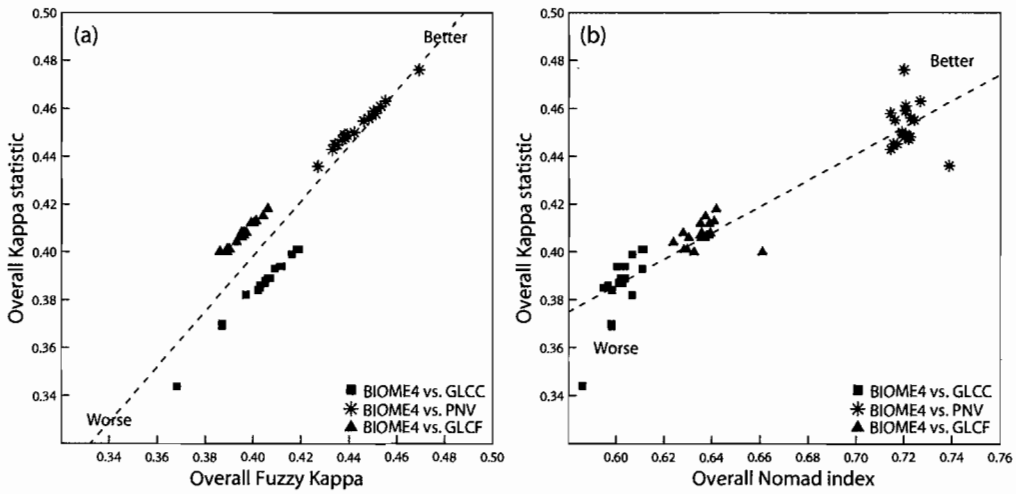

Figure 3.5 Overall Kappa statistic versus overall Fuzzy Kappa values (left) and overall Kappa statistic versus overall Nomad index values (right) from the comparisons the GLCC, PNV, and GLCF observed vegetation with the BIOME4 vegetation simulated under each of the 19 climatologies. The BIOME4-simulated overall vegetation pattern for Asia under the 19 simulations agrees more with the PNV data than does with either the GLCC or the GLCF data as illustrated by the relatively higher three statistics under the comparison of "BIOME4 vs. PNV".

BIOME4 was originally developed to simulate potential natural vegetation and thus it is not surprising that the BIOME4 simulated vegetation better matches the PNV data than it does either the GLCC or GLCF data. The PNV data used in this study were derived from a combination of the DISCover land cover data set (Loveland *et al.*, 2000) and the Haxeltine and Prentice (1996) potential natural vegetation data (Ramankutty & Foley, 1999). In the PNV data, the vegetation types in regions dominated by human land

use were based on the Haxeltine and Prentice (1996) potential natural vegetation data, which in turn were based primarily on the vegetation maps of Melillo *et al.* (1993). In contrast, both the GLCC and GLCF data were developed completely from remotely-sensed AVHRR data, which were snapshots of the actual vegetation over the period of April 1992 to March 1993. Although we excluded all grid cells with human-altered land cover types in both the "BIOME4 vs. GLCC" and "BIOME4 vs. GLCF" comparisons, other human-induced effects on terrestrial vegetation (e.g. past deforestation, changes in disturbance regimes) may still exist in the reclassified GLCC and GLCF data.

The extent to which the observed data must be reclassified to be compared with the simulated data will also affect the accuracy assessment of a model to simulate a given biome. For example, the Kappa statistic (κ>0.55) indicates that BIOME4 has a good ability to simulate the spatial distribution of barren and desert areas (the only common category classified in all three comparisons) in continental Asia when compared with the GLCC and PNV data (Tables 3.7 and 3.8), but a poor ability (κ=0.35) when compared with the GLCF data (Table 3.9). This difference in accuracy is mainly a result of how barren and desert areas are classified in the three observed data sets (Figure 3.6). In the GLCF data, "unvegetated" areas were reclassified as barren and desert (Figure 3.6f), which excluded areas with little vegetation. In contrast, the reclassified barren and desert consists of either "bare desert and sand desert" in the GLCC data or "desert and polar/rock/ice" in the PNV data, both of which were largely based on the "barren or sparsely vegetated" land cover type in IGBP DISCover data set (Ramankutty & Foley, 1999; Loveland *et al.*, 2000) and thus included areas with little vegetation (e.g. the spatial extent of reclassified barren and desert in west China is much larger in both GLCC (Figure 3.6b) and PNV (Figure 3.6d) data than in GLCF data (Figure 3.6f)). Because the definitions and attributes of the reclassified barren and desert biome are different in these three datasets, the spatial pattern of the GLCC- and PNV-based barren and desert biomes display better visual agreement with the BIOME4-simulated barren and desert biome than with the GLCF-based biome (Figure 3.6).

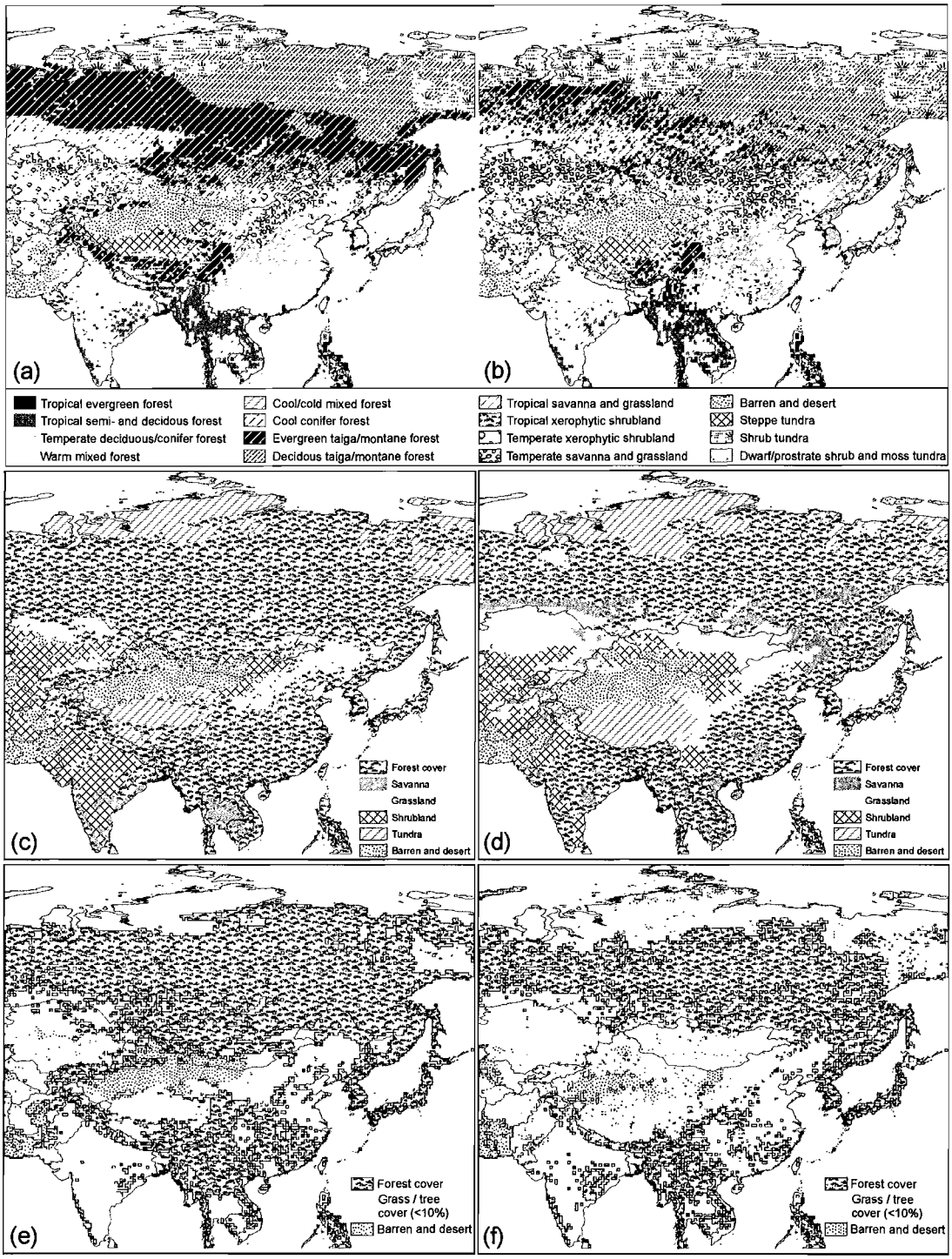

Figure 3.6 Comparison between the BIOME4-simulated vegetation for Asia (a, c and e) under the 1963-1992 30-year mean climatology and the observed vegetation from the (b) GLCC, (d) PNV and (f) GLCF data. The white areas in (a), (b), (e) and (f) refer to human-modified land and inland water.

Table 3.9 Comparison of GLCF biomes with the BIOME4 biomes simulated under the 1963-1992 30-year mean climatology

Reclassified biome types	Kappa statistic	Fuzzy Kappa	Nomad index
1) Forest cover	0.52	0.50	0.68
2) Grassland/ percent tree cover less than 10%	0.33	0.27	0.58
3) Barren and desert	0.35	0.36	0.71
Overall statistics	0.42	0.41	0.64

Effect of map comparison methods on accuracy assessment

The choice of map comparison methods will affect the accuracy assessment of a model simulation. Given the same observed and simulated vegetation data, different comparison methods can produce similar judgments of a model's ability to simulate a given biome. For example, the individual Kappa statistic, Fuzzy Kappa and Nomad index all indicate that BIOME4 can accurately predict temperate deciduous/conifer forest, deciduous taiga/montane forest, temperate savanna and grassland, temperate xerophytic shrubland, steppe tundra and barren/desert (Table 3.7 & Figure 3.6a vs. b), forest cover, tundra and barren/desert (Table 3.8 & Figure 3.6c vs. d), and forest cover (Table 3.9 & Figure 3.6e vs. f) in continental Asia. These reclassified biomes consist of a large number of continuously distributed grid cells in the two compared maps. In contrast, the three statistics suggest that BIOME4 less accurately simulates cool conifer forest (Table 3.7 & Figure 3.6a vs. b) and tropical/temperate savanna (Table 3.8 & Figure 3.6c vs. d). These biomes often consist of a small number of discretely distributed grid cells spread over a large area.

Different conclusions about a model's ability to simulate a given biome may also occur when different comparison methods are used for the assessment. For example, for tropical/temperate shrubland in the "BIOME4 vs. PNV" comparison, the low Kappa (0.37) and Fuzzy Kappa (0.37) values suggest an inability of BIOME4 to correctly simulate shrubland in our research area. In contrast, the high Nomad index value (0.75) indicates that BIOME4 has a relatively good ability to simulate shrubland. Figures 6c and 6d indicate that the pattern of the BIOME4 simulated shrubland resembles to some

degree that of the PNV shrubland. Because the Nomad index assesses pattern agreement based on geographic distance instead of location accuracy (i.e. the correct location of a category), the relatively good agreement of spatial pattern (especially in the mid-latitude areas) between observed and simulated shrubland and a large number of total compared grid cells (see equation 4) result in the high Nomad index. However, because the Kappa and Fuzzy Kappa statistics depend on a pixel-by-pixel comparison that emphasizes location accuracy, the large disagreement between observed and simulated shrubs in India produces low Kappa and Fuzzy Kappa values.

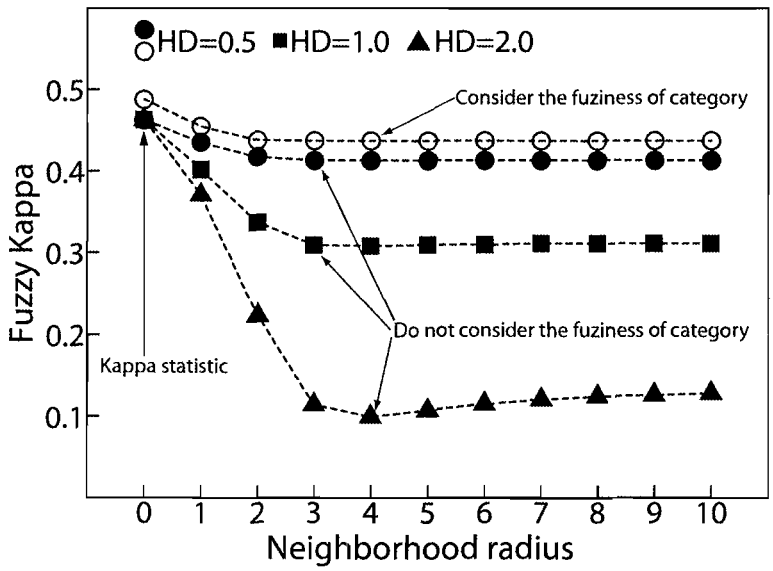

Figure 3.7 Sensitivity of the Fuzzy Kappa under the "BIOME4 vs. PNV" comparison to different settings of the neighborhood radius and the exponential decay function halving distance (HD). Without considering category fuzziness and when the neighborhood radius is zero, the Fuzzy Kappa equals the Kappa statistic.

Although the Kappa and Fuzzy Kappa statistics in this study are approximately equal to each other under all comparisons, the simulated vegetation accuracy assessment is still sensitive to how they are used. For example, Figure 3.7 illustrates how the Fuzzy Kappa varies with changes in the neighborhood radius and the fuzzy membership function, two parameters that need to be specified to calculate the Fuzzy Kappa. The

Fuzzy Kappa values decrease as the neighborhood radius increases largely because of an increased expected similarity. In this case, the Fuzzy Kappa value tends to be lower than the Kappa statistic if category fuzziness is not considered (Figure 3.7). If category fuzziness is considered, the Fuzzy Kappa is likely to be higher than the Kappa statistic. Therefore, when using the Fuzzy Kappa to assess the accuracy of simulated vegetation model, users must exercise care in choosing the values of neighborhood radius, the "fuzzy membership function," and category fuzziness values. For 0.5-degree data, the Fuzzy Kappa calculated using a neighborhood radius of 2 and exponential decay function halving distance of 2 will greatly underestimate the accuracy of simulated vegetation (Figure 3.7).

Conclusion

First, the evaluation of global vegetation model accuracy is sensitive to the selection of input climatologies and their associated atmospheric CO_2 concentrations. The BIOME4 simulations run with the most recent 30-year (1963-1992) CRU TS 2.0 climatology and its associated atmospheric CO_2 concentration simultaneously result in the highest agreement when the simulated biomes are compared to each of the three land- and tree-cover data sets. In addition, the simulations driven by 25-, 30- and 35-year climatologies most accurately simulate the greatest number of individual biomes. Our results support the use of 30-year (or longer) climatologies (and their associated atmospheric CO_2 concentrations) when using an equilibrium vegetation model to simulate terrestrial vegetation, particularly the 30-years that correspond to the time period represented by the observed vegetation data that will be used to evaluate the simulated results.

Second, the results reveal that the choice of which observed data set to compare with the simulated data will affect the assessment of a vegetation model's ability to simulate terrestrial vegetation patterns at global-to-regional scales. The BIOME4-simulated Asian terrestrial vegetation displays better agreement with the PNV data than with either the GLCC or GLCF data, because both the BIOME4 simulations and the PNV

data share the same goal of describing potential vegetation determined largely by climate and in the absence of human activity. However, the agreement between the BIOME4-biomes and those reclassified from the GLCC and GLCF data is lower because these two AVHRR-derived data sets are snapshots of modern vegetation at a particular time (April 1992 to March 1993) and include the effects of human activities on vegetation (even though we excluded the human-influenced grid cells in our comparison). Therefore, when choosing observed data for model evaluation, model users must take into account the nature of both the model and the observed data. A correct assessment of a model's accuracy requires that the attributes and definitions of the simulated vegetation match that defined or classified from observed data.

Third, the results demonstrate that the use of different map comparison methods will affect the evaluation of a model's accuracy. Our results reveal that the accuracy assessments of the BIOME4 simulations based on the Kappa statistic, Fuzzy Kappa and Nomad index agree well when the compared vegetation types consist of a large number of continuously distributed grid cells on both the simulated and observed maps. However, when the patterns of the simulated and observed biomes are similar but consist of a large number of grid cells that are not continuously distributed, the Nomad index tends to indicate better agreement than the Kappa or Fuzzy Kappa statistics because it stresses pattern agreement instead of location accuracy. In contrast, the Kappa statistic and Fuzzy Kappa are better suited for accuracy assessments that emphasize the location accuracy of the simulated vegetation. In addition, this study suggests that when using the Fuzzy Kappa to assess a model's simulated vegetation accuracy it is essential to consider the spatial resolution of the compared data. Our results indicate that a neighborhood radius of 1.0 and exponential decay function halving distance of 0.5 are good for data with a 0.5^{o} spatial resolution and that cover a broad area, largely because a larger radius increases the potential for underestimating a model's simulation accuracy by increasing the expected similarity between compared categories (Figure 3.7).

Bridge

As discussed in Chapter III, the accuracy assessment of model results is sensitive to the choice of map comparison approaches because different map comparison approach has different weakness and strength. Therefore, new approach that can address the weaknesses of existing comparison approaches is still needed for vegetation modeling and other applications that use spatial accuracy assessments. Chapter IV aims to develop a new metric for evaluating the correspondences of spatial patterns in vegetation models and to demonstrate its application.

CHAPTER IV

A NEW METRIC FOR EVALUATING THE CORRESPONDENCE OF SPATIAL PATTERNS IN VEGETATION MODELS

This chapter was published in 2008 in the journal "*Global Ecology and Biogeography*, volume 17, page 465-478".

Introduction

Vegetation models have been recognized as key analytical tools with high potential for investigating the spatiotemporal dynamics of ecological variables such as net primary productivity (NPP) and leaf area index (LAI) of forests (Cramer *et al.*, 1999). However, simulation results are often worth challenging because of: (i) uncertainties inherent in the models themselves, such as their structure, assumptions and parameterization (Allen *et al.*, 2001; Barrett *et al.*, 2001); (ii) the quality of input data used to run the models (Kickert *et al.*, 1999); and (iii) the inadequacy of vegetation models in simulating or incorporating all factors that may have important effects on vegetation. Therefore, model simulations must be tested for their ability to reproduce features of real vegetation. This can generally be done by analyzing the agreement between simulated and observed behaviors of terrestrial vegetation.

Large-scale spatial and long-term time-series data are often not available to validate simulation results. In addition, simulation results may vary substantially from one model to another. As a result, effective and efficient tools are critical for evaluating the agreement and differences between simulations, and between simulated and observed data. Such agreement analyses allow researchers to better understand model behavior, to assess the robustness of inferred mechanisms used to build the model, and to measure the sensitivity of particular variables (Kicklighter *et al.*, 1999; Bolliger *et al.*, 2000; Knorr & Heiman, 2001). They also allow researchers to weigh analytical results and to estimate

the predictive uncertainty of ecological dynamics (Kicklighter *et al.*, 1999). The Potsdam NPP Model Intercomparison Project (e.g. Cramer *et al.*, 1999; Kicklighter *et al.*, 1999) is one example of an attempt to survey agreement-related research on different model outputs.

The approaches for analyzing the agreement between two simulation results or between simulated and observed data can be broadly classified into two categories: the categorical-data and the continuous-data comparison approaches. The categorical-data comparison approaches, such as the Kappa statistic (Congalton & Green, 1999), Fuzzy Kappa (Hagen, 2003), Tau (Ma & Redmond, 1994), Kappa-for-location (Pontius, 2000) and the receiver (or relative) operating characteristic (ROC) technique (e.g. Pontius & Schneider, 2001; Luoto *et al.*, 2005), are used to quantify the agreement between two categorical datasets, such as the distribution patterns of simulated plant functional types or of species presence or absence. The continuous-data comparison approaches, such as correlation and regression analysis, root mean squared error (RMSE) (e.g. Murphy, 1988; Potts *et al.*, 1996), measures of absolute and relative error (e.g. Gordon *et al.*, 2004) and analysis of variance, are used to assess the correspondence between two continuous datasets, such as time-series dynamics of terrestrial NPP and LAI.

However, both categorical-data and continuous-data comparison approaches may be problematic in some cases. For example, the Kappa statistic lacks the ability to measure error magnitude (Congaltong, 1991; Foody, 2002) and tends to underestimate the overall similarity between two simulated spatial patterns of terrestrial vegetation (Foody, 1992). Fuzzy Kappa considers the grades of similarities between pairs of cells in two maps, but may underestimate the overall agreement between two maps by overestimating the expected similarity (Hagen, 2003; Hagen-Zanker *et al.*, 2005). The ROC technique has gained widespread use in evaluating ecological presence-absence models (e.g. Luoto *et al.*, 2005), but it is most suitable for maps with exactly two land-cover types (Fielding & Bell, 1997; Pontius & Schneider, 2001).

Like the categorical-data comparison approaches, correlation cannot determine whether two patterns have the same amplitude of variation, such as the difference in the

average anomalies of two datasets relative to their means (Taylor, 2001). It is also insensitive when the compared data differ by a constant factor (Murphy & Epstein, 1988; Storch & Zwiers, 1999). In addition, correlation and regression analyses are very sensitive to influential data and outliers (e.g. Belsley *et al.*, 1980), and thus are not always able to accurately quantify the agreement between two datasets. RMSE can be used to quantify the magnitude of the difference of variation between two datasets, but it is very sensitive to systematic errors because the penalty grows as the square of the error (Storch & Zwiers, 1999). Moreover, most statistics are based on the assumption that the values in two compared datasets are independent of one another. However, the research subjects of ecological modeling are often spatiotemporally autocorrelated. New approaches to analyzing the agreement between two simulation results are therefore essential in order to address these limitations.

This study presents a new cell-by-cell-based numerical approach, the "opposite and identity" (OI) index, to quantify the agreement between two simulation results or to evaluate simulation results against observed data. The study first introduces the geometry and definition of the OI index. A comparison of the OI index with the correlation coefficient highlights the similarity and dissimilarity of concepts underlying both approaches. A case study demonstrates the application of this method and the reliability of the OI index in quantifying the agreement between two simulated time-series NPP dynamics for Asia (ranging from 60.0°E to 150.0°E and from 8.0°N to 80.0°N) from 1982 to 2000; this demonstrates the utility of the OI index in model-related comparison and evaluation research.

The geometry and definition of the opposite and identity (OI) index

The geometry of the OI index

In math, vectors are used to conveniently denote physical quantities with both a magnitude and a direction (such as force). In the field of ecological modeling, the spatiotemporal dynamics of an ecological variable, such as terrestrial NPP, can be expressed as either an anomaly or as a ratio of change relative to its long-term mean. In a

sense, both anomaly and change ratio are direction- (positive or negative) and magnitude- (the amplitude of change) related quantities. Therefore, vectors can be used in the Cartesian plane to conveniently denote them. For example, the origin of the Cartesian plane can be used to represent both of the long-term means of an ecological variable derived from the two sets of the simulations or observations being compared. Thus, the vectors starting from the origin and on the y-axis, such as A1, A2, A3 and A4 (Figure 4.1a), can be used to denote a set of anomalies (or change ratios) from one simulation and those on the x-axis, such as B1, B2, B3 and B4 (Figure 4.1a), can be used to denote another set of anomalies from another simulation. The length of a vector represents the magnitude of an anomaly, and the direction of a vector indicates the positivity (if a vector is directed upward or rightward) or negativity (if a vector is directed downward or leftward) of an anomaly.

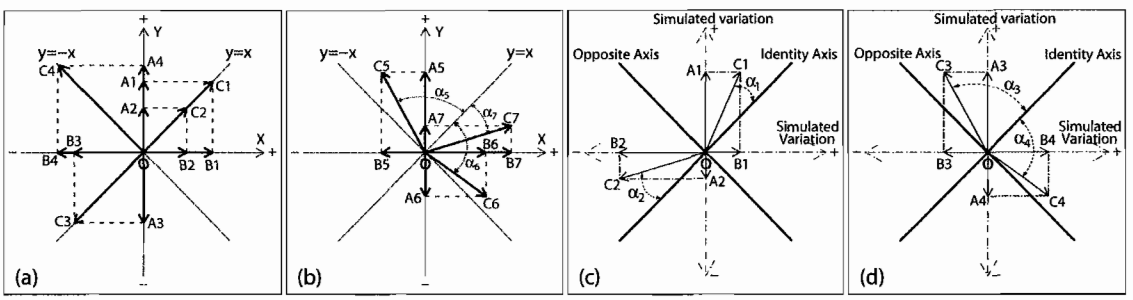

Figure 4.1 (a,b) Using pairs of vectors in the Cartesian plane, such as A1 vs. B1, A2 vs. B2, A3 vs. B3, A4 vs. B4, A5 vs. B5, A6 vs. B6, and A7 vs. B7, to denote compared time-series anomalies of an ecological variable. The length of a vector stands for the magnitude of an anomaly and its direction indicates the positivity (if upward or rightward) or negativity (if downward or leftward) of an anomaly. The vector C1, C2, C3, C4, C5, C6 and C7 are the corresponding vector sum, respectively. (c,d) The definitions of the identity axis and the opposite axis and their implications for comparing two simulation results. For any pair of vectors, such as A1 and B1 in (a), if the vector sum, such as C1, is on the line y=x (i.e. the defined identity axis), their magnitudes and directions are identical. In contrast, for any pair of vectors, such as A4 and B4 in (b), if the vector sum, such as C4, is on the line y=-x (i.e. the defined opposite axis), their magnitudes are the same but directions are opposite. In general, the size of the acute angle between the vector sum and the identity axis, such as α_1, α_2, α_3 and α_4 in (c) and (d), indicates the differences in both magnitudes and directions of compared anomalies.

If the direction and magnitude of any pair of compared vectors are the same (such as A1 vs. B1, A2 vs. B2, or A3 vs. B3), then the vector sum (such as C1, C2 and C3) is always on the line y= x (Figure 4.1a), which means that the compared anomalies of an ecological variable are identical. In this case, the variations of two simulation results are identical. On the other hand, if the direction or magnitude of any pair of compared vectors (such as A5 vs. B5, A6 vs. B6, or A7 vs. B7) is different, then their vector sum (such as C5, C6 and C7) will deviate from the line y= x at an angle (such as α_5, α_6 and α_7) between each of the resultant vectors and the line y= x (Figure 4.1b). The existence of such an angle implies that the variations of two simulation results are not identical. Likewise, when the direction of any pair of compared vectors are opposite but their magnitudes are the same (such as A4 vs. B4), the vector sum (such as C4) is always on the line y= -x (Figure 4.1a). This study defines the line y= x as the identity axis (i.e., the compared anomalies are identical) and the line y= -x as the opposite axis (i.e., the direction of the compared anomalies is opposite but the magnitude is identical) (Figure 4.1c & d).

In theory, the size of the acute angle between the vector sum and the defined identity axis reflects the difference between two simulation results at a given time or location. In particular, when the angle is less than 45.0° (such as α_1 and α_2 in Figure 4.1c), the two simulation results generally agree, largely because the direction of the compared anomalies is identical. In contrast, when the angle is greater than 45.0° (such as α_3 and α_4 in Figure 4.1d), the two simulation results do not agree well because the direction of the compared anomalies is opposite. The smaller the acute angle, the greater the agreement between the two simulation results.

The definition of the OI index

Assume that a and b refer to two sets of time-series simulations. Let vector $a_{i,j}$ and $b_{i,j}$ $(i = 1,2,\ldots,m;\ j = 1,2\ldots,n)$ be the simulated anomalies of an ecological variable in grid cell i at time step j, where m and n are the total numbers of grid cells and time steps respectively. Let $c_{i,j}$ be the vector sum of $a_{i,j}$ and $b_{i,j}$, and $\alpha_{i,j}$ be the acute angle

between the vector sum $c_{i,j}$ and the identity axis. Then, the opposite and identity (OI) index of the two simulation results in grid cell i and at all time is defined as:

$$OI_i = 1 - \theta_i / 90.0° \quad i = 1,2,\ldots,m \tag{1}$$

where $\theta_i = \tan^{-1}(\sum_{j=1}^{n}|c_{i,j}|\sin\alpha_{i,j} / \sum_{j=1}^{n}|c_{i,j}|\cos\alpha_{i,j})$. Correspondingly, the overall opposite and identity (OOI) index of the two simulation results in all grid cells and at all time is defined as:

$$OOI = 1 - \theta / 90.0° \tag{2}$$

where $\theta = \tan^{-1}(\sum_{i=1}^{m}\sum_{j=1}^{n}|c_{i,j}|\sin\alpha_{i,j} / \sum_{i=1}^{m}\sum_{j=1}^{n}|c_{i,j}|\cos\alpha_{i,j})$. The derivations of the OI and OOI indices (equations 1 and 2) are described in Appendix S1 (see Appendix A in Supplementary Material).

Comparison between the OI index and the correlation coefficient

The basic concepts underlying the OI index and Pearson correlation coefficient are somewhat similar, because both are based on the means of two datasets and the deviation of each value in the two datasets from these means. Taking the OOI index (see equation 2) as an example, let $a_{i,j}$ and $b_{i,j}$ be the deviations of $A_{i,j}$ and $B_{i,j}$ from the means of datasets A and B, respectively. Let point P (Figure 4.2a) be a random sample of the points ($a_{i,j}$, $b_{i,j}$) derived from datasets A and B. The coordinates of P are OL=$a_{i,j}$ and LP=$b_{i,j}$. Let the perpendicular distance PM be denoted by $d_{i,j}$, and the acute angle between OP and the line $b_{i,j} = a_{i,j}$ be denoted by $\alpha_{i,j}$. Thus (see Appendix B in Supplementary Material), the OOI index between A and B can also be expressed as:

$$OOI = 1 - \tan^{-1}(\sum_{i=1}^{m}\sum_{j=1}^{n}(b_{i,j} - a_{i,j}) / \sum_{i=1}^{m}\sum_{j=1}^{n}(b_{i,j} + a_{i,j}))/90.0° \tag{3}$$

According to Jackson (1924), the correlation (r) between A and B is mathematically expressed as:

$$r = \begin{cases} 1-(\sum_{i=1}^{m}\sum_{j=1}^{n}(b_{i,j}-a_{i,j})^2/(2m*n)) & a_{i,j}b_{i,j} \geq 0 \\ -1+(\sum_{i=1}^{m}\sum_{j=1}^{n}(b_{i,j}+a_{i,j})^2/(2m*n)) & a_{i,j}b_{i,j} < 0 \end{cases} \quad (4)$$

Equations 3 and 4 suggest that both the OOI index and the correlation reach their maximum value 1 when $b_{i,j}$ equals $a_{i,j}$. When the magnitudes of $b_{i,j}$ and $a_{i,j}$ are identical but their signs are opposite, the OOI index has its minimum value 0 and the correlation has the value -1. When the OOI index approaches 0.5, the correlation coefficient approaches zero. In addition, an OOI index near 0.5 suggests that the averaged deviations are large between the two compared simulations. In general, the OOI index varies from 0 to 1, and the correlation coefficient changes from -1 to 1 (Figure 4.2b). The OI index is also not a substitute for the square of correlation coefficient.

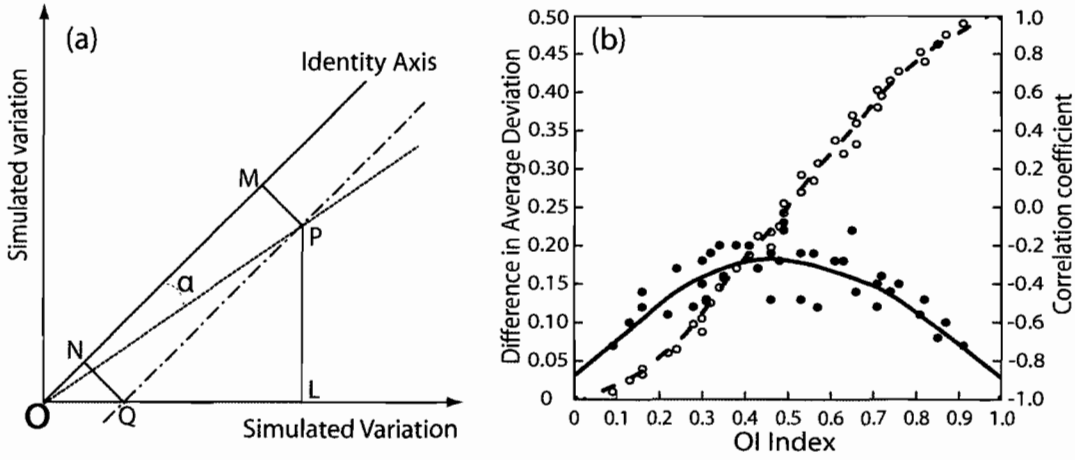

Figure 4.2 (a) For any point P, the OI index depends on the measure of the acute angle α and the correlation is associated with the perpendicular distance PM. (b) The relationship (as shown by the dashed line) between the OI index and the correlation, and the relationship (as shown by the solid black curve) between the OI index and the difference in the averaged deviations of two compared datasets from their corresponding means. Each data point in (b) is based on two sets of data points that are randomly created with values between 0 and 1. The total number of data points in each dataset is 16.

Although the basic concepts underlying the OI index and the correlation are similar, the two quantities are different from each other. Algebraically, correlation measures the direction and strength of the linear association between two datasets. The OI index, however, measures the directions and magnitudes of variations between two datasets. Geometrically, correlation is related to the perpendicular distance from one point to the identity axis, such as the PM in Figure 4.2a (Jackson, 1924). The OI index, on the other hand, depends on the acute angle between the vector sum and the identity axis, such as the α in Figure 4.2a. This study shows that correlation is more sensitive than the OI index to influential data or outliers from two datasets. In some cases, this allows the OI index to more accurately quantify the agreement between two datasets.

The resistance of the OI index to influential data or outliers from the two datasets X and Y (two randomly created sets of 50 data points) is illustrated in Figure 4.3. Figure 4.3a shows that X is strongly negatively correlated with Y ($r=-0.74$, $p<0.01$). In this case, the OI index is 0.22, which implies there is little agreement between X and Y. However, the addition of only two influential data points (the filled dark points in Figure 4.3b) increases the correlation coefficient by 0.74 to 0.0, indicating that X is no longer negatively correlated with Y. The OI index, on the other hand, only increases by 0.12 to 0.34, which still suggests that the agreement between X and Y is low. A similar situation occurs in Figure 4.3c and 4.3d. In Figure 4.3d, the addition of two influential data points (the filled dark points in Figure 4.3d) causes X to be no longer positively correlated with Y (as it is in Figure 4.3c). However, the OI index only decreases by 13% from 0.71 to 0.62, which still suggests a good agreement between X and Y. Under all four comparisons, the t-statistic ($-2.0<t<2.0$, $p>0.05$) between the means implies no significant difference between the means of any pair of compared datasets. The rating system for the OI index in quantifying the agreement between two datasets is described in Table 4.1. Like other statistics, such as Kappa statistic, the rating system for the OI index is more or less subjective and therefore could be adjusted in related research.

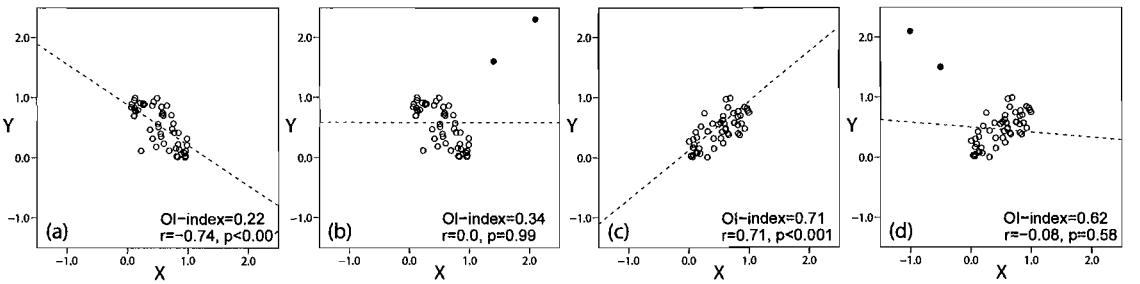

Figure 4.3 The OI index is more resistant to outliers or influential data from the two datasets X and Y (two randomly created sets of 50 data points) than are correlation and regression analysis. (a) Both the OI index and the correlation suggest a poor agreement between the dataset X and Y. (b) An addition of two influential data points (filled black points) to X and Y in (a), the correlation suggests that X and Y are no longer negatively correlated but the OI index still suggests a poor agreement. (c) Both the OI index and the correlation suggest a good agreement between the dataset X and Y. (d) An addition of two influential data points (filled black points) to X and Y in (c), the correlation suggests that X and Y are no longer positively correlated but the OI index still suggests a good agreement. The dashed line is fitted regression line.

Table 4.1 The rating systems for using the OI index to quantify the agreement between two datasets

OI index	Corresponding correlation	The meaning of the OI index		
		Changing direction	Changing magnitude	Agreement levels
0.7-1.0	0.6-1.0	Identical	Almost the same	Very good
0.6-0.7	0.3-0.6	Identical	No big difference	Good
0.5-0.6	0.0-0.3	Mostly identical	Big difference	Fair
0.4-0.5	-0.3 to 0.0	Mostly opposite	Big difference	Poor
0.3-0.4	-0.6 to -0.3	Opposite	No big difference	Worse
0.0-0.3	-1.0 to -0.6	Opposite	Almost the same	Worst

Changing direction suggests if the positivity (or negativity) of compared anomalies (or ratio changes) in most grid cells is identical or opposite. Changing magnitude measures the difference in the averaged anomalies (or ratio changes) between two compared datasets. The definition of the OI index levels and the corresponding ranges of the correlation, the meaning of changing direction and magnitude are based on their general relationship (see Figure 4.2b) and are also inferred from their mathematical expressions. The definition of agreement levels is based on the classifications of changing direction and magnitude.

A case study using the OI index

Two simulated time-series NPP dynamics in Asia

In order to demonstrate the applicability and reliability of the OI index, this study used the Lund-Potsdam-Jena (LPJ) dynamic global vegetation model (Sitch *et al.*, 2003; Gerten *et al.*, 2004) to simulate a set of Asian terrestrial NPP dynamics from 1982 to 2000. The study then derived another set of Asian terrestrial NPP dynamics for the same period from the Global Inventory Modeling and Mapping Studies (GIMMS) NDVI data (Pinzon, 2002; Tucker *et al.*, 2005) by following the Carnegie-Ames-Stanford Approach (CASA) (Potter & Klooster, 1999). The two approaches and the simulated and derived NPP dynamics for Asia are described in more detail in Tang and Bartlein (by personal communication).

Data required for estimating Asian terrestrial NPP dynamics

The climate data required to run the LPJ model include monthly mean temperature (°C), monthly mean precipitation (mm), monthly mean percent cloudiness (%) and monthly mean wet-day frequency (days). These data are based on a 0.5 degree geospatial resolution and come from the CRU TS 2.0 data sets developed by the Climate Research Unit (CRU) at the University of East Anglia (U.K.) (New *et al.*, 2000; Mitchell & Jones, 2005). The monthly mean temperature and monthly mean precipitation data from the CRU TS 2.0 are also used to calculate the temperature and water stress scalars required to derive NPP from NDVI. The soil data used in the LPJ model were obtained from the derived soil properties defined in the FAO world digital soil map (Food & Agriculture Organization, 1995). Annual CO_2 values needed to run LPJ for the years 1901-1998 were originally provided by the Carbon Cycle Model Linkage Project (Kicklighter *et al.*, 1995). The atmospheric CO_2 concentrations in 1999 and 2000 were set at the 367.7- and 369.0-ppm levels, respectively, by referencing other observations (e.g. Keeling *et al.*, 2002).

An additional set of Asian terrestrial NPP dynamics was derived using the GIMMS-NDVI monthly dataset for Asia with a spatial resolution of 0.5 degree for the years 1982-2000. This dataset provides a multi-year satellite record of monthly changes

in terrestrial vegetation (Pinzon, 2002; Tucker *et al.*, 2005). Grid cells missing the original NDVI data were excluded in the estimate of NPP dynamics. The ten LPJ-simulated plant functional types were selected as basic biomes to summarize the NDVI-derived NPP.

Simulating Asian terrestrial NPP dynamics by LPJ-DGVM

LPJ (Sitch *et al.*, 2003; Gerten *et al.*, 2004) combines process-based, large-scale representations of terrestrial vegetation dynamics and the exchanges of carbon and water between land and atmosphere. Ten plant functional types (PFTs) (Figure 4.4) are defined in LPJ by their physiological, morphological, phenological, bioclimatic and fire-response attributes. In LPJ, the vegetation type in a grid cell is determined by the dominant PFT, which has the largest fractional foliage coverage. The NPP of each PFT is calculated as the difference between its gross primary productivity and total respiration, and is updated monthly and annually. The LPJ simulation starts from unvegetated ground and 'spins up' for 1000 model years until approximate equilibrium is reached regarding the carbon pools and vegetation cover (Sitch *et al.*, 2003). LPJ has been used to examine terrestrial NPP dynamics at regional and global scales (e.g. Cowling & Shin, 2006).

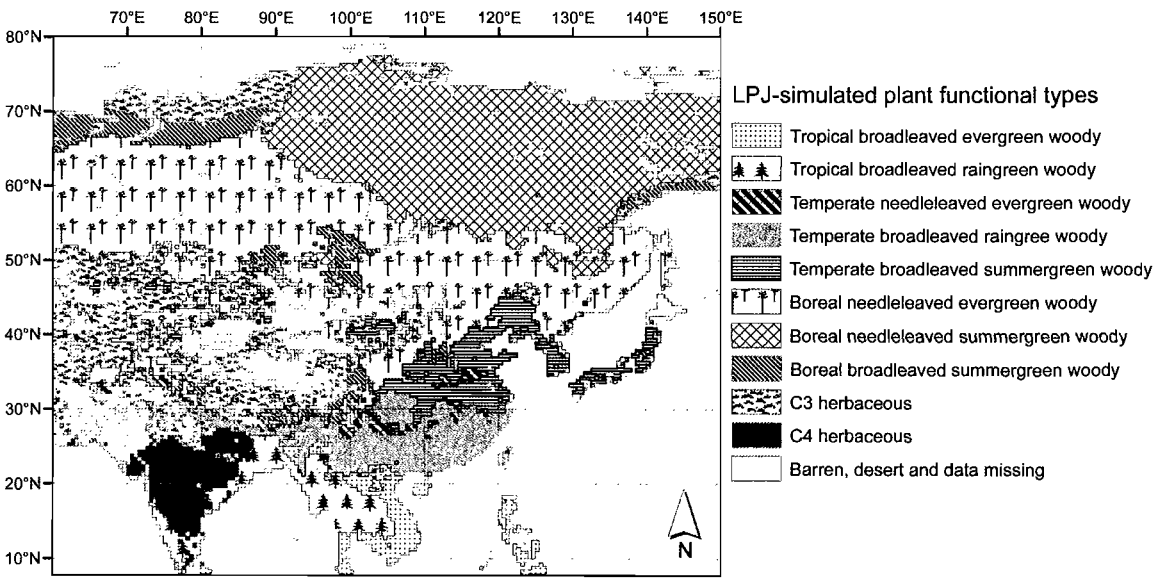

Figure 4.4 The spatial pattern of the 10 LPJ-simulated plant functional types (Sitch *et al.*, 2003) for Asia

Deriving Asian terrestrial NPP dynamics from NDVI data

In CASA, monthly NPP is calculated as the product of cloud-corrected solar irradiance (S) (Bishop & Rossow, 1991), fractional intercepted photosynthetically active radiation (*FPAR*) and a maximum light-use-efficiency term ($\varepsilon_{\max}$), adjusted by temperature and moisture stress scalars (T_s & W_s). The CASA approach is mathematically expressed as:

$$NPP = S \times FPAR \times \varepsilon_{\max} \times T_s \times W_s \tag{5}$$

where the estimation of FPAR at regional-to-global scales is based on a vegetation index derived from remotely sensed NDVI data and is calculated as a linear function of a NDVI-derived simple ratio (SR) as follows:

$$SR = (1 + NDVI)/(1 - NDVI) \tag{6}$$

$$FPAR = \min[(SR - SR_{\min})/(SR_{\max} - SR_{\min}),\quad 0.95] \tag{7}$$

where $SR_{\min}$ represents the *SR* for unvegetated land area. This study sets $SR_{\max}$ and $SR_{\min}$ in each grid cell as the approximate maximum and minimum NDVI-derived *SR* from 1982 to 2000, respectively.

The $\varepsilon_{\max}$ value for major biomes varies from one biome to another and is determined by local NPP inventory data (see Appendix C in Supplementary Material). In each basic biome, the monthly temperature stress scalar ($T_{(s,m)}$) is determined by the deviation of temperature from the low and high temperature limits for CO_2 uptake and by the optimum photosynthetic temperature as follows:

$$T_{(s,m)} = \begin{cases} 0.15 & if \quad T_m < T_{low} \quad or \quad T_m > T_{high} \\ (T_m - T_{low})/(T_{opt1} - T_{low}) & if \quad T_{low} \le T_m < T_{opt1} \\ (T_{high} - T_m)/(T_{high} - T_{opt2}) & if \quad T_{opt2} < T_m \le T_{high} \\ 0.95 & if \quad T_{opt1} \le T_m \le T_{opt2} \end{cases} \tag{8}$$

where T_m represents monthly mean temperature, T_{low} and T_{high} refer to the low and high temperature limits for CO_2 uptake, and T_{opt1} and T_{opt2} represent the lower and upper limits of the temperature range for optimum photosynthesis. The specific values of T_{low}, T_{high},

T_{opt1} and T_{opt2} for the basic biomes under study come from other research (e.g. Sitch *et al.*, 2003) (see Appendix D in Supplementary Material).

The monthly moisture stress value in each biome derives from a comparison of monthly estimated and potential evapotranspiration (EET & PET) (Potter *et al.*, 1999):

$$W_{(s,m)} = \min(0.5 + 0.5EET_m / PET_m, \quad 1.0) \tag{9}$$

The LPJ-simulated and NDVI-derived NPP estimates: basic results

The LPJ-simulated NPP estimates for Asia are similar to those derived by NDVI in most biomes (difference less than 10%). Both simulations suggest that the lowest annual mean NPP estimate occurs in C3 grasslands (from 154 to 300 gC m^{-2} $year^{-1}$), and that the highest annual mean NPP estimate occurs in tropical broadleaf evergreen forest (from 745 to 910 gC m^{-2} $year^{-1}$). Estimates of NPP decrease with increasing latitude in East Asia, as the climate shifts from tropical to temperate to boreal (Figure 4.5). In addition, estimates of NPP are relatively low in most of mid-latitude Asia, such as southern Mongolia, western China and the Tibetan Plateau, southeastern Pakistan and northwestern India, in which the dominant biomes are grasses. Estimates of NPP are higher in South Asia and the southeastern peninsula of Asia, where tropical forests are dominant. However, LPJ-simulated NPP estimates are more spatially homogenous within regions than NDVI-derived NPP estimates, which include human effects on terrestrial vegetation. In general, the two model-simulated NPP estimates resemble other model-based research such as BIOME3 (e.g. Ni *et al.*, 2001) and CASA (e.g. Potter *et al.*, 1999).

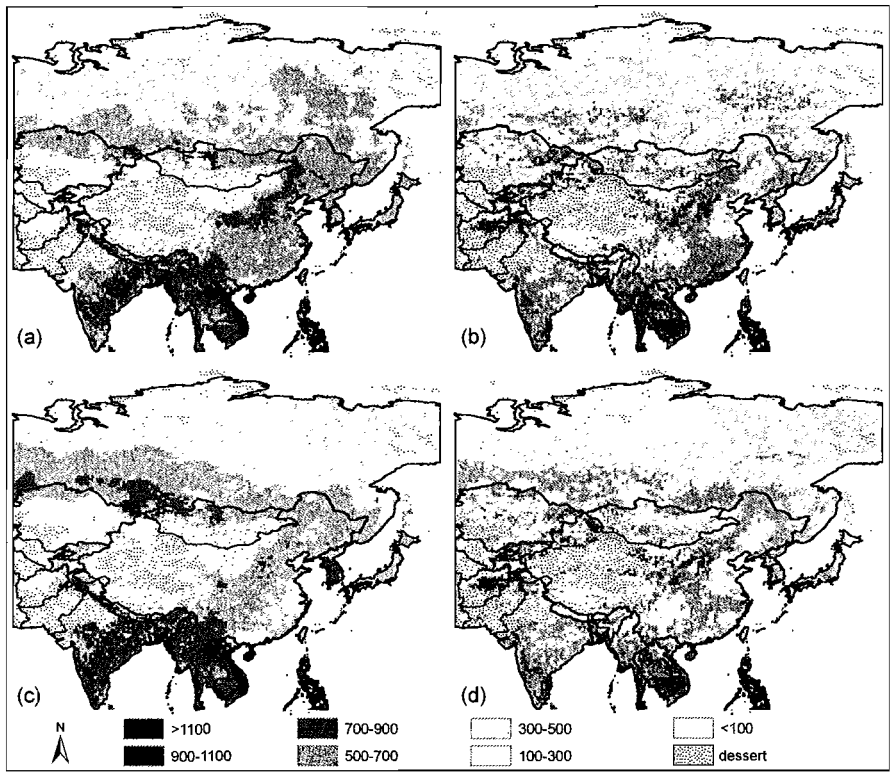

Figure 4.5 NPP values for the most similar (OI index=0.67) pattern of NPP estimates of 1990 by (a) the LPJ-simulation and (b) the NDVI-derivation; the most dissimilar (OI index=0.56) pattern of NPP estimates of 1997 by (c) the LPJ-simulation and (d) the NDVI-derivation. Annual NPP is measured in gC m^{-2} $year^{-1}$.

Quantifying the spatial agreement of NPP estimates

The OI indices calculated for each grid cell are used to map the spatial variations in the extent of agreement between LPJ-simulated and NDVI-derived NPP estimates (Figure 4.6a). To test the spatial agreement on the basis of OI indices, the correlation coefficients are used to create another map of spatial agreement of NPP estimates (Figure 4.6b). According to the grayscale of the map, the visual agreement is good between areas with an OI index larger than 0.5 (or smaller than 0.5) and areas with a correlation larger than 0 (or smaller than 0) (an OI index equal to 0.5 is equivalent to a correlation close to 0), which suggests the spatial pattern of agreement measured by the OI indices matches that measured by the correlation coefficients. After transforming all the OI indices and the correlation coefficients whose values are within a specific range specified for the

same agreement level (Table 4.1) into the same category for comparison, the calculated Kappa statistic for five levels of agreement, i.e., very good, good, fair, bad and worse, between that measured by the OI indices in Figure 4.6a and those measured by correlation coefficients in Figure 4.6b are 0.78, 0.59, 0.61, 0.71 and 0.67, respectively. This proves that the spatial pattern of agreement as measured by the OI index coincides with that measured by correlation. The overall pattern of agreement as measured by the OI index is also consistent with that measured by correlation (the overall Kappa statistic is 0.66).

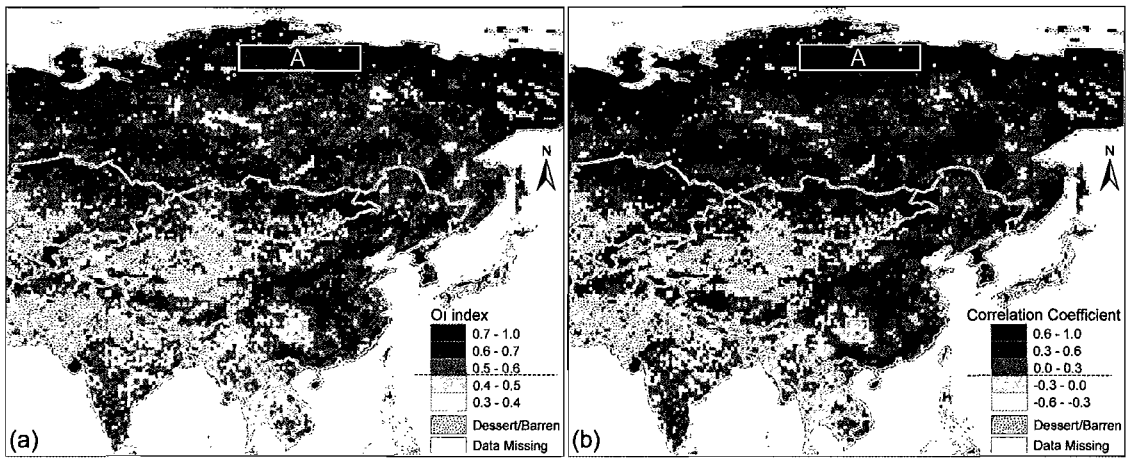

Figure 4.6 The spatial pattern of agreement between LPJ-simulated and NDVI-derived NPP variations from 1982 to 2000 in Asia measured by (a) the OI indices and (b) the correlation coefficients. Area A with high OI index and area B with low OI index are randomly selected for testing.

The spatial pattern of agreement as measured by the OI index allows researchers to pinpoint the extent to which compared variations between two simulations agree or disagree. To demonstrate this, an area with strong agreement (area A in Figure 4.6) and another with low agreement (area B in Figure 4.6) as suggested by the OI index were randomly selected for testing. According to the rating system for the OI index (Table 4.1), the high OI index (0.75) in area A suggests that the LPJ-simulated NPP dynamics agree well with the NDVI-derived dynamic; concordant with the strong correlation ($r=0.69$, $p<0.01$) between the two simulation results (Figure 4.7a). In addition, the grid

cells in which the direction of the LPJ-simulated NPP anomalies is the same as those derived from NDVI account for 69.6% out of 3021 compared grid cells. The difference of the average NPP anomalies between the two simulation results is less than 5.3%. The standard deviations of LPJ-simulated and NDVI-derived NPP estimates are 47.9 and 48.1, respectively. All these statistics illustrate that the LPJ-simulated NPP variation resembles that derived by NDVI in area A.

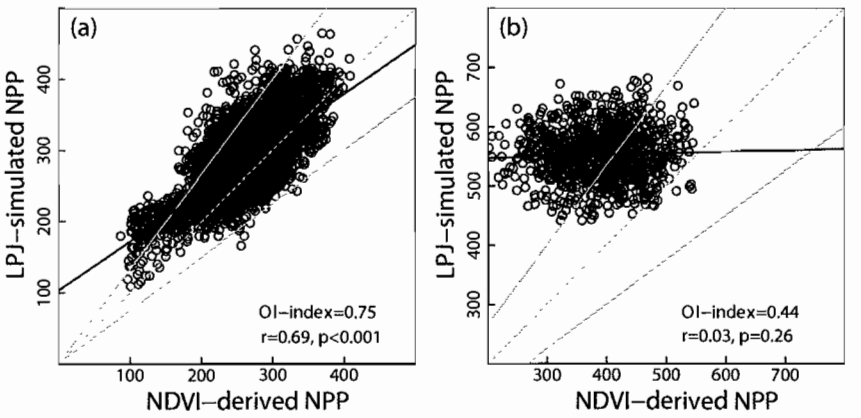

Figure 4.7 Comparisons of LPJ-simulated and NDVI-derived annual NPP estimates (gC m^{-2} $year^{-1}$) in two selected areas (a) A and (b) B in Figure 4.6. (a) Both the OI index and the correlation suggest a good agreement. (b) Both the OI index and the correlation suggest a poor agreement. The solid black line is fitted regression line. For points inside the region enclosed by the lower and upper solid grayish line, the absolute difference between two simulation results is less than 25%. The grid cells in area A and B are 3021 and 1654, respectively.

The low OI index (0.44) in area B, on the other hand, suggests that the LPJ-simulated NPP dynamics do not coincide with those derived by NDVI. The non-significant relationship (r=0.03, p=0.26) between LPJ-simulated and NDVI-derived annual NPP variation in area B (Figure 4.7b) can somewhat justify the agreement as measured by the OI index. Other statistics can further prove the rationality of the agreement as measured by the OI index. For example, the grid cells in which the direction of LPJ-simulated NPP anomalies is opposite to the NDVI-derived direction account for 48.8% out of 1654 compared cells in area B. The difference between the

average NPP anomalies between the two simulation results is as high as 35.9%, which indicates that the amplitude of LPJ-simulated NPP variation does not resemble that derived by NDVI (Figure 4.7b). The standard deviations of LPJ-simulated and NDVI-derived NPP estimates are 44.1 and 67.9 respectively, indicating that the LPJ-simulated NPP estimates are less variable than the NDVI-derived estimates.

The dominant biome types in areas A and B are boreal needleleaved summergreen woody PFT (BoBS) and temperate broadleaved raingreen woody PFT (TeBR), respectively (Figures 4.4 & 4.6a). Compared to area A, which is located in uppermost northern Russia and has little human activity, area B is located in the Yungui Plateau of China, which is characterized by a high level of human social and economic activity. Unlike the LPJ simulation, which depends largely on input climate and soil data without considering human effects on terrestrial vegetation, the NDVI derivation involves direct observations of the spatiotemporal dynamics of terrestrial vegetation shaped by human activities, such as land-use change. Therefore, the spatial homogeneity of climate and NDVI data used to run both models contributes to the strong agreement between the two simulation results in BoBS as confirmed by other model-based intercomparison research (e.g. Cramer *et al.*, 1999; Kicklighter *et al.*, 1999). The effects of human activities on terrestrial vegetation help explain why the NDVI-derived NPP estimates are apparently smaller than the LPJ-simulated estimates in area B (Figure 4.7b). For example, Fang *et al.* (2003) and Piao *et al.* (2003) argued that terrestrial NPP decreased in areas of China that experienced rapid urbanization.

Quantifying the agreement of NPP estimates in a given biome

The OOI index calculated from equation 2 can be used to quantify the agreement between two simulation results in a given biome or for the overall simulated vegetation. For example, the calculated OI index in tropical broadleaved raingreen woody PFT (TrBR) is 0.51 (Table 4.2), which suggests that there is some agreement between LPJ-simulated and NDVI-derived NPP dynamics in TrBR. The negative relationship ($r=-0.21$, $p<0.01$) based on 10,556 compared cells also reveals that the two simulation results do

not coincide; this is illustrated by the standardized annual NPP variations from 1982 to 2000 (Figure 4.8), in which the direction of LPJ-simulated NPP anomalies are clearly opposite those derived by NDVI in the years of 1984, 1988, 1989, 1992, 1997 and 2000. In addition, the value of the OI index (close to 0.5) implies that the difference in the amplitudes of variations between the two simulations is large. The difference of the average NPP anomalies between the two simulation results is relatively large (Table 4.2), which confirms the difference in the amplitudes of LPJ-simulated NPP variation and NDVI-derived data.

Table 4.2 Using the OI index to measure the agreement between LPJ-simulated and NDVI-derived NPP estimates for the 10 LPJ-simulated plant functional types in Asia and its approving by other statistics.

PFTs	OI index	Correlation coefficient	AveDev1 (LPJ)	AveDev2 (NDVI)	ΔDev (absolute)	RMSE	NPP (LPJ)	NPP (NDVI)
TrBE	0.51	-0.17	49.0	71.5	22.5	276.7	909.7	744.7
TrBR	0.51	-0.21	44.2	58.3	14.1	188.2	710.6	689.4
TeNE	0.55	0.44	45.4	48.5	3.1	324.9	458.9	434.9
TeBE	0.53	0.34	58.3	47.1	11.2	238.7	560.4	504.1
TeBS	0.59	0.62	45.6	47.3	1.7	248.6	455.4	419.4
BoNE	0.61	0.57	47.6	56.5	8.9	226.6	458.9	464.7
BoNS	0.67	0.79	33.0	39.0	6.0	85.4	357.5	304.5
BoBS	0.69	0.82	47.2	45.8	1.4	120.4	345.8	355.6
TeH	0.59	0.60	48.4	44.5	3.9	264.7	153.7	300.7
TrH	0.54	0.12	112.3	60.3	52.0	285.4	641.5	554.9
Overall	0.60	0.53						

Annual NPP (net primary productivity) is measured in gC m^{-2} $year^{-1}$. AveDev is short for 'Average NPP deviations from the 19-year mean' calculated at grid cell level. LPJ refers to the Lund-Potsdam-Jena dynamic global vegetation model. NDVI is normalized difference vegetation index. ΔDev is the absolute difference between two average NPP deviations. RMSE stands for 'Root Mean Squared Error'. The full name of each plant functional type (PFT) is as follows: TrBR—Tropical broadleaved evergreen woody PFT; TrBR—tropical boradleaved raingreen woody PFT; TeNE—Temperate needleleaved evergreen woody PFT; TeBE—temperate broadleaved evergreen woody PFT; TeBS—Temperate broadleaved summergreen woody PFT; BoNE—Boreal needleleaved evergreen woody PFT; BoNS—boreal needleleaved summergreen woody PFT; BoBS—boreal broadleaved summergreen woody PFT; TeH—C3 herbaceous; TrH—C4 herbaceous (see Sitch *et al.*, 2003).

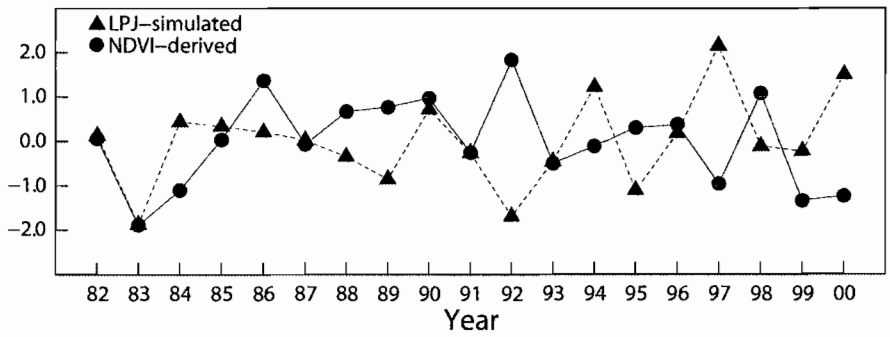

Figure 4.8 The standardized annual NPP variation in tropical broadleaved raingreen woody PFT from 1982 to 2000.

The dissimilarity between LPJ-simulated and NDVI-derived NPP dynamics in TrBR is caused primarily by the input data used to run LPJ and to derive NPP from NDVI. The LPJ-simulated TrBR is mainly distributed in the southeastern peninsula of Asia, in places such as Thailand, Cambodia and part of India (Figure 4.4). Compared to the climate and soil data used to run LPJ, the NDVI data used to derive NPP estimates are more spatially heterogeneous because of the direct effects of human activities on terrestrial vegetation and the complexity of topography. As a result, the NDVI-derived NPP estimates are more spatially heterogeneous than the LPJ-simulated results (Figure 4.5). For example, the calculated Moran statistics based on the four nearest neighbors algorithm for 567 compared cells show that the LPJ-simulated NPP estimates in 2000 ($I=0.81$, $p<0.01$) are more spatially autocorrelated than those derived by NDVI ($I=0.67$, $p<0.01$).

Quantifying the agreement of NPP estimates at a given time

Keeping the time dimension variable (see Appendix S1 in Supplementary Material) allows the OOI index to be used to analyze the agreement between two simulation results at a given time (e.g. Figure 4.9a & b). For example, the calculated OI index is high (0.75) for the simulation of 1989 in BoBS (Figure 4.9b), suggesting that the LPJ-simulated NPP estimates agree well with the NDVI-derived estimates in this year. Table 4.3 shows that the LPJ-simulated annual mean NPP and average NPP anomaly approximately equal those derived by NDVI. In addition, given that there are 672

compared grid cells and that the annual mean NPP is as high as 348, the relatively low RMSE (95.8) suggests that the two simulation results in 1989 are largely similar. The regression analysis robustly proves that the LPJ-simulated NPP estimates in 1989 are strongly linearly correlated with the NDVI-derived estimates ($r=0.69$, $p<0.01$) (Figure 4.10). The agreement between two model-simulated NPP estimates in 1989 may be due to: (i) the spatial homogeneity of the climate data, especially that of temperature, which may be the dominant factor controlling NPP dynamics in boreal forests, and NDVI data used to run two models; and (ii) the BoBS not being strongly influenced by human activities.

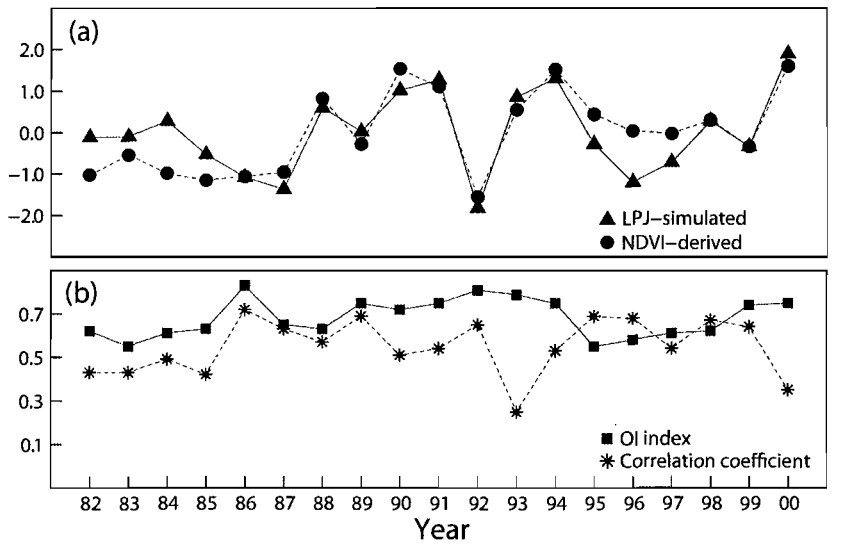

Figure 4.9 (a) The standardized annual NPP variation in boreal broadleaved summergreen woody PFT (BoBS) from 1982 to 2000. (b) The OI index and the correlation calculated for each year's simulation in TrBR. Note: the OI index for each year's simulation is based on the acute angle between the summation of all anomalies (each of them is treated as a vector) at all grid cells of BoBS. Standardizing annual NPP estimates in a year may bias the real relationship between two simulated NPP estimates, which helps explain why the standardized annual NPP variations in 1984 and 1995 appear to be opposite between two simulations but the corresponding OI indices are above 0.5.

Table 4.3 Comparison between LPJ-simulated and NDVI-derived annual NPP estimates in 1989 and 1993 in boreal broadleaved summergreen woody PFT.

	1989		1993	
Statistics	LPJ	NDVI	LPJ	NDVI
OI index	0.75		0.79	
Correlation coefficient	0.48		0.06	
Compared cells	672		695	
Common cells	514		587	
Percentage of common cells	76.5		84.5	
Annual mean NPP	348.3	348.6	369.2	369.1
Annual NPP difference	0.08%		0.02%	
Average NPP anomaly	48.4	43.8	62.9	66.9
Anomaly difference	10.5%		6.0%	
Root mean squared error	95.8		126.7	

LPJ refers to the Lund-Potsdam-Jena dynamic global vegetation model. NDVI is normalized difference vegetation index. Common cells are the number of cells in which the positivity or negativity of compared NPP (net primary productivity) anomalies is identical. Percent of common cells is the ratio of common cells to all compared cells. Annual NPP difference and anomaly difference are in reference to the NDVI-derived values. Annual mean NPP and average NPP anomaly are measured in gC m^{-2} $year^{-1}$.

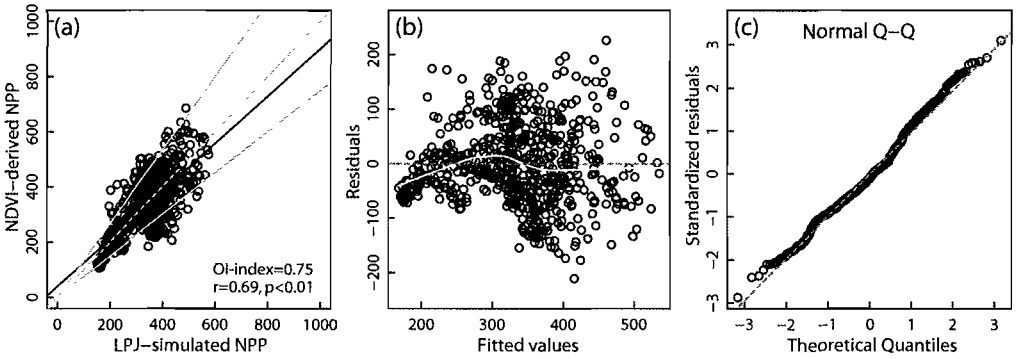

Figure 4.10 Comparison between LPJ-simulated and NDVI-derived NPP estimates in boreal broadleaved summergreen woody PFT in 1989. The number of compared grid cells is 672. The solid black line in (a) is fitted regression line. For points inside the region enclosed by the lower and upper solid grayish line, the difference between two simulation results is less than 25%. The grayish solid line in (b) is fitted loess curve.

Accurately quantifying the agreement between two simulated NPP estimates

The resistance of the OI index to influential data and outliers is important in model-related comparison and evaluation research. For example, linear regression shows

that LPJ-simulated NPP estimates are not strongly correlated with NDVI-derived ones in 1993 in BoBS (r=0.24, p<0.01) (Figure 4.11a, b & c). However, the OI index is as high as 0.79, indicating that the two simulation results agree well in this year as illustrated by the standardized annual NPP variation (Figure 4.9a). The OI index-measured agreement is consistent with that suggested by other statistics (Table 4.3).

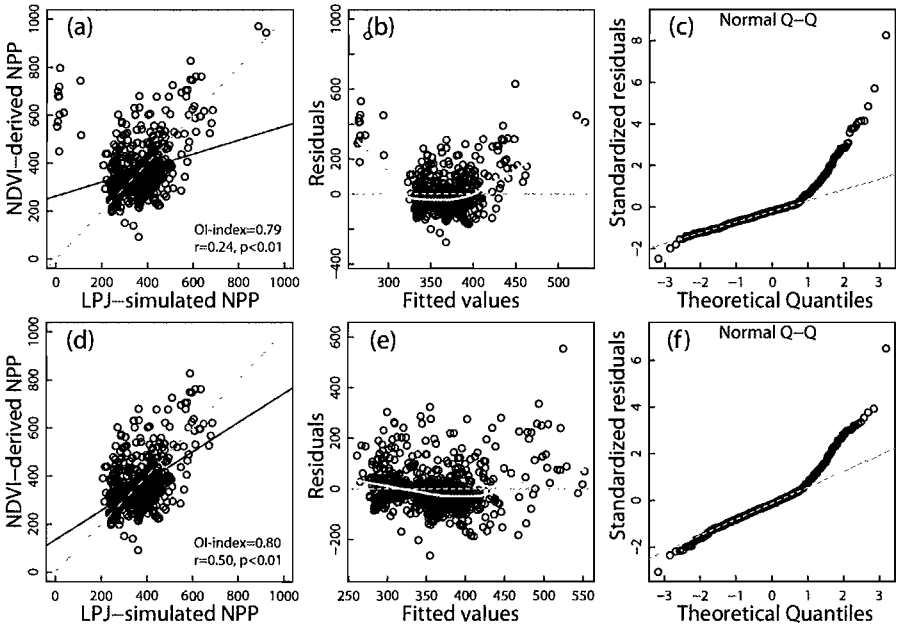

Figure 4.11 The linear regression analysis may bias the real agreement between two simulation results in 1993 in boreal broadleaved summergreen woody PFT. (a) Without leaving out some influential points and outliers in two compared simulations (695 compared cells), the linear relationship is low (r=0.24, p<0.01) as illustrated in (b) and (c). (d) After leaving out 13 cells, the linear relationship is greatly improved (r=0.50, p<0.01). Under both comparisons, however, the OI index (above 0.70) consistently suggests a good agreement between two simulation results. The solid black line in (a) and (d) is fitted regression line and the grayish solid line in (b) and (e) is fitted loess curve.

The failure of the regression to correctly quantify two simulation results in 1993 results from its sensitivity to influential simulations and outliers in the two compared simulations. A plot of LPJ-simulated against NDVI-derived annual NPP estimates (Figure 4.11a) shows that there are influential outliers as illustrated by the residual (Figure 4.11b) and Normal Q-Q plots (Figure 4.11c). These outliers indicate either that

the two simulation results are distinct from each other or that the results of the two simulations deviate from the major overall pattern of NPP estimates in some grid cells. Consequently, the agreement measured based on regression analysis differs from the results of the OI index and other statistics. In fact, after leaving out some influential simulations and outliers (13 out of 695 compared cells), the linear association between the two model simulations is greatly improved ($r=0.50$, $p<0.01$) (Figure 4.11d, e & f).

Conclusion

This study created and introduced a novel cell-by-cell-based numerical approach, the "opposite and identity" (OI) index, intended to quantify the agreement between two simulation results or to evaluate simulation results against observed spatiotemporal data. The OI index is built on the vector addition rule and is a novel cell-by-cell-based numerical comparison approach. By comparing the directions and magnitudes of variations of two datasets, the results reveal the following.

(1) The OI index provides an intuitive measure of agreement between two simulated variations of an ecological variable. The suggested rating system of the OI index is straightforward and easy to use. Like other numerical comparison approaches, the OI index can be used not only to analyse the agreement between two simulated spatiotemporal dynamics of ecological variables, but also has potential for evaluating simulation results when observed data are available.

(2) The OI index provides researchers with multiple and flexible ways to analyze the agreement of two simulation results. The OI indices calculated in each grid cell can be used to map the spatial agreement of variations between two simulation results, allowing researchers to pinpoint the extent to which two simulation results agree or disagree. The OI indices calculated for time-series simulations allow researchers to analyze why two simulation results agree more at one time but less at another, which is important for improving model's structure. The OI index can also be calculated for different biomes, allowing researcher to examine why two simulations are good in one

biome but poor in another, which is useful for analyzing the sensitivity of model simulations to the input data used to run the model.

(3) This study shows that the OI index is more resistant to influential data and outliers of two datasets than are correlation and regression analysis. In practice, because of the difference in input data and model structure, two simulation results may be similar in most grid cells but distinct in just a few. These few outliers can unduly influence the measurement of agreement in correlation and regression analysis, resulting in a biased measurement of agreement. In addition, because the target of ecological modeling is often spatiotemporally autocorrelated with simulated values that are spatially clustered in a scatter plot, the agreement measurement based on correlation and regression analyses can also be biased because the underlying assumptions are violated, stressing the linear association but overlooking the difference in the magnitudes of variations in two simulation results.

(4) The calculation of the OI index requires that two compared datasets be time-series data with the length of time steps greater than 1. The longer the time steps in two compared datasets, the better the performance of the OI index in evaluating the agreement of variations in two compared datasets. Like the correlation, the OI index should not be used to measure the difference in the absolute magnitudes of values in two compared datasets, largely because it is based on the means of two datasets and the deviation of each value in the two datasets from these means.

Bridge

So far, Chapter III has examined the sensitivity of vegetation model simulation to input data, to observed validation data and to map comparison approach, and Chapter IV developed a new metric for comparing two simulation results or evaluating model results against observed data, which are two goals of this dissertation. The foci of Chapter V and VI are on analyzing the climate sensitivity of terrestrial NPP, soil moisture and actual evapotranspiration in China, which are another two goals of this dissertation.

CHAPTER V

VARIATION AND CLIMATE SENSITIVITY OF TERRESTRIAL NET PRIMARY PRODUCTIVITY IN CHINA DERIVED FROM SATELLITE-BASED NDVI DATA

This chapter contains unpublished coauthored material with Patrick J. Bartlein (Department of Geography, University of Oregon). It is intended for submission as an article to a journal like "Climatic Change". Guoping Tang prepared the first draft of manuscript and Patrick J. Bartlein edited the paper and provided guidance and comments on the paper.

Introduction

The net primary productivity (NPP) of terrestrial vegetation has been the subject of considerable research over the past several decades because of its important role in the global carbon cycle and in ecosystem processes (Raich *et al.* 1991; Fang *et al.* 2003; Chen *et al.* 2004). As a key component of terrestrial carbon cycle, NPP provides the basic energy source for the growth and maintenance of most organisms (Wang *et al.* 2003), and forms an important link between the biosphere and atmosphere, which has profound influences on water fluxes, nutrient cycles and climate variation (Prentice *et al.* 2000). Terrestrial NPP varies spatially and temporally because the rates of photosynthesis and respiration of plants are sensitive to changes in environmental conditions caused by both natural and human activities (Jenkins *et al.* 1999). Study of the spatio-temporal pattern of terrestrial NPP is therefore pivotal for understanding the feedbacks between climate systems and terrestrial ecosystems (Potter *et al.* 1998; Piao *et al.* 2003) and the sustainable human utilization of the global biosphere (Schellnhuber *et al.* 2006).

Because the distribution and variation of terrestrial NPP cannot be observed directly at the regional or global scales (Cramer *et al.* 1999), forest-inventory data, satellite-based

vegetation indices and results from vegetation modeling (e.g. dynamic global vegetation model (DGVM)-based simulations) are typically used to analyse the large-scale dynamics of terrestrial NPP. Forest-inventory data can be used estimate forest NPP and carbon budget at landscape and regional scales (Luo *et al.* 2002; Ni, 2004; Zhao and Zhou, 2006). However, such data are often limited and do not describe fine-grained spatial variation of terrestrial vegetation, and must be interpolated to describe large-scale patterns of NPP. Satellite-based vegetation index, such as Normalized Difference Vegetation Index (NDVI) data, can be incorporated into light-use efficiency models such as LULUE (Brogaard *et al.* 2005) to estimate the spatio-temporal dynamics of terrestrial NPP over large areas (Clein *et al.* 2002; Markon and Peterson, 2002; Dawson *et al.* 2003). However, such estimates of NPP are often based on an empirical relationship between NPP and other environmental factors, such as fractional intercepted photosynthetically active radiation (Jenkins *et al.* 2001; Nabuurs *et al.* 2003), which themselves must be estimated, and the data are necessarily limited by the length of the satellite record. Vegetation models such as BIOME-BGC (Running and Coughlan, 1988), BIOME4 (Kaplan *et al.* 2002), CENTURY (Parton *et al.* 1987), LPJ (Lucht *et al.* 2002; Sitch *et al.* 2003), and MC1 (Daly *et al.* 2000), include mechanistic representations of the processes of ecosystem carbon cycle variations and their dynamic responses to environmental alterations and therefore are capable of quantifying NPP (Cramer *et al.* 2001), but do not explicitly consider anthropogenic land-cover changes. Consequently, there is no single approach that may be optimal for describing the temporal and spatial variations of NPP.

Unlike forest-inventory NPP data, which are a direct measure of forest NPP in the field, both NDVI-derived and DGVM-simulated NPP estimates involve the use of some kind of a model and of observed climate data. However, they are different in some aspects. For example, NDVI-derived NPP estimates are often based on the empirical relationship between NPP and satellite-based NDVI data, but also use direct observations of spatio-temporal variation in terrestrial vegetation. In contrast, the DGVM-simulated NPP estimates are based on the parameterizations of some mechanistic processes of terrestrial vegetation, and the model simulations may require only climate, soil and other environmental data (e.g. CO_2), and thus some spatio-temporal variations in terrestrial vegetation (e.g. human-induced land cover change) are not simulated.

Several studies have examined the spatio-temporal dynamics of terrestrial NPP in China using forest-inventory data (e.g. Luo *et al.* 2002; Ni, 2004; Zhao and Zhou, 2006), satellite-based NDVI data (e.g. Fang *et al.* 2003; Brogaard *et al.* 2005; Piao *et al.* 2003, 2005), and vegetation models (e.g. Cao *et al.* 2003, 2004; Ni, 2000; Fang *et al.* 2003). However, uncertainty may still exist in the estimates of NPP dynamics in China because of: (i) limitations inherent in vegetation models (e.g. the parameterization of physiological, biological and biogeochemical processes of plants); (ii) the quality of input data used to run a model (e.g. the quality of NDVI and climate data); and (iii) the spatio-temporal scale or resolution of analytical data (e.g. scaling-up local forest-inventory data to estimate NPP dynamics at the regional scale may ignore the heterogeneity of environmental conditions at different locations). To address these limitations, additional and novel research is necessary for accurate quantification of the spatio-temporal pattern of terrestrial NPP in China.

Climate in China can be generalized into three zones: the eastern monsoon zone, the north-west arid zone and the Tibetan Plateau frigid zone. The corresponding dominant vegetation in each climatic zone is forest, grass steppe and alpine tundra respectively. Because the attribute and variation of temperature and precipitation are considered two major factors for controlling the dynamics of terrestrial NPP in China (Ni *et al.* 2001; Cao *et al.* 2003; Kimball *et al.* 2003; Piao *et al.* 2006), the spatio-temporal pattern of NPP across different locations should be relatively homogenous within each climate zone, while differing across climate zones because of the difference in prevailing climate among each zone.

The goals of this study are: (i) to analyse the interannual and seasonal variation of terrestrial NPP in China over the years 1982-2000, and (ii) to examine climatic (temperature and precipitation) controls on the dynamics of NPP in each climatic zone of China. Toward these ends, we first used satellite-based NDVI data to derive a set of terrestrial NPP dynamics in China over the years 1982-2000. Then, we employed a DGVM to simulate another set of NPP dynamics with the same spatio-temporal resolution for comparing with the NDVI-derived NPP dynamics. Finally, the variability and climate sensitivity of terrestrial NPP in each climate zone are examined based on the NDVI-derived NPP estimates and the observed temperature and precipitation variation.

The first approach uses direct observation of vegetation, but relies on empirical correlations with climate to illustrate the sensitivity of NPP to climate variations. In contrast,

the second approach uses mechanistic approaches to simulate NPP using observed climate data, but those data do not include the direct effects of land-use and land-cover change on terrestrial NPP.

Material and Methods

The basic biomes used to summarize the NPP estimates

The biomes classified in the Potential Natural Vegetation (PNV) data (Ramankutty and Foley, 1999) are used to describe the basic biomes for China. The gridded global PNV data are classified into 15 biome types, of which ten occur in China (Figure 5.1a). These biome types fall into three main categories: forests (including tropical, temperate and mixed forests), grassland (including grass and savanna) and tundra, with spatial distribution patterns that largely agree with the three general climate zones in China, i.e. the eastern monsoon zone (Area A in Figure 5.1a), the north-west arid zone (Area B in Figure 5.1a) and the Tibetan Plateau frigid zone (Area C in Figure 5.1a). Moreover, the biome types classified in the PNV data match well with the ten plant functional types specified in the Lund-Potsdam-Jena global dynamic vegetation model (LPJ-DGVM). Consequently, the DGVM-simulated NPP variations can be used to compare with the NDVI-derived NPP dynamics.

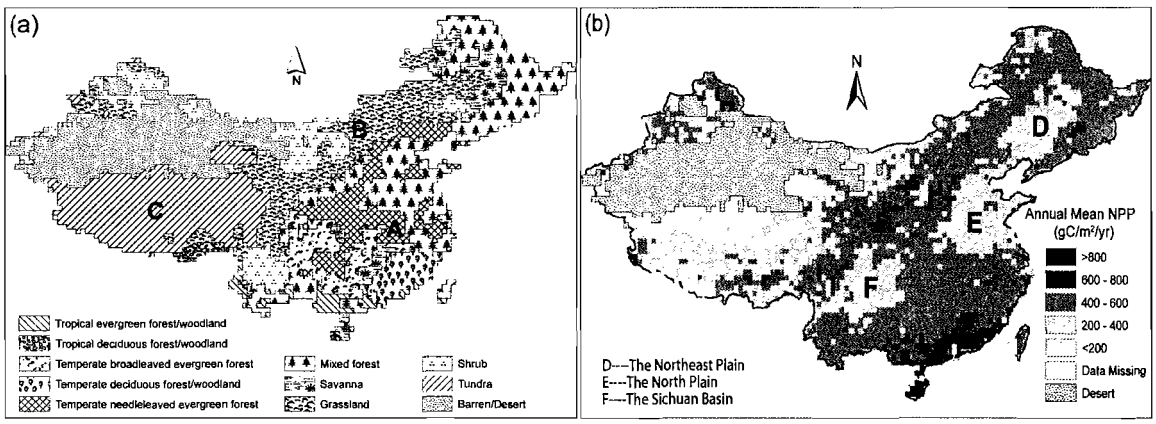

Figure 5.1 (a): the basic biomes for China derived from the PNV data (Ramankutty and Foley, 1999). The spatial resolution of PNV data used in this study is 0.5°. The areas A, B and C approximate the eastern monsoon zone, the north-west arid zone and the Tibetan Plateau frigid zone respectively. (b): The spatial pattern of annual mean NPP over the years 1982-2000 in China derived from NDVI data.

To examine the variation and climate sensitivity of terrestrial NPP in China, we will aggregate the NDVI-derived NPP into four biomes: forests, grassland, shrub, and tundra. We did not combine shrub with forests because shrubs are common in the north-west arid zone dominated by grass (Figure 5.1a). The inclusion of shrub into forests would therefore be likely to affect the accuracy of the climate-sensitivity analysis. In addition, aggregating NPP into four biomes rather than ten will greatly simplify the analysis of interannual and seasonal variability of NPP in China under historical climatic variation.

The climate and NDVI data used to run the models

The input climatology data used in this study to derive NPP from NDVI and to run the LPJ-DGVM come from the CRU TS 2.0 data sets developed by Climate Research Unit (CRU), University of East Anglia (U.K.). The CRU TS 2.0 data sets are supplied on a 0.5-degree global land grid at a monthly time-step for 1901-2000, and build upon several previously gridded data sets created by the CRU (New *et al.* 2000; Mitchell and Jones, 2005). Monthly mean temperature (°C) and precipitation (mm) from the CRU TS 2.0 data sets are used to estimate the temperature and water stress scalars required to derive NPP from NDVI. In addition to monthly mean temperature and precipitation, other climate data from the CRU TS 2.0 data sets required to run the LPJ-DGVM include monthly mean percent cloudiness (%), and monthly wet-day frequency (days). The soil data used to run the LPJ-DGVM were obtained from the derived soil properties defined in the FAO digital soil map of the world (Food and Agriculture Organization, 1995). Annual CO_2 values to run the LPJ-DGVM for the period of 1901 to 1998 were originally provided by Carbon Cycle Model Linkage Project (Kicklighter *et al.* 1995). For 1999 and 2000, the CO_2 concentration is set at 367.70 and 369.00-ppm level respectively by referencing other observations (e.g. Keeling *et al.* 2002).

The GIMMS (Global Inventory Modeling and Mapping Studies) NDVI data sets for China at a monthly time-step for the period of 1982 to 2000 are used to derive terrestrial NPP dynamics in each of basic biomes at the same time-series scale. These data sets provide a multi-year satellite record of monthly changes in terrestrial vegetation. New features of these data sets include reduced NDVI variations arising from calibration, view geometry, volcanic aerosols, and other effects not related to actual vegetation change (Pinzon, 2002; Tucker *et al.* 2005). The spatial resolution of GIMMS NDVI data used in this study is 0.5°. For the

grid cells in which the NDVI data were missing due to high solar zenith angle or other factors in the original GIMMS-derived NDVI data will be excluded in the estimate of NPP dynamics.

Estimates of NPP variation from NDVI data

Estimates of NPP from NDVI data in each biome under study follow the logic of the CASA model (Carnegie-Ames-Stanford Approach) (Potter and Klosster, 1999). Monthly NPP in CASA is calculated as a product of cloud-corrected solar irradiance (S) (Bishop and Rossow, 1991), fractional intercepted photosynthetically active radiation (*FPAR*), and a maximum light-use-efficiency term ($\varepsilon_{\max}$), which is adjusted by temperature- and moisture-stress scalars (T_s and W_s). The CASA approach is expressed in the following equation:

$$NPP = S \times FPAR \times \varepsilon_{\max} \times T_s \times W_s \quad (1)$$

The estimation of FPAR at regional-to-global scales is based on a vegetation index derived from remotely sensed NDVI data and is calculated as a linear function of the NDVI-derived simple ratio (*SR*) as follows:

$$SR = (1 + NDVI)/(1 - NDVI) \quad (2)$$

where $SR_{\min}$ represents *SR* for unvegetated land area. In this study, the $SR_{\max}$ and $SR_{\min}$ for each grid cell approximate the maximum and minimum NDVI-derived simple ratio *SR* over the period of 1982 to 2000 respectively. *FPAR* is then estimated as:

$$FPAR = \min[(SR - SR_{\min})/(SR_{\max} - SR_{\min}), \quad 0.95] \quad (3)$$

The $\varepsilon_{\max}$ value in major biomes under study is determined by local NPP inventory data (Table 5.1). For shrub and tundra, the $\varepsilon_{\max}$ is set as 0.56 as in other research (e.g. Potter *et al.* 1999). In theory, the value of $\varepsilon_{\max}$ has no influence on the NPP trend analysis if the trend analysis is based on NPP anomalies or percentage variations.

Table 5.1 Description of selected NPP inventory data for determining the ε_{max} of biomes under study

Biome types	NPP inventory data	Location	Data description	ε_{max}
Tropical forests	Zheng *et al.* (2003)	Asia	NPP data for multi-biomes	0.67
Temperate forests	Zheng *et al.* (2003)	Asia	NPP data for multi-biomes	0.56
Savanna and Grassland	Xiao & Ojima, (1996)	China	NPP grassland for 1980-1989	0.46
	Xiao & Ojima, (1999)	China	NPP grassland for 1981-1990	

Tropical forests include tropical evergreen and deciduous forest/wood land; Temperate forests include temperate broadleaf and needle leaf evergreen forest, temperate deciduous forest/woodland and mixed forests.

In each biome, the monthly temperature stress scalar ($T_{(s,m)}$) is determined by the deviation of temperature from the low and high temperature limits for CO_2 uptake and the optimum photosynthesis temperature as follows:

$$T_{(s,m)} = \begin{cases} 0.15 & if \quad T_m < T_{low} \quad or \quad T_m > T_{high} \\ (T_m - T_{low})/(T_{opt1} - T_{low}) & if \quad T_{low} \le T_m < T_{opt1} \\ (T_{high} - T_m)/(T_{high} - T_{opt2}) & if \quad T_{opt2} < T_m \le T_{high} \\ 0.95 & if \quad T_{opt1} \le T_m \le T_{opt2} \end{cases} \tag{4}$$

Where, T_m represents monthly mean temperature; T_{low} and T_{high} refer to the low and high temperature limits for CO_2 uptake; T_{opt1} and T_{opt2} represent the lower and upper range of temperature optimum of photosynthesis. The specific values of T_{low}, T_{high}, T_{opt1} and T_{opt2} for the basic biomes under study are listed in Table 5.2.

Monthly estimated and potential evapotranspiration (EET and PET) calculated by referring to BIOME4 (Kaplan *et al.* 2002) and LPJ (Sitch *et al.* 2003) are used to define the monthly moisture-stress value in each biome as follows (Potter *et al.* 1998, 1999):

$$W_{(s,m)} = \min(0.5 + EET_m / PET_m, \quad 1.0) \tag{5}$$

Table 5.2 The temperature limits for CO_2 uptake and the temperature optimum for photosynthesis

Classified biomes in PNV data	T_{low} (°C)	T_{opt1} (°C)	T_{opt2} (°C)	T_{high} (°C)
Tropical evergreen forest/wood land (TrEFW)	2.0	25.0	30.0	55.0
Tropical deciduous forest/wood land (TrDFW)	2.0	25.0	30.0	55.0
Temperate broad-leaved evergreen forest (TeBEF)	-4.0	20.0	30.0	42.0
Temperate deciduous forest/woodland (TeDFW)	-4.0	20.0	25.0	38.0
Temperate needle-leaved evergreen forest (TeNEF)	-4.0	20.0	30.0	42.0
Mixed forest	-4.0	20.0	30.0	42.0
Tundra	-4.0	10.0	30.0	45.0
Shrub	-4.0	10.0	30.0	45.0
Savanna and Grass	6.0	20.0	45.0	55.0

The values of T_{low}, T_{opt1}, T_{opt2} and T_{high} for each biome refer to other research (e.g. Sitch *et al.*, 2003)

Estimates of NPP variation by DGVM simulation

Simulations of NPP dynamics by LPJ-DGVM are used to compare the NDVI-derived NPP dynamics at the same temporal and spatial scale. LPJ-DGVM combines process-based, large-scale representations of terrestrial vegetation dynamics and the exchanges of carbon and water between land and atmosphere. Ten plant functional types (PFTs) are differentiated in LPJ-DGVM by their physiological, morphological, phonological, bioclimatic, and fire-response attributes (Sitch *et al.* 2003). Vegetation type in a grid cell is determined by the dominant PFT, i.e. the one that has the largest fractional foliage coverage (FPC). Photosynthesis, evapotranspiration and soil water dynamics in LPJ-DGVM are modeled at a daily time-step, while vegetation structure, PFT population densities and NPP of each PFT are updated monthly and annually.

In LPJ-DGVM, the calculation of gross primary productivity (GPP) in each grid cell is based on the climate data and the current FPC, which is used as a surrogate for FPAR. The maintenance respiration of each PFT is calculated in each simulation based on the size of the living tissue pools, their assigned C:N ratio and climate data. The growth respiration of each PFT is taken as a fraction of NPP. NPP of each PFT is then calculated as the difference between its GPP and the total respiration (maintenance respiration plus growth respiration). The LPJ-DGVM simulation starts from unvegetated ground and 'spins up' for 1,000 model

years until approximate equilibrium is reached with respect to carbon pools and vegetation cover (Sitch *et al.* 2003).

Results and Discussion

The NDVI-derived estimates of NPP in China: the basic results

The NDVI-derived estimates of NPP in China not only vary from one biome to another but also vary spatially within biomes (Figure 5.1b). At the grid-cell level, annual NPP estimates in China range from below 200 gC m^{-2} per year to above 800 gC m^{-2} per year (Figure 5.1b). Among different biomes, the lowest annual NPP estimates mainly occur in tundra (around 344 gC m^{-2} per year) and the highest annual mean NPP estimates occur in tropical broadleaved evergreen forest (around 565 gC m^{-2} per year). In addition, the NDVI-derived NPP estimates are higher in mountainous areas than areas of relatively flat terrain (e.g. the northeast plain, the north plain and the Sichuan basin in China) with an exception of the Tibetan Plateau, in most areas of which annual NPP is less than 400 gC m^{-2} per year (Figure 5.1b). Overall, the range of NDVI-derived estimates of NPP for China is similar to other model-simulated estimates such as LPJ (Sitch *et al.* 2003) and BIOME3 (e.g. Ni, 2001).

Comparison between NDVI-derived and DGVM-simulated annual NPP variation

Interannual variations in NDVI-derived annual NPP values agree well with the DGVM-simulated values in most of the individual biomes for China. For example, the calculated correlation coefficients between NDVI-derived and DGVM-simulated annual NPP variation over the years 1982-2000 for forested biomes are 0.81 ($p<0.001$) in temperate needleleaved evergreen forest (TeNEF), 0.47 ($p<0.05$) in temperate deciduous forest/woodland (TeDFW), 0.47 ($p<0.05$) in mixed forests, and 0.31 ($p<0.20$) in tropical evergreen forests/woodland (TrEFW) (Figure 5.2). Tropical deciduous forest and woodland (TrDFW) accounts for only a small part of total forests under study (<5%). For non-forested biomes, the NDVI-derived interannual NPP variation is linearly correlated with the DGVM-simulated NPP variations in savanna ($R^2=0.25$, $p<0.04$), grassland ($R^2=0.64$, $p<0.001$) and tundra ($R^2=0.36$, $p<0.005$). For annual NPP variations in shrubs, the correlation of NDVI-derived and DGVM-simulated NPP is relatively low ($R^2=0.07$, $P=0.28$), partially because in

regions where the PNV shrubs are dominant the DGVM-simulated biomes consist of grass and temperate broadleaved evergreen tree (LPJ-DGVM does not simulate shrubs).

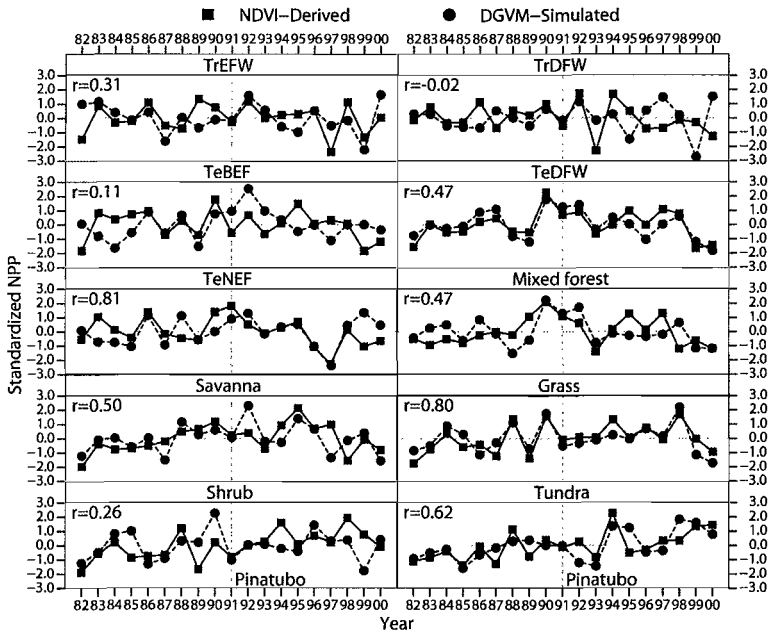

Figure 5.2 Comparison between the NDVI-derived and DGVM-simulated NPP variations in China over the years 1982-2000. The standardized NPP (or Z-score) is summarized for each of the ten biomes classified in the PNV data. The "r" refers to correlation.

The spatial pattern of annual NPP dynamics derived from NDVI data also agrees well with that simulated by the DGVM in most areas of China (as illustrated by the correlation coefficients in Figure 5.3). Especially in areas of relatively flat terrain, such as in the Northeastern Plain, the North Plain and the Pearl River Plain of China, the NDVI-derived NPP variation is highly consistent with the DGVM-simulated. In each of these regions, the homogeneity of the NDVI values, climate, and soil characteristics across different locations is high, which resulted in the high consistency between the NDVI-derived NPP dynamics and the DGVM-simulated. However, the interannual variability of NPP derived from NDVI data does not agree well with that simulated by the DGVM in the Yungui Plateau of China (Figure 5.3). In this region, the NDVI-derived annual NPP is much larger than the DGVM-simulated annual NPP.

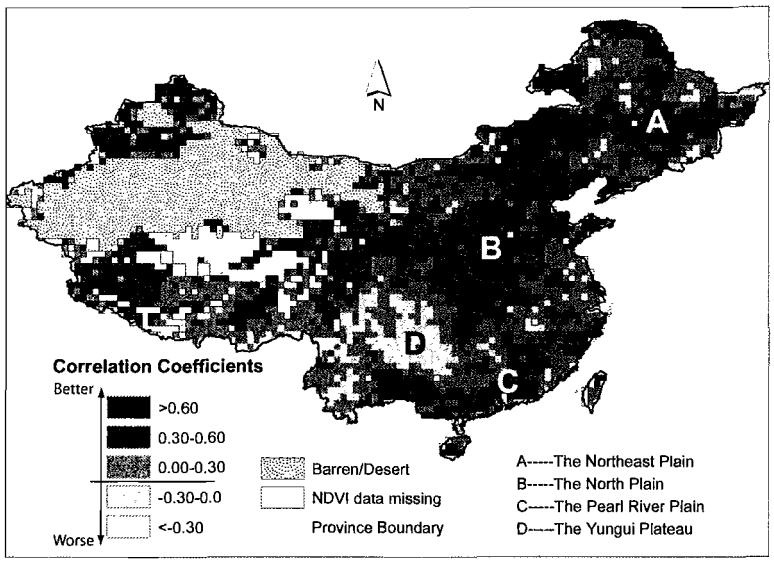

Figure 5.3 The performance of NDVI-derivation in each grid cell as shown by the calculated correlation coefficients between the NDVI-derived and the DGVM-simulated annual NPP variation over the years of 1982 to 2000. The white area in inland China is a result of NDVI data missing.

Comparison between NDVI-derived and DGVM-simulated seasonal NPP variation

The seasonality of NDVI-derived NPP is broadly similar to the DGVM-simulated across different latitudinal bands (Figure 5.4). In general, the seasonal cycles of NDVI-derived NPP resembles the DGVM-simulated NPP when the latitude is greater than 30°N, where seasonal NPP is relatively high from June to September but low from November to March. When the latitude is less than 30°N, the NDVI-derived seasonal NPP clearly differs from the DGVM-simulated. The difference mainly occurs in the estimation of winter and summer NPP. The relative distribution of NDVI-derived winter NPP is higher (Figure 5.4a) than the DGVM-simulated (Figure 5.4b). In summer, the relative distribution of NPP estimates under both NDVI-derivation and DGVM-simulation is high but the pattern is more complicated under the DGVM-simulation. In spring and autumn, seasonal NPP derived from NDVI data matches to some degree that simulated by the DGVM, which may suggest that the climate transition from winter to summer or from summer to winter is not very significant in areas south of 30°N.

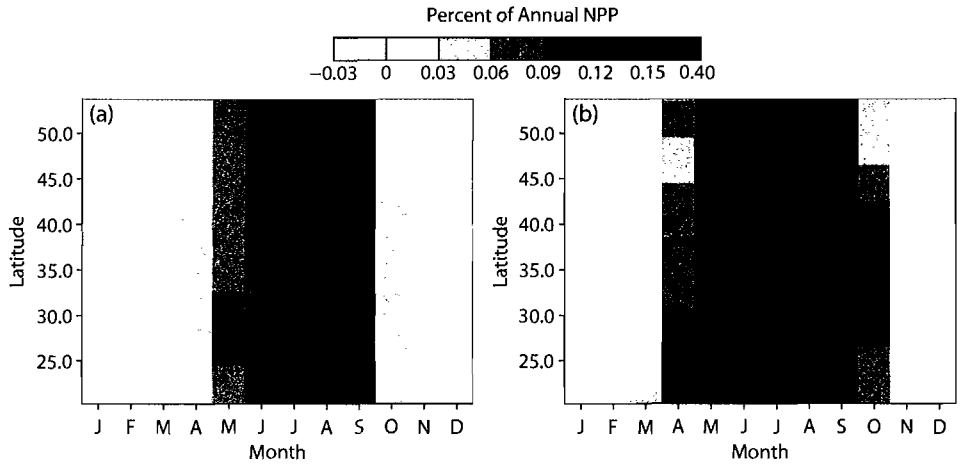

Figure 5.4 Comparison between the NDVI-derived (a) and DGVM-simulated (b) monthly NPP across different latitude (0.5° band), expressed as percentages of the annual total NPP in each latitudinal band.

In detail, both the NDVI-derivation and DGVM-simulation estimate a negative NPP in winter at latitudes higher than about 30°N, which indicates that plant respiration is greater than the uptake of carbon by plants during winter. In contrast, the estimates of NPP in summer from both NDVI data and DGVM-simulated data are greater than the annual mean, concordant with the concept that the release of carbon due to plant respiration is generally smaller than the uptake of carbon by plants during summer. In addition, the proportion of annual NPP represented by the summer NPP peak is relatively higher under the NDVI-derivation than that under the DGVM-simulation (Figure 5.4a and b).

The interannual and seasonal variability of NPP in China

The interannual variability of annual NPP in China

The general trend of terrestrial NPP dynamics in China over the years 1982-2000 appears in Figure 5.5, in which loess curves (Cleveland, 1979) are used to describe annual NPP variation over the years 1982-2000 in each of four biomes. The results show that annual NPP in forests varies from -16.7 below to 21.5 gC m^{-2} above its 19-years' mean (470.4 gC m^{-2} per year). The variation of NPP anomaly in forests is least among the four aggregated biomes. Over the whole period, annual NPP in forests tended to increase during the 1980s and decrease during the 1990s (Figure 5.5). Compared to annual NPP in 1990, it decreased by 7.4% in 1991 and 1992 and continued to decrease in 1993. This short-term decrease is

associated with the negative anomaly in both temperature and precipitation, which (at least for temperature) was partially a result of the Pinatubo eruption and the resulting cooling effects as mentioned by other studies (e.g. Lucht *et al.* 2002; Cao *et al.* 2003; Piao *et al.* 2006). In addition, estimates of annual NPP in forests show a decrease during the El Niño years of 1987-1988 and 1997-1998. However, it did not show a decrease during the El Niño year of 1982-1983 (Figure 5.5), which suggests that the El Niño-related climatic variation in the eastern monsoon zone was spatially complex, or that other factors contributed to the NPP dynamics in forests in these particular years.

Unlike the forests, annual NPP in grassland tended to increase over most of the 1982-2000 period though it showed a decrease in the last two years of 1990s. The rate of increase was 0.005 gC m^{-2} per year (R^2=0.17, p<0.08). Especially over the years 1982-1998, the annual NPP increase was as high as 4.2 gC m^{-2} per year (R^2=0.39, p<0.01). Such an increasing trend is highly consistent with studies by Cao *et al.* (2004). On average, the magnitude of NPP change in grassland varied from 25.0 to 25.1 gC m^{-2} per year, which accounts for 5.5 percent of its 19-years' mean (451.1 gC m^{-2} per year). Like annual NPP in forests, annual NPP in grassland diminished in 1991 largely due to the cooling effects introduced by the Pinatubo eruption.

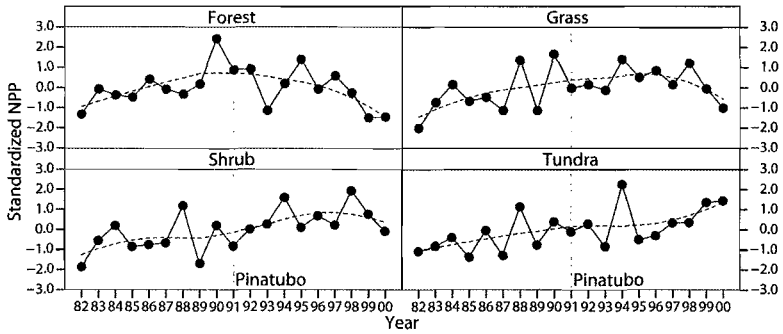

Figure 5.5 The NDVI-derived Annual NPP variation as shown by the solid line in China over the years 1982-2000. The dashed horizontal line (fitted loess curve) helps visualize the generalized NPP trend. The dashed vertical line locates the year in which Mt. Pinatubo erupted.

Annual NPP in shrubs and tundra increased slightly over the years 1982-2000. The increasing rate was 0.01 gC m^{-2} per year (R^2=0.36, p<0.007) in both shrubs and tundra. The

averaged annual NPP in shrubs is 383.4 gC m^{-2} per year, which is larger than the average annual NPP of 305.5 gC m^{-2} per year in tundra. Even though the increasing rate of annual NPP in shrubs and tundra is similar, the specific variation of NPP differs from one biome to another. For example, the fitted loess curve shows annual NPP in shrubs increased gradually from 1982 to 1998. After 1998, there was a decreasing trend for NPP in shrubs. In contrast, annual NPP in tundra tended to increase gradually over the whole research period. In addition, our results indicate that annual NPP in both shrubs and tundra decreased in the year (1991) when Mt. Pinatubo erupted. However, annual NPP in shrubs tended to increase during the El Niño years of 1982-1983, 1986-1987 and 1997-1998 (Figure 5.5).

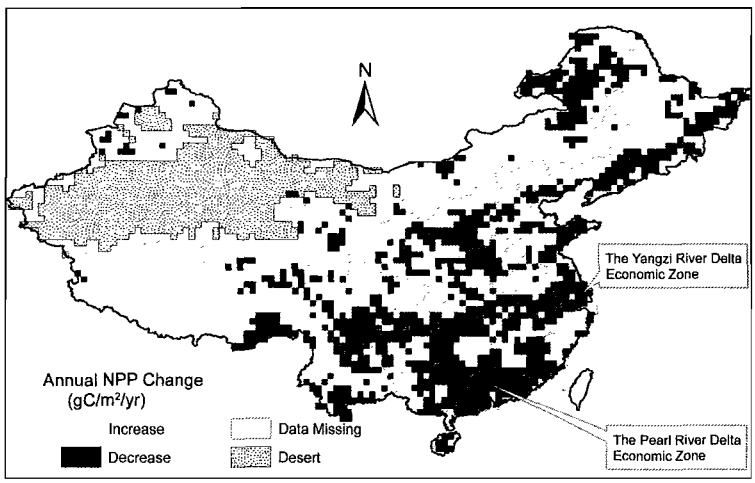

Figure 5.6 The changes of annual mean NPP between 1980s and 1990s (Here we only show the change direction rather than the magnitude of averaged-annual NPP change).

When the difference between the averaged-annual NPP in 1980s and that in 1990s was mapped, we found the spatial pattern of annual NPP change was relatively complicated in the eastern monsoon zone (dominated by forests). In contrast, the spatial pattern of annual NPP change in the north-west arid zone (dominated by grass) and the Tibetan Plateau frigid zone (dominated by tundra) of China is more uniform, showing an increasing trend (Figure 5.6). The complexity of the annual NPP pattern in the eastern monsoon zone of China may be explained by the climatic gradient from south to north and the rapid land use change, such as urban sprawl and agricultural activities. For example, the NDVI-derived annual NPP in the

Pearl River Delta Economic Zone and The Yangtze River Delta Economic Zone of China decreased sharply from 1980s to 1990s, concordant with other research (e.g. Fang *et al.* 2003; Piao *et al.* 2003). The decreasing magnitude of annual NPP in these two areas was beyond 60 gC m^{-2} per year, which was the highest among all decreasing areas.

The variability of seasonal NPP in China

This study reveals that NPP in winter (December, January and February) varied slightly in all four combined biomes as might be expected. Especially in grassland and tundra, NPP in winter seemed to be consistent over the years 1982-2000 (Figure 5.7A). In forests and shrubs, the NPP anomaly in winter varied from -7.2 below to 6.1 gC m^{-2} above their 19-years' mean respectively (47.9 gC m^{-2} per season in forests and 34.3 gC m^{-2} per season in shrubs). In contrast, NPP in spring (March, April and May), summer (June, July and August), and autumn (September, October and November) varied more acutely than that in winter (Figure 5.7B, C and D). For example, NPP in spring tended to increase gradually at a rate of 0.66 gC m^{-2} per season (R^2=0.16, $p<0.10$) in forests, 0.48 (R^2=0.15, $p<0.10$) in grassland and 0.72 (R^2=0.68, $p<0.01$) in tundra, respectively. The increasing trend of spring NPP is consistent with the concurrent increase of spring temperature, which will likely advance the onset of the growing season or of budburst of terrestrial ecosystems (Lucht *et al.* 2002; Fang *et al.* 2003).

In contrast to NPP in spring, the variation of NPP in summer was more complicated. Our results show that summer NPP in forests and grassland had no clear increasing trend. However, summer NPP in tundra increased gradually over the years 1982-2000 at a rate of 1.60 gC m^{-2} per season (R^2=0.21, $p<0.05$). In autumn, the statistics suggest that seasonal NPP increased gradually at a rate of 0.60 gC m^{-2} per season (R^2=0.17, $p<0.08$) in grassland, 1.00 gC m^{-2} per season (R^2=0.24, $p<0.04$) in shrubs, and 0.52 gC m^{-2} per season (R^2=0.15, $p<0.10$) in tundra. Our results also reveal that seasonal NPP in most biomes tended to decrease in the year (1991) when Mt. Pinatubo erupted. However, seasonal NPP differed both from one biome to another and from one season to the next during the El Niño years of 1982-1983, 1986-1987 and 1997-1998 (Figure 5.7), which suggest other factors contributed to the NPP dynamics in China or the climatic variation during different El Niño years was spatially complex in China.

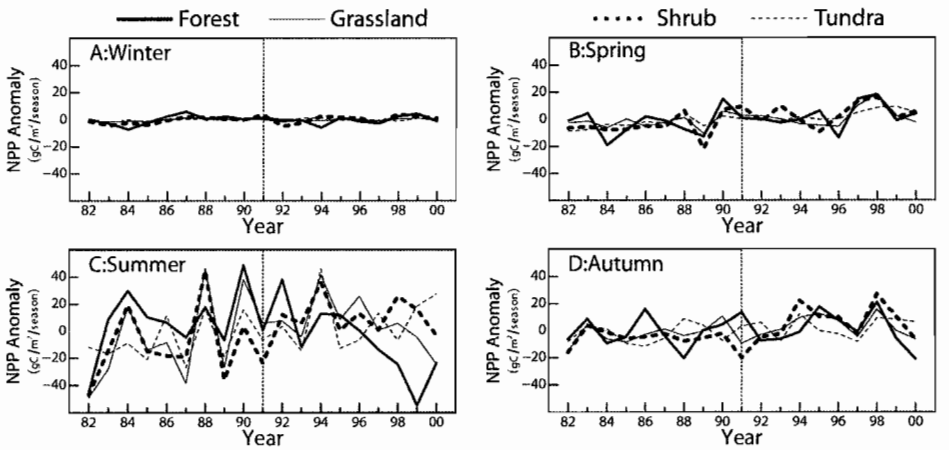

Figure 5.7 The variability of seasonal NPP in China over the years 1982-2000. The dashed vertical line locates the year in which Mt. Pinatubo erupted.

Sensitivity of NPP to precipitation and temperature variation in China

The relationship of annual NPP to annual mean temperature and precipitation

To examine the relationship of terrestrial NPP dynamics in China to the spatial variation of annual mean precipitation and temperature, we first averaged the 19-years' annual mean NPP, precipitation and temperature in each grid cell respectively and then plotted them using an enhanced scatter plot (Figure 5.8). The results reveal that the highest estimates of annual NPP in China are in regions where annual mean temperature is above 20°C (warm) and annual mean precipitation beyond 1500 mm (wet). These regions are mainly distributed in southeast China such as Hainan, Guangdong and part of Guangxi and Fujian provinces (Figure 5.1b), in which the dominant vegetation is tropical forest. Our estimates of the highest NPP are consistent with other research. For example, Jiang *et al.* (1999) and Ni (2000) found that the highest productivity in China was in tropical seasonal and rain forests. In addition, a study based on inter-comparison of multiple model-based results at the global scale revealed a similar conclusion (e.g. Schloss *et al.* 1999).

In contrast, the lowest estimates of annual NPP occur in regions where annual mean precipitation is less than 500 mm and annual mean temperature is below zero. These regions are mainly located in the Tibetan Plateau frigid zone and the western part of Inner Mongolia of China (Figure 5.1b), in which the dominant vegetation is alpine tundra and grass/steppe and desert respectively. The lowest NPP estimates in these areas are largely attributed to the

low temperature and moisture deficit (Ni, 2004). However, the relatively low estimates of NPP in the Northeastern and North plain and Sichun Basin of China are caused by the low NDVI value, which are largely a result of the local socio-economic activities such as urbanization and agriculture practises. For example, Piao *et al.* (2003) argued rapid urbanization resulted in a sharp decrease in NDVI in the Yangtze River and Pearl River deltas. In the whole of China, estimates of NPP tended to increase as both temperature and precipitation increase (Figure 5.8). The high temperature and precipitation in summer results in high actual evapotranspiration. But, because precipitation mainly occurs in summer, it greatly minimizes the water stress on plant growth and in return causes the highest NPP to occur in summer (Ding *et al.* 2005).

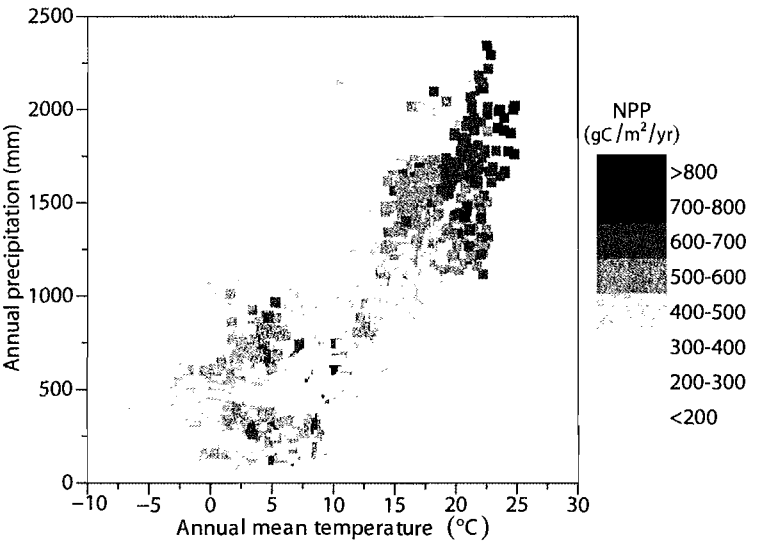

Figure 5.8 The general relationship of annual NPP to annul mean temperature and precipitation in China. Annual NPP does not increase uniformly and consistently with increase in annual mean temperature and precipitation because of the effects of human social and economical activities on terrestrial NPP in China, and because there are areas where actual crops were treated as forests in summarizing NDVI-derived NPP.

The sensitivity of annual NPP to the variation of temperature and precipitation

Our results show that the climate sensitivity of annual NPP estimates differs from one biome to another. In forests, the interannual variability of NPP was not significantly correlated with the variation of temperature and precipitation (Figure 5.9a and Table 5.3).

The non-significant relationship implies other factors may have important effects on the dynamics of annual NPP in forests or the climatic conditions were not limiting for plant growth in the eastern monsoon zone. For example, Jiang *et al.* (1999) argued that the spatial pattern of NPP in Chinese forests was a result of both natural environmental factors and human land use patterns. Land use change can either enhance terrestrial NPP in cropping-grazing transition zone (Gao *et al.* 2005) or decrease it in areas undergoing rapid urbanization (Fang *et al.* 2003; Piao *et al.* 2003).

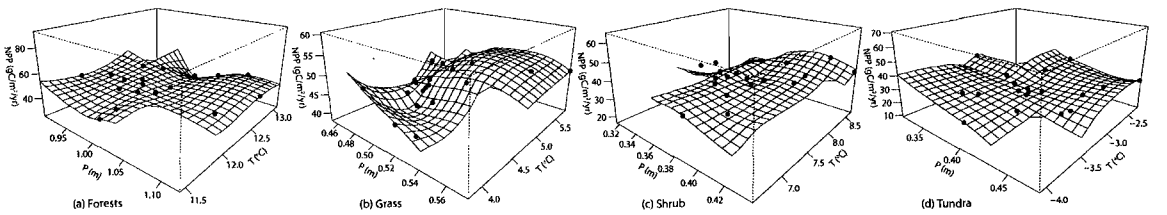

Figure 5.9 The sensitivity of annual NPP to the temperature and precipitation change in four biomes as illustrated by the loess surface, which is derived from the 19 black points. Each of points refers to the NDVI-derived NPP (the NPP values on Z-axis are reduced by an order of 10 for plotting), the observed precipitation and temperature in a specific year.

In contrast to forests, the variations of annual NPP in grassland were significantly correlated with the variation of temperature and precipitation. Our results show that the increase of precipitation tended to decrease annual NPP in grassland when annual mean temperature is less than 4.5°C. However, when annual mean temperature is greater than 4.5°C, the variation of annual NPP was positively correlated with the variation of precipitation (Figure 5.9b). The bivariate regression analysis also indicates that annual NPP in grassland was positively and linearly correlated with the variation of precipitation (Table 5.3). Such a positive relationship between precipitation and annual NPP in grassland suggests that soil moisture was limiting and a major factor for controlling the spatial distribution and temporal variation of NPP in the north-west arid zone of China (Ni, 2004; Lu and Ji, 2006). Compared to precipitation, the variability of annual NPP was more strongly and positively correlated with the variation of temperature (Figure 5.9b), which indicates temperature also played an important role in controlling the NPP dynamics in grassland. For example, Ni

(2004) stated that belowground and total productivity in the temperate grassland of China was influenced more by temperature than by precipitation.

Table 5.3 The bivariate regression analyses between NPP and temperature or precipitation

		Forests			Grass			Shrub			Tundra		
		Slope	R^2	P (<)	Slope	R^2	P (<)	Slope	R^2	P (<)	Slope	R^2	P (<)
Annual	T	-	-	-	-	-	-	-	-	-	34.2	0.32	0.01
	P	-	-	-	3.18	0.39	0.01	2.88	0.34	0.01	-	-	-
DJF	T	2.54	0.42	0.01	0.41	0.22	0.04	1.26	0.24	0.03	0.68	0.31	0.01
	P	-	-	-	-	-	-	-	-	-	-	-	-
MAM	T	12.2	0.50	0.01	5.26	0.33	0.01	-	-	-	5.23	0.35	0.01
	P	-	-	-	0.32	0.39	0.01	-	-	-	-	-	-
JJA	T	-	-	-	-	-	-	-	-	-	30.7	0.29	0.01
	P	-0.29	0.23	0.04	0.65	0.41	0.01	0.50	0.34	0.01	-	-	-
SON	T	-	-	-	8.11	0.42	0.01	7.35	0.21	0.05	8.25	0.36	0.01
	P	-0.11	0.13	0.08	-	-	-	-	-	-	-0.29	0.27	0.03

DJF (December, January, February), MAM (March, April, May), JJA (June, July, August) and SON (September, October, November) refer to winter, spring, summer and autumn respectively. T and P stand for temperature and precipitation respectively. "-" means there is no statistically significant linear relationship.

Similar to grassland, the variation of annual NPP in tundra was significantly correlated with the variation of temperature and precipitation. In particular, our results reveal the increase of temperature increased annual NPP in tundra and so did the decrease in precipitation (Figure 5.9d). Given that there was a positive relationship between annual NPP and temperature in tundra (Table 5.3), and that temperature increased gradually at a rate of 0.05°C per year (R^2=0.43, $p<0.002$) over the years 1982-2000 in tundra, we argue that temperature was limiting for plant growth in the Tibetan Plateau frigid zone. In addition, the negative relationship between annual NPP and precipitation implies that soil moisture was sufficient for the growth of plants in the Tibetan Plateau frigid zone. For example, the bivariate regression between NDVI-derived annual NPP and observed precipitation shows that annual NPP in tundra decreased by 1.09 gC m^{-2} per year (R^2=0.14, $p<0.11$) as a result of precipitation increase by 1 percent. In shrubs, annual NPP tended to increase as both the temperature and precipitation increase (Figure 5.9c).

The sensitivity of seasonal NPP to the variation of temperature and precipitation

Although the sensitivity of seasonal NPP to temperature and precipitation variations is more complex than that of annual NPP, several patterns appear when seasonal NPP dynamics were assumed to be a result of the combination of temperature and precipitation variations. First, winter and spring NPP dynamics in four biomes were mostly and positively correlated with the temperature variations, especially in forests, grassland and tundra (Table 5.3). However, NPP dynamics in these two seasons appeared to be insensitive to the precipitation variations in most biomes, as suggested by relevant non-significant statistics in Table 5.3. Second, summer NPP appeared to be insensitive to the combination of temperature and precipitation variations though the precipitation variations alone increased summer NPP in grassland and tundra (Table 5.3). Third, temperature increase in autumn tended to increase autumn NPP in grassland, shrub and tundra. Fourth, compared to seasonal NPP in other biomes, seasonal NPP in tundra was consistently and positively correlated with the temperature variations in all seasons (Table 5.3), indicating that the temperature or solar radiation is a major factor associated with changes of NPP in the Tibetan Plateau frigid zone (Piao *et al.* 2006).

Conclusion

This study examined both the variability and the climate sensitivity of terrestrial NPP in China over the last two decades. Through comparing the NDVI-derived NPP estimates with the DGVM-simulated NPP data, and through combining the spatiotemporal variation of NPP estimates with three general climatic zones in China, our results reveal that:

(i) The NDVI-derived interannual variability of NPP agrees well with the DGVM-simulated variability of NPP in most areas of China. Specifically, the NDVI-derived seasonality of NPP agrees better with the DGVM-simulated seasonality when the latitude is greater than 30°N, in which both estimates show plant respiration is greater than the uptake of carbon by plants in winter but smaller in summer. South of 30°N, winter NPP is slightly higher under the NDVI-estimation. Over China as a whole, the NDVI-derived annual NPP variations are consistent with the DGVM-simulated variations in areas whose terrain is relatively flat, such as in the Northeastern Plain, the North Plain and the Pearl River Plain of

China. This consistency is largely a result of the homogeneity of the NDVI-values, climate and soil condition inside each of the regions.

(ii) Annual NPP in forests had an increasing trend in the 1980s but showed a decreasing trend in the 1990s. Annual NPP in grassland, shrubs and tundra increased respectively over the whole period of 1982-2000. The increase was 0.01 gC m^{-2} per year (R^2=0.17, $p<0.08$) in grassland, and 0.01 gC m^{-2} per year (R^2=0.36, $p<0.01$) in both shrubs and tundra. In addition, NPP in spring, summer and autumn varied more acutely than that in winter. NPP in spring also increased at a rate of 0.66 gC m^{-2} (R^2=0.16, $p<0.10$) in forests, 0.48 (R^2=0.15, $p<0.10$) in grassland and 0.72 (R^2=0.68, $p<0.01$) in tundra, respectively. However, NPP in summer did not show an increasing trend in both grassland and forests with an exception of tundra, in which summer NPP increased gradually over the years 1982-2000.

(iii) The dominant factor controlling the spatiotemporal patterns of NPP in China varies from one climatic zone to another. In specific, our results reveal that the interannual variability of NPP in grassland (or in the north-west arid zone) was sensitive to both temperature and precipitation change. In contrast, the dynamics of annual NPP in tundra (or in the Tibetan Plateau frigid zone) depended more on temperature than on precipitation. In the eastern monsoon zone in which forests dominate, the dynamics of annual NPP did not correlate well with both the temperature and precipitation variation, which suggests that the complex spatial pattern of NPP variation is largely a result of both climate change and human socio-economic activities.

Bridge

Chapter V investigated the sensitivity of terrestrial NPP in China to historical climate variation. Like terrestrial NPP being a key ecological variable in soil-vegetation-atmosphere transfer (SVAT) schemes and being sensitive to climate variation, soil moisture and actual ET are two key hydrological variables in the SVAT schemes and are also sensitivity to climate change. Chapter VI will analyze how historical climate variation affected soil moisture and actual ET in China by modifying a dynamic global vegetation model.

CHAPTER VI

SIMULATING THE VARIATION AND CLIMATE SENSITIVITY OF SOIL MOISTURE AND EVAPOTRANSPIRATION IN CHINA OVER THE YEARS 1961-2002

This chapter contains unpublished coauthored material with Patrick J. Bartlein (Department of Geography, University of Oregon). Guoping Tang developed the LH model and prepared the first draft of manuscript. Patrick J. Bartlein provided guidance on the paper and edited the manuscript.

Introduction

Soil moisture and evapotranspiration (ET) are two major components of the hydrologic cycle at the land surface, and affect many important processes in the soil-vegetation-atmosphere system (Lu *et al.*, 2003; Murphy & Lodge, 2004). For example, soil moisture can influence near-surface atmospheric variability (Arora & Boer, 2006) and can also influence atmospheric circulation on seasonal-to-interannual time scales (Shukla & Mintz, 1982; Manabe & Delworth, 1990). Soil-moisture deficits can restrict the respiration and productivity of plants and thus can influence species composition, type, and structure of vegetation (Brabson *et al.*, 2005; Evans & Trevisan, 1995). Similarly, changes in actual and potential ET have implications for nutrient flux, forest function, and plant productivity (Chattopadhyay & Hulme, 1997; Kosugi *et al.*, 2007), and for the global carbon cycle (Engstrom *et al.*, 2006).

Climate change can trigger changes in the hydrologic cycle by altering the spatial and temporal patterns of precipitation, temperature, and other hydrologically important variables (Arora & Boer, 2001; Burns *et al.*, 2007), and by influencing potential interactions among hydrologic variables. For example, higher temperature can reduce soil

moisture either by increasing the energy available for evaporation (Arora, 2002) or by enhancing forest ET by lengthening the growing season of plants (Chiew & McMahon, 2002; Glenn *et al.*, 2007; Huntington, 2003). Precipitation directly influences the availability of water and thus can affect soil and actual ET. For example, Guo *et al.* (2004) found that terrestrial ET is more sensitive to the spatiotemporal distributions of precipitation than is soil moisture. In addition, an increase in atmospheric CO_2 concentration can change the state of the water balance at the land surface through increasing temperature (Claessens *et al.*, 2006), contributing to changes in vegetation structure and distribution (Leipprand & Gerten, 2006), and inducing the stomatal closure of plants that increases their water use efficiency (Claessens *et al.*, 2006; Edraki *et al.*, 2004).

Approaches for estimating soil moisture and ET can be classified into experimental and model-based approaches. Direct measurement based on instruments such as moisture-flux towers (e.g. Glenn *et al.*, 2007), and indirect measurement based on the eddy-correlation method (e.g. Running *et al.*, 1999; Wever *et al.*, 2002) and the Bowen-ratio approach (Bowen, 1926) have been used to quantify soil moisture or actual ET at the land surface. However, measurement of soil moisture and ET are often costly and time-consuming, and difficult at the regional scales (Song *et al.*, 2000). As a result, observed data are confined to low temporal resolutions and small spatial scales (Miller *et al.*, 2007; Rodell *et al.*, 2004). To address these limitations, hydrologic models, either conceptual or physical, have been developed to study various water-related issues because they can provide finer spatiotemporal resolution of the hydrologic variables than do experimental approaches (Hamlet *et al.*, 2007). In addition, most current climate models such as HadCM3 (e.g. Pope *et al.*, 2000) or terrestrial biosphere models such as LPJ (e.g. Stich *et al.*, 2003) contain some kind land-surface or hydrologic model and have been used to simulate terrestrial soil moisture and ET (e.g. Gerten et al., 2004; Gordon & Famiglietti, 2004; Hirschi *et al.*, 2007).

Water is one of the most critical resources in China (Tao *et al.*, 2005). To date, efforts have been made to examine the climate-related hydrologic variation in China,

including the historical trend of ET (e.g. Gao *et al.*, 2007) and soil water deficit (e.g. Thomas, 2000), the climatic controls on water balance in lakes of Tibet (e.g. Morrill, 2004), and future climate-induced changes in the water cycle (e.g. Tao *et al.*, 2003). However, because the spatiotemporal changes in hydrologic variables are very complex and depend on multiple factors, and because the climatic controls on water balance at the land surface are still poorly understood (Kosugi & Katsuyama, 2007; Wilson *et al.*, 2004), additional study of their historical dynamics is still important for improving the management of water resource and agricultural systems (Chiew & McMahon, 2002; Hailemarian, 1999), and for understanding the roles of vegetation in the interactions between the atmosphere and the biosphere (Metcalfe & Buttle, 1999).

The importance of soil moisture and ET for human well being and terrestrial ecosystem sustainability requires that we be able to simulate the water balance at the land surface. This requires a model that can correctly simulate the roles of climatic variation, vegetation, soil characteristics, and atmospheric composition (i.e. CO_2) in controlling terrestrial soil moisture and ET. Dynamic global vegetation models (e.g. LPJ) have illustrated a strong ability to simulate transient responses of vegetation and water balance to climate variation at the global scale. However, they may not correctly simulate vegetation at the regional scale because they do not include many factors that have important roles in determining vegetation and water dynamics, and because of human modification of land cover. Ideally, when applying such a model to a regional-scale study with known vegetation, we would specify vegetation instead of dynamically simulating it. The specification of vegetation can help in theory to more accurately simulate the effects of climate and vegetation on soil moisture and ET.

The goals of this study are (1) to present an attempt to modify the LPJ dynamic global vegetation (DGVM) (Sitch *et al.*, 2003; Gerten *et al.*, 2004) in order to simulate terrestrial soil moisture and ET under predefined vegetation, (2) to evaluate the ability of this model, named LH (LPJ-hydrology), to simulate soil moisture and ET at the land surface, and (3) to demonstrate its application in China. Toward these ends, we first describe the structure of the LH model and the parameterization of some key hydrologic

variables in the LH model. As input to the LH model, we develop the necessary data sets, including climate, soils, vegetation type, foliar vegetation cover for each specified vegetation type and CO_2. Then, a series of simulations on a 0.5-degree global land grid are run using the historical climate and CO_2 data. Both observed and simulated data for runoff, soil moisture and ET at the different spatial scales are used to evaluate the LH simulations. Finally, the model results for China are used to analyze the variation and climate sensitivity of soil moisture and ET.

Methods and Data

The development of the LH model

The stand-alone LH (LPJ-hydrology) model was developed by modifying LPJ-DGVM (Stich *et al.*, 2003; Gerten *et al.*, 2004), and shares many of its features. The input data needed to run the LH model include climate, vegetation, foliar vegetation cover, soil and atmospheric CO_2 concentration (Figure 6.1). The climate data include monthly mean values of temperature (^{o}C), precipitation (mm), wet-day frequency (days) and percent cloudiness (%). LH defines the global vegetation into 11 biome types with reference to the global potential natural vegetation data set (Ramankutty & Foely, 1999), of which seven types are forests (two tropical, three temperate and two boreal) and four are non-forest (one savanna, one grassland, one shrub land and one tundra) (Table 6.1). The input vegetation data are used (1) to initialize some biome-related parameters (Table 6.1 & 6.2), (2) to define the phenological characteristics of each predefined biome type as one of four types, i.e. evergreen, summergreen, raingreen and other, and (3) to specify the photosynthetic pathway of plants (i.e. C4 vs. C3). The foliar vegetation cover data are used to calculate biome-specific minimum canopy conductance and the total amount of interception loss of precipitation. The soil data used in LH consists of two layers with fixed thickness (upper, 50cm; lower, 100cm) and includes parameters such as water holding capacity in both layers. The CO_2 data are used to calculate non-water-stressed canopy conductance and intercellular CO_2 partial pressure (Haxeltine & Prentice, 1996).

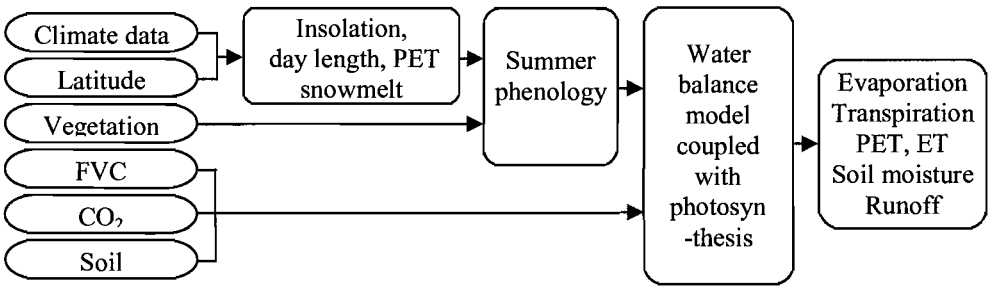

Figure 6.1 A flowchart to describe the process of LH (LPJ-hydrology) model for calculating several hydrological variables based on input climate, vegetation, foliar vegetation cover (FVC), CO_2 and soil data. PET and ET are short for potential and actual evapotranspiration, respectively.

Table 6.1 Hydrologically relevant parameters for each predefined biome type

PNV-based biome types	*LeL* (years)	*f*	*W* min	*CaC* (mm/s)	*E* max (mm/day)	*Ints*
Tropical evergreen forest	2.00	0.85	0.00	0.5	7.0	0.02
Tropical deciduous forest	0.50	0.60	0.10	0.5	7.0	0.02
Temperate broadleaf evergreen forest	2.00	0.70	0.00	0.5	5.0	0.02
Temperate needleleaf evergreen forest	4.00	0.70	0.00	0.3	5.0	0.06
Temperature deciduous forest	0.50	0.70	0.10	0.8	5.0	0.02
Boreal evergreen forest	4.00	0.90	0.00	0.3	5.0	0.06
Boreal deciduous forest	2.00	0.83	0.10	0.8	5.0	0.06
Savanna	0.50	0.57	0.20	0.5	7.0	0.01
Grassland	0.50	0.83	0.20	0.5	5.0	0.01
Shrubland	0.50	0.93	0.00	0.8	1.0	0.01
Tundra	0.50	0.93	0.00	0.8	1.0	0.01

LeL—leaf longevity; *f*—fraction of roots in soil upper layer; *W* min—minimum water scalar at which leaves shed by drought deciduous biome; *CaC*—canopy conductance component that is not associated with photosynthesis; *E* max—maximum evapotranspiration rate; *Ints*—interception storage parameter. The specific value of each parameter refers to Sitch et al. (2003) and Kaplan et al. (2002).

LH consists of three main sub-models, i.e. (1) the potential evapotranspiration model that calculates pseudo-daily photosynthetic active radiation flux, day length and daily potential ET in each grid cell using input climate data with latitude information, (2) the summer phenology model that evaluates daily phenology of each specified biome type, and (3) the coupled water balance model with plant photosynthesis that simulates

major componens of the water balance among the soil, vegetation and atmosphere, including surface evaporation, plant transpiration, soil moisture and surface runoff (Figure 6.1). In the application, to better initialize some important variables such as soil moisture content and fraction available water in two soil layers, the water balance model is run twice. Soil moisture of each layer is updated at daily time-steps, updating the previous day's soil moisture by balancing the amount of water infiltrating into the soil and that removed from the soil layers through runoff, percolation and actual ET.

The parameterization of LH model

Unlike LPJ, LH does not consider bioclimatic limits that determine whether or not a biome can survive under the climatic condition prevailing in a particular grid cell at a particular time because the biome type in a grid cell is specified, not simulated. LH also ignores the dynamics of vegetation, the competition between different vegetation types, and the biogeochemical dynamics among soil, vegetation and atmosphere. Consequently, the biome-related parameters (or attributes) in LH are greatly reduced and can be classified into two categories: (i) parameters that govern the dynamics of water balance (Table 6.1), and (ii) parameters necessary for simulating plant photosynthesis (Table 6.2). The reduction of parameters aims to strengthen LPJ's application to questions such as how climate change alone will affect the hydrology of a region with known or specified vegetation.

Parameters that govern the dynamics of the water balance include leaf longevity (LeL), the fraction of roots in two soil layers (f), the minimum water scalar value at which leaves are shed by drought-deciduous biomes (W min), the canopy conductance component not associated with photosynthesis (CaC), the maximum ET rate (E max), and the interception storage of vegetation ($Ints$). The leaf longevity of each biome type is used to calculate its leaf area. The fraction of roots in two soil layers (f_1 and f_2) affects relative soil mositure (wr) that is given by:

$$wr = w_1 \times f_1 + w_2 \times f_2 \quad (1)$$

where w_1 and w_2 are the fractions of available water in the upper and lower layer of soil respectively. The minimum water scalar (W min) adjusts daily drought phenology

because drought-deciduous plants shed their leaves when their water scalar falls below a specific threshold. The canopy conductance component (CaC) is a part of total non-water-stressed canopy conductance (gp) averaged over a grid cell as follows (Haxeltine & Prentice, 1996):

$$gp = ((1.6 \times adt / (ca \times (1.0 - \lambda))) / Dt\text{sec}) + CaC \quad (2)$$

where adt is total daytime net photosynthesis ($gC/m^2/day$); ca is the mole fraction of atmospheric CO_2; λ is the optimal ratio of intercellular to ambient CO_2 concentration; and $Dt\text{sec}$ refers to the length of daylight in seconds.

The maximum daily transpiration rate ($E\max$) is necessary for simulating the water supply function ($Suppl$) through the following expression:

$$Suppl = E\max \times wr \times dphen \times fvc \quad (3)$$

where $dphen$ is daily phenology of a biome and fvc is foliar vegetation cover (%) in a grid cell. The interceptation storage parameter ($Intc$) is used to calculate biome-specific interception storage ($Ints$) (Kergoat, 1998) as follows:

$$Ints = Intc \times LAI \times dphen \times \Pr \quad (4)$$

where LAI is leaf area index and $\Pr$ is adjusted daily precipitation.

Table 6.2 Photosynthetic relevant parameters and leaf area index for predefined biome types under study

PNV-based biome types	$N\max$ (mg/g)	T_l (°C)	T_1 (°C)	T_2 (°C)	T_h (°C)	LAI
Tropical Evergreen forest	100.0	2.0	25.0	30.0	55.0	5.2
Tropical deciduous forest	100.0	2.0	25.0	30.0	55.0	4.0
Temperate broadleaf evergreen forest	100.0	-4.0	20.0	30.0	42.0	6.0
Temperate needleleaf evergreen forest	100.0	-4.0	20.0	30.0	42.0	6.7
Temperature deciduous forest	120.0	-4.0	20.0	25.0	38.0	5.1
Boreal evergreen forest	100.0	-4.0	15.0	25.0	38.0	3.5
Boreal deciduous forest	100.0	-4.0	15.0	25.0	38.0	2.7
Savanna	100.0	6.0	20.0	45.0	55.0	2.6
Grassland	100.0	-4.0	10.0	30.0	45.0	2.5
Shrubland	1.0	-4.0	10.0	30.0	45.0	2.2
Tundra	1.0	-4.0	10.0	30.0	45.0	2.5

Nmax is the maximum foliar N content; T_l and T_h are the low and high temperature limits for CO_2 uptake; T_1 and T_2 are the lower and upper ranges of optimum temperature for photosynthesis; LAI is leaf area index. The specific value of each parameter except for LAI refers to Sitch *et al.* (2003) and Kaplan *et al.* (2002). The LAI for each PNV-based biome type refers to the Global Leaf Area Index Data from Field Measurements compiled at the Oak Ridge National Laboratory Distributed Active Archive Centre (DAAC) (http://daac.ornl.gov/VEGETATION/lai_des.html) and approximately equals to the long-term mean LAI of the corresponding biome/land cover type in the DAAC LAI data set.

Parameters needed for simulating plant photosynthesis include the maximum foliar N content (Nmax), the low (T_1) and high (T_2) temperature limit for CO_2 uptake, and the lower (T_l) and upper (T_h) ranges of optimum temperature for plant photosynthesis (Table 6.2). These parameters are used to calculate total daytime net photosynthesis ($gC/m^2/day$) of plant and to convert the daytime net photosynthesis to gas ($mm/m^2/day$) using an ideal gas equation (Haxeltine & Prentice, 1996), which is later used to simulate canopy conductance (see equation 2). The specific value of each parameter refers to both LPJ (Sitch *et al.*, 2003) and BIOME4 (Kaplan *et al.*, 2002).

The calculation of major hydrologic variables

The calculation of each hydrologic variable in LH is almost the same as that described in Gerten *et al.* (2004). We briefly introduce the calculation of each output variables (see Figure 6.1) here. Daily PET rate (E_q) at the regional scale is expressed as:

$$E_q = [\Delta/(\Delta+\gamma)]R_n / L \quad (5)$$

where R_n refers to net radiation calculated from latitude, day of the year, sunshine hours and air temperature; Δ is the rate of the saturation vapor pressure increase with temperature; γ and L are the psychrometric values of air and the latent heat of water vaporization adjusted by daily temperature, respectively. To avoid abrupt change in the values of variables such as the ratio of ET and PET in high latitude area, LH assigns daily E_q a new value 10^{-6} when the calculated E_q is zero.

Actual ET is the aggregation of interception loss, vegetation transpiration, and evaporation from bare soil. Daily interception loss ($Intcl$) is a product of daily PET (E_q) and the fraction of day-time (ω) when the canopy is wet as follows:

$$Intcl = E_q \times \alpha \times \omega \tag{6}$$

where α is the Priestley-Taylor coefficient with a value 1.32. The value of ω is related to the canopy interception storage capacity (see equation 4). Vegetation transpiration is based on the comparison between an atmosphere-controlled demand function and a plant-controlled supply function (see equation 3).

Daily evaporation (E_s) from bare soil is expressed following Huang *et al.* (1996) as:

$$E_s = E_q \alpha wr(1 - fv) \tag{7}$$

where wr represents the relative moisture in the upper layer of the soil column.

Daily soil water content in both layers at day i is updated taking account of the water content at previous day, and snowmelt (M_i), precipitation, interception loss, transpiration (E_i), evaporation ($E_{s,i}$), percolation ($p_{1,i}$) through two layers and runoff ($R_{1,i}$) during the current day i:

$$\begin{cases} \Delta w_{1,i} = \Delta w_{1,i-1} + \mathrm{Pr}_{t,i} + M_i - \beta_{1,i} \times E_{T,i} - E_{s,i} - p_{1,i} - R_{1,i} \\ \Delta w_{2,i} = \Delta w_{2,i-1} + p_{1,i} - \beta_{2,i} \times E_{T,i} - R_{2,i} - p_{2,i} \end{cases} \tag{8}$$

where $\Delta w_{1,i}$ and $\Delta w_{2,i}$ are daily changes in soil water content of both layers at day i; β_1 and β_2 represent the fractions of water extracted for transpiration from each layer (such that $\beta_1 + \beta_2 = 1$). The model simulates surface runoff (R_1) and subsurface runoff (R_2) from the excess of water over field capacity of the upper and the lower soil layer, respectively. The total runoff in a grid cell is the sum of surface and subsurface runoff.

Model input data

Monthly mean values of temperature (°C), precipitation (mm), percent cloudiness (%) and wet-day frequency (days) required to run LH are provided by the CRU TS 2.1 data sets developed by the Climatic Research Unit (CRU) at the University of East

Anglia (U.K.) (Mitchell & Jones, 2005). CRU TS 2.1 was built from a database of monthly weather-station data that were mostly checked for data inhomogeneities. Records from different sources were combined into a single database through the World Meteorological Organization codes attached to the stations. Station anomalies relative to long-term mean for 1961-1990 were interpolated onto 0.5 degree grid and applied to published long-term mean values on the same grid (e.g. New *et al.*, 1999). The final monthly climate grids were constructed for nine climate variables spanning 1901 to 2002 and are available from http://www.cru.uea.ac.uk/.

The global potential natural vegetation (PNV) data (Ramankutty & Foley, 1999) used to specify input biome type at each grid cell describe the distribution of global potential natural vegetation types that would most likely exist without human interventions. The PNV data are grouped into 11 biome types (Table 6.1) at a 0.5 degree geospatial resolution. The Vegetation Continuous Fields (VCF) data (Hansen *et al.*, 2000, 2003) produced at the University of Maryland (http://glcf.umiacs.umd.edu/data/vcf/description.shtml) are used to define the foliar vegetation cover (%) of a PNV-based biome in a grid cell. The VCF data contain proportional estimates for three vegetative cover types: woody vegetation, herbaceous vegetation and bare ground. Compared to the traditional classification schemes, the VCF data depict areas of different land cover and thus show better the percentage (from 0 to 100) of a land cover in a grid cell. The total percentage cover for three vegetation cover types in a grid cell is 100 percent (Hansen *et al.*, 2000).

The soil data used to run LH were from the derived soil properties data defined in the FAO world digital soil map (Food & Agriculture Organization, 1995). Annual atmospheric CO_2 concentrations for the period of 1961-2002 were originally from the Climate Research Group at the University of Illinois at Urbana-Champaign (see Schlesinger & Malyshev, 2001).

Model validation data

Several different data sets of observed (and simulated using other approaches) hydrological variables were used to evaluate the performance of the LH model. The soil

moisture data used to evaluate the LH simulations are the Illinois Soil Moisture (ISM) data (http://climate.envsci.rutgers.edu/soil_moisture/illinois.html) produced originally by Hollinger and Isard (1994). The ISM data consist of total soil moisture measured at 19 stations in the state of Illinois (U.S.). In specific, the ISM data set includes measurements for the top 10 cm of soil, and then for 20 cm layer intervals (e.g., 10-30 cm, 30-50 cm ...) continuously down to a depth of 2 m. The ISM data spanning the interval from January 1981 to June 2004 were calibrated with gravimetric observations. We did not use the first three years of data (1981, 1982 and 1983) to validate the LH simulations because they have smaller variability than the rest of data (Hollinger & Isard, 1994). Although ISM data represent a limited area relative to the size of the 0.5-degree grid cells being used here, the data do offer the possibility of examining monthly soil-moisture simulations over a 20-year period.

Two ET data sets are used to validate the LH-simulated ET at both the global and the local scales. The local ET in the Everglades of Florida (U.S.) (German, 2000) was evaluated on the basis of the Bowen-ratio energy budget method (Bowen, 1926) and is given by:

$$ET = (R_n - G - W)/[\lambda p_w(1+B)] \tag{9}$$

where R_n is net radiation measured by a net radiometer; G is soil heat storage estimated by measured values of heat flux, soil temperature and soil moisture, together with estimated values of soil bulk density and particles heat capacity; W refers to storage of heat in water estimated from measurements of water level and water temperature; λ is the latent heat of vaporization of water; p_w is the density of water (mass per volume); B is the Bowen ratio, which is expressed as a function of vertical differences of temperature and vapor pressure in the air:

$$B = \gamma(t_2 - t_1)/(e_2 - e_1) \tag{10}$$

where γ is a function of air temperature and barometric pressure; t_1 and t_2 are air temperatures measured at two points with different elevation; e_1 and e_2 are vapor pressures measured at the same two points. All data needed for the application of the

Bowen-ratio method were measured at 15-minute intervals spanning from 1996 to 2000 and at 9 sites ranging from 24.75°N to 26.25°N and from 79.75°W to 81.25°W (German & Vecchioli, 1996; German, 2000).

The second data set consists of global ET data from Tateishi and Ahn (1996), in which ET was derived from precipitation (P), soil moisture (SM) and potential evapotranspiration (PET) in the following way:

$$\begin{cases} ET_i = P_i + (SM_i - SM_{i-1}) & if \quad P_i < PET_i \\ ET_i = PET_i & if \quad P_i \geq PET_i \end{cases} \tag{11}$$

The Global Runoff Data Centre (GRDC) composite runoff fields (CRF) data set (Fekete *et al.*, 2002) at global scale were used to evaluate the LH-simulated monthly and annual runoff. The GRDC CRF data were developed by combining observed river discharge information with climate-driven water balance model outputs. The observed information was derived from selected gauging stations available from the World Meteorological Organization GRDC data archive (http://www.grdc.sr.unh.edu/html/Data/index.html). These station data were coregistered to a simulated topological network at a 0.5 degree land grid spatial resolution. The simulated runoff in each grid cell was multiplied by the ratio of observed to simulated runoff of the corresponding interstation region from the GRDC data sets. The composite monthly and annual runoff data are used in this study to evaluate the LH-simulated monthly and annual runoff at the continental scale.

Results and Discussion

The evaluation of the LH simulations against model validation data

The LH-simulated monthly mean runoff (an average value based on all grid cells in a continent) for five continents agrees well with the composite monthly runoff (Fekete *et al.*, 2002) (Figure 6.2). For example, the LH-simulated monthly runoff in Africa averages about 12.7 mm, which is close to the composite monthly runoff of 17.3 mm (Figure 6.2d). Although the LH-simulated monthly runoff appears not to be correlated well with the composite monthly runoff in Oceania ($r=0.43$, $p<0.16$), the magnitudes of

monthly runoff are similar in most months except for January (Figure 6.2e). Given the big discrepancy of monthly runoff between January and December in the composite, we argue that the LH-simulated monthly runoff in January appears to be more reasonable than the composite, largely because the values of LH-simulated monthly runoff vary more smoothly from one month to the next, and particularly from December to January. After aggregating the LH-simulated and the composite annual runoff into 1 degree latitudinal bands, they agree well ($r=0.86$, $p<0.01$) (Figure 6.2f), which demonstrates that LH captures the spatial variation of monthly runoff at the global land surface. However, LH might still underestimate annual runoff in high latitudes of both the hemispheres as LPJ does (Gerten *et al.*, 2003) when compared to the composite annual runoff data (if composite runoff data were not biased). For example, the LH-simulated annual runoff is smaller than the composite annual runoff when latitude is greater than 20°N in the northern hemisphere (Figure 6.2f), which is largely a result of underestimation of spring and summer runoff in North America (Figure 6.2a) and Eurasia (Figure 6.2c).

When LH-simulated monthly mean soil moisture (an average value based on simulated monthly soil moisture in all grid cells ranging from -91.25°W to -88.25°W and from 37.25°N to 42.25°N, a spatial extent that approximately matches the extent of observed soil moisture in Illinois of U.S.) was compared to observed monthly mean soil moisture at the top 50 cm layer of soil in Illinois of U.S. over the years 1984-2002 (Hollinger *et al.*, 1994), the statistics ($r=0.81$, $p<0.001$) suggest that LH can accurately capture the variation of monthly soil moisture (Figure 6.3). The LH-simulated monthly soil moisture averages 141.1 mm, accounting for 89.4% of the observed monthly soil moisture (159.0 mm). The root mean square error (RMSE) between the LH-simulated and observed monthly soil moisture for 228 months is 26.8, which demonstrate that LH does well in simulating monthly soil moisture in this particular region although it may underestimate soil moisture in some months.

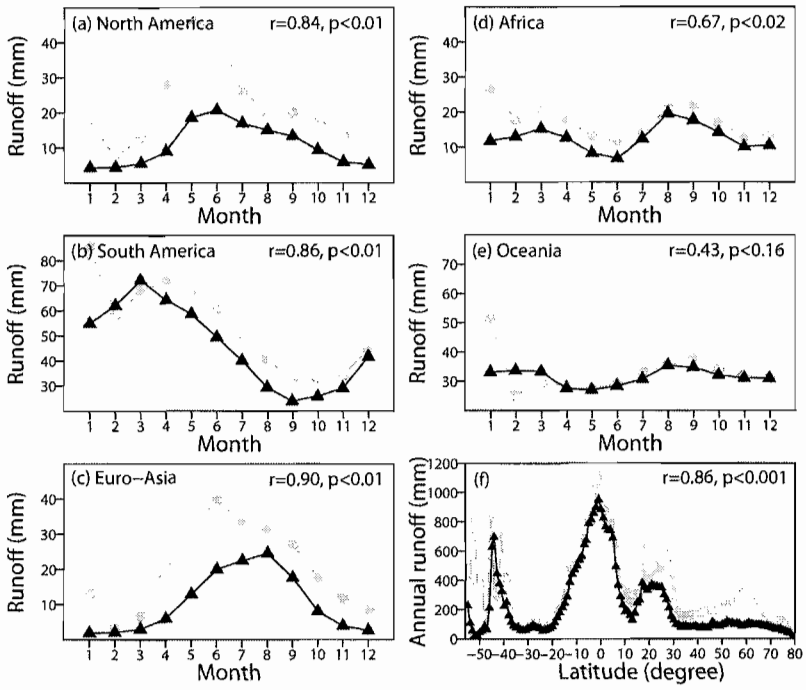

Figure 6.2 Comparisons between the LH-simulated 30-year (1961-1990) monthly mean runoff (triangle) and composite monthly runoff (circle) based on time periods with different length (Fekete *et al.*, 2002) in (a) North America, (b) South America, (c) Euro-Asia, (d) Africa and (e) Oceania, and (f) between the LH-simulated 30-year (1961-1990) annual mean runoff (circle) and composite annual runoff (triangle) across 1 degree latitudinal band.

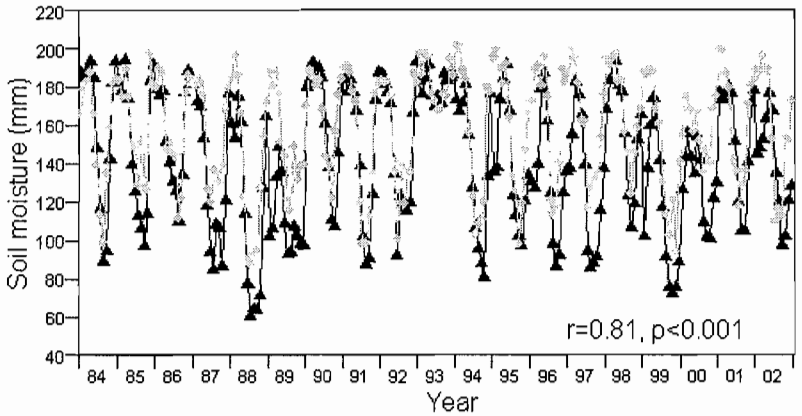

Figure 6.3 Comparison between the LH-simulated (triangle) and observed (diamond) soil moisture (Hollinger *et al.*, 1994) at the top 50cm of soil over the years 1984-2002 in Illinois of the United States.

As was the case for soil moisture, LH is able to accurately simulate monthly and annual actual ET (Figure 6.4). For example, the variation of the LH-simulated monthly ET over the years 1996-1999 corresponds well ($r=0.78$, $p<0.001$) to that derived from other measured data in the Everglades of the south Florida (U.S.), and area that ranges from 24.75°N to 26.25°N and from 79.75°W to 81.25°W (German & Vecchioli, 1996; German, 2000) (Figure 6.4a). The average monthly ET is 98.0 mm, approximating 99.6 mm of derived monthly ET. The RMSE is 16.6 for 48 data points, which is less than 17% of average monthly ET from both simulated and derived values. When compared to Tateishi and Ahn (1999) global annual ET data, the correlation between aggregated ET values in 1 degree latitudinal band is as high as 0.99, indicating that LH captures well the spatial pattern of annual ET at the global scale (Figure 6.4b) with an exception of ET estimates in the tropics, in which Tateishi and Ahn simulated annual ET are higher than LH-simulated annual ET.

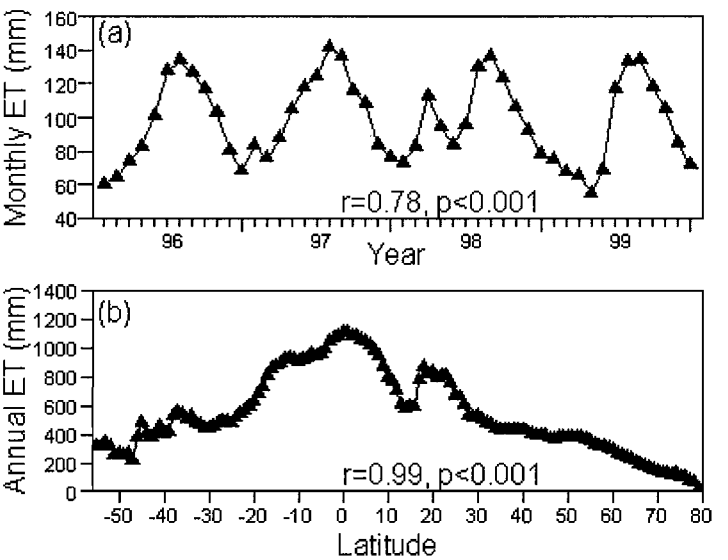

Figure 6.4 Comparison between (a) the LH-simulated monthly ET (triangle) and observed ET (square) over the years 1996-1999 in a region of Florida, ranging from 24.75°N to 26.25°N and from 79.75°W to 81.25°W (German & Vecchioli, 1996); and between (b) the LH-simualted annual ET (triangle) and a water-balance model-simulated annual ET (square) (Tateishi & Ahn, 1999) aggregated into 1 degree latitudinal band.

Overall, the LH evaluation against both observed and simulated hydrological data indicate that LH does well in simulating soil moisture, actual ET and runoff at the local to regional scales. However, because of the spatiotemporal heterogeneity of soil and climate conditions and the complexity of factors affecting the water balance at the land surface, further improvements on input soil and climate data and on the model's structure are still needed for the LH model. For example, the vertical soil profile in the LH model includes only two layers, which are not enough to describe the detailed physical dynamics of soil moisture within the soil profile. In addition, the LH model ignores the impacts of human activities such as land-use change and irrigation on the hydrologic cycle, which can cause the LH-simulated data not to perfectly match the observed.

The application of the LH simulations in China

The spatial patterns and climate sensitivity of soil moisture and ET in China

When the LH-simulated annual soil moisture and actual ET for China were mapped at the 0.5-degree grid-cell resolution over China as a whole (Figure 6.5a & b), annual soil moisture is around 76.2 mm and tends to decrease from the southeast to the northwest China (Figure 6.5a). The simulated annual mean soil moisture in the top 50 cm layer shows two distinct maxima, in southern and northeast China, with generally lower values in the interior and northwest. Annual soil moisture has the lowest value of 28.3 mm in west China, which is about 73.6 mm lower than that in the Tibetan Plateau of China. Similar to annual soil moisture, annul actual ET decreases from the southeast to the northwest China. In south China, annual actual ET was over 800 mm, a value of 600 mm higher than actual ET in west China (less than 200 mm). In other regions, annual ET varied from 600 mm to 400 mm in northeast and north China, and from 400 mm in southeast corner to 200 mm in northwest corner of the Tibetan Plateau (Figure 6.5b).

The spatial patterns of annual soil moisture and ET in China depend highly on the spatial patterns of annual temperature (Figure 6.5c) and precipitation (Figure 6.5d). Our results show that annual soil moisture tends to increase with increasing annual precipitation but decrease with increasing annual mean temperature (Figure 6.6a). When

temperature remains constant, an increase of 100 mm in annual precipitation will increase annual soil moisture by 10 mm. In contrast, when precipitation remains constant, an increase of temperature by 1 Celsius degree will decrease soil moisture by 2.05 mm. In contrast to annual soil moisture, annual actual ET tended to increase with the increase in both annual temperature and precipitation (Figure 6.6b). The reason is that higher temperature and precipitation will greatly increase surface water evaporation thus increasing actual ET. Because temperature and precipitation are both higher in southeast China and lower in northwest China (Figure 6.5c & d), annual soil moisture and actual ET tend to decrease from the southeast to the northwest China.

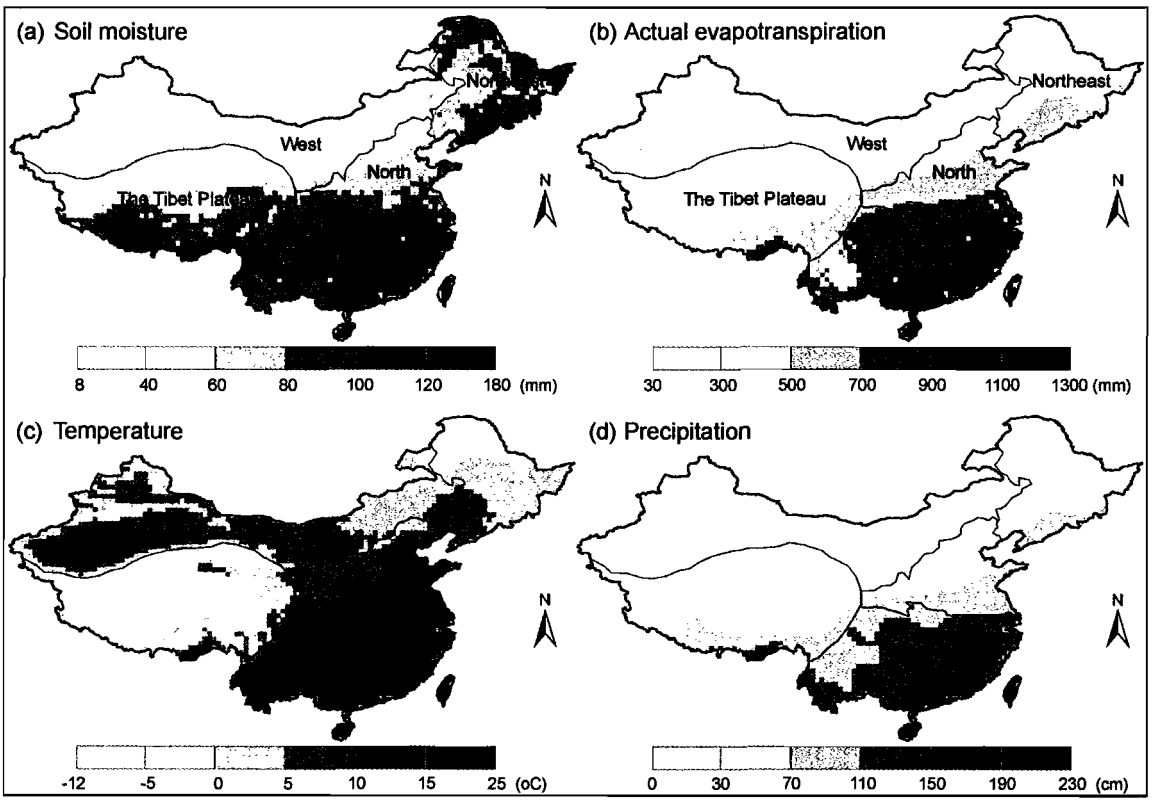

Figure 6.5 The spatial patterns of the LH-simulated 30-yrs (1961-1990) (a) annual mean soil moisture at the top 50cm layer of soil and (b) annual mean actual evapotranspiration in China, and the 30-yrs (1961-1990) (c) annual mean temperature and (d) precipitation in China. The stippled areas in (a) and (c) are desert and the white areas stand for either water or cities.

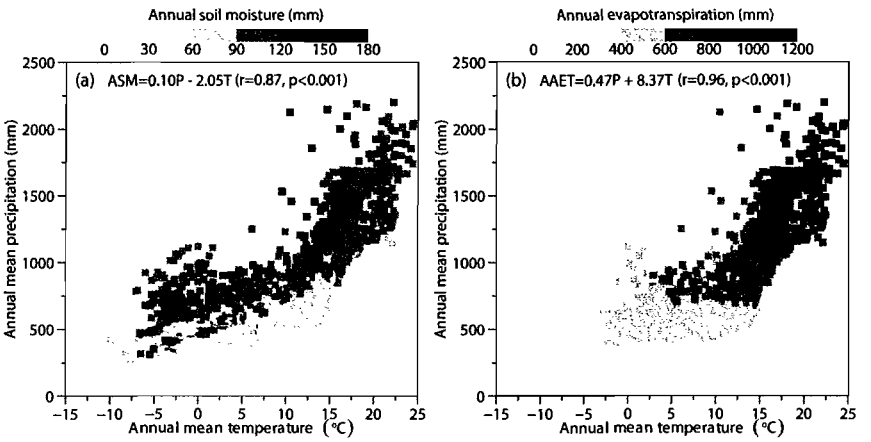

Figure 6.6 The relationship of (a) annual soil moisture (mm) and (b) annual actual evapotranspiration (mm) with annual mean temperature and precipitation over the whole China

In more detail, our results show that when annual precipitation is less than 500 mm, annual soil moisture and actual ET are neither negatively or positively correlated with annual temperature respectively (Figure 6.6a & b). This pattern indicates that the controls of temperature on soil moisture and actual ET highly depend on the availability of water. In areas where annual precipitation is less than 500 mm, annual temperature does not play an important role in controlling the state of soil moisture and actual ET because of the limitation of water. In other words, annual precipitation plays a more important role in controlling soil moisture and actual ET in areas where annual precipitation is less than 500 mm. These areas are mainly distributed in west China and the northern corner of the Tibetan Plateau (Figure 6.5d). In contrast, in areas annual precipitation is more than 500 mm, such as in south China and in the southern corner of the Tibetan Plateau (Figure 6.5d), annual temperature and precipitation jointly control the dynamics of soil moisture and actual ET at the land surface.

The temporal variation and climate sensitivity of soil moisture and ET in China

The annual variation of soil moisture and ET over the years 1961-2002

When the standardized (z-score) values of annual soil moisture and actual ET were plotted against time (Figure 6.7), they show that annual soil moisture tended to

decrease at a rate of 0.02 mm/yr ($r=-0.27$, $p<0.08$) in north China over the years 1961-2002 (Figure 6.7b). In contrast, annual soil moisture shows an increase at a rate of 0.03 mm/yr ($r=0.32$, $p<0.04$) in south China over the research period (Figure 6.7c). In other regions and over the whole of China, the linear trend of annual soil moisture variation was not significant over the years 1961-2002 (Figure 6.7a, d, e & f). Compared to annual soil moisture, annual actual ET tended to increase at a rate of 0.04 mm/yr ($r=0.52$, $p<0.01$) in south China (Figure 6.7c) and at a rate of 0.03 mm/yr ($r=0.31$, $p<0.05$) in the Tibetan Plateau (Figure 6.7e). In other regions, the linear trend of annual actual ET variation was non-significant.

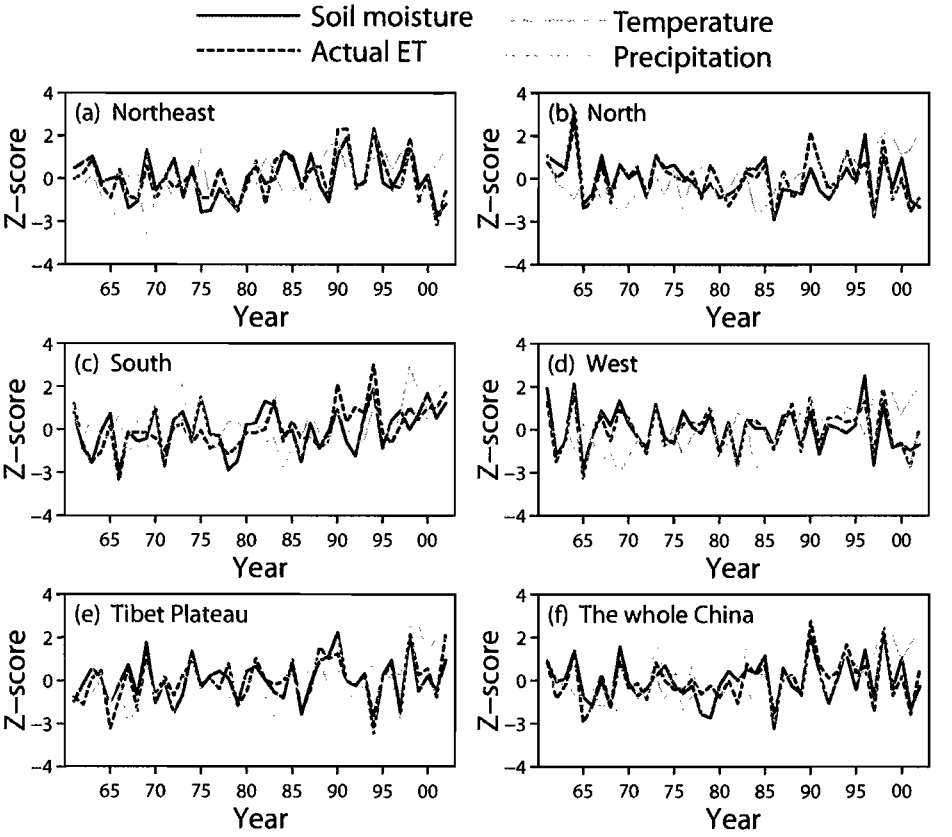

Figure 6.7 The variation of standardized (z-score) annual soil moisture (dashed blackish line) and evapotranspiration (ET) (dashed bluish line) over the years 1961-2002. The solid blackish and bluish lines are the plotted regression lines for soil moisture and ET respectively.

The sensitivity of soil moisture and ET to the variation of temperature

By allowing temperature to vary while other input climate and CO_2 variables were held constant (at the monthly average for 1961-1990) for the purpose of separating the direct effects of temperature on soil moisture and ET from others, the results suggest that the observed temperature increases from 1961 to 2002 consistently decrease annual soil moisture but increase actual ET in all regions. However, when other input variables were allowed to vary (a more realistic simulation), the negative relationship between the variation of temperature and soil moisture was significant only in west China (Figure 6.8d), in which temperature increase (annual temperature increased at a rate of 0.03 °C/yr ($r=0.60$, $p<0.01$) over the years 1961-2002 in west China) decreased annual soil moisture at a rate of 2.18 mm/yr ($r=0.33$, $p<0.04$). Further statistics suggest that surface water evaporation was not correlated with the temperature increase ($r=-0.07$, $p=0.66$) and had no increasing trend over the research period, indicating that other factors also played an important role in declining soil moisture in west China. For example, annual precipitation did not increase in west China over the years 1961-2002 (Figure 6.7d), suggesting that surface water evaporation under higher temperature condition was constrained by the limitation of water. In other regions, the non-significant relationship between temperature increase and the variation of soil moisture indicated that water was sufficient for a temperature-induced increase in surface water evaporation in all regions (Figure 6.7).

When temperature and other input data are allowed to vary, annual actual ET was significantly and positively correlated with temperature variation in south China (Figure 6.8i) and in the Tibetan Plateau of China (Figure 6.8k). In these regions, temperature increase increased annual actual ET at a rate of 22.8 mm/yr ($r=0.43$, $p<0.01$) in south China and at a rate of 12.2 mm/yr ($r=0.37$, $p<0.02$) in the Tibetan Plateau of China. The increase in annual actual ET resulted mainly from the increase in surface evaporation. For example, surface evaporation in south China increased at a rate 0.29 mm/yr ($r=0.35$, $p<0.10$) in south China as a result of temperature increase from 1961 to 2002. In addition, annual precipitation increased at a rate of 2.02 mm/yr ($r=0.27$, $p<0.09$) in south China over the research period (Figure 6.7c), indicating that surface water evaporation under

higher temperature condition was not limited by the availability of water. However, in northeast, north and west China (Figure 6.8g, h & j), annual actual ET was not significantly correlated with the temperature increase, largely because annual precipitation had no increasing trend over the years 1961-2002 (Figure 6.7a, b & d). As a result, the temperature increase tended to augment soil water stress on plants by increasing potential ET in north, northeast and west China. For example, the Priestley-Taylor soil moisture index (a ratio of actual to potential ET) was negatively correlated with temperature increase in northeast ($r=-0.23$, $p<0.15$), north ($r=-0.23$, $p<0.14$) and west China ($r=-0.25$, $p<0.11$).

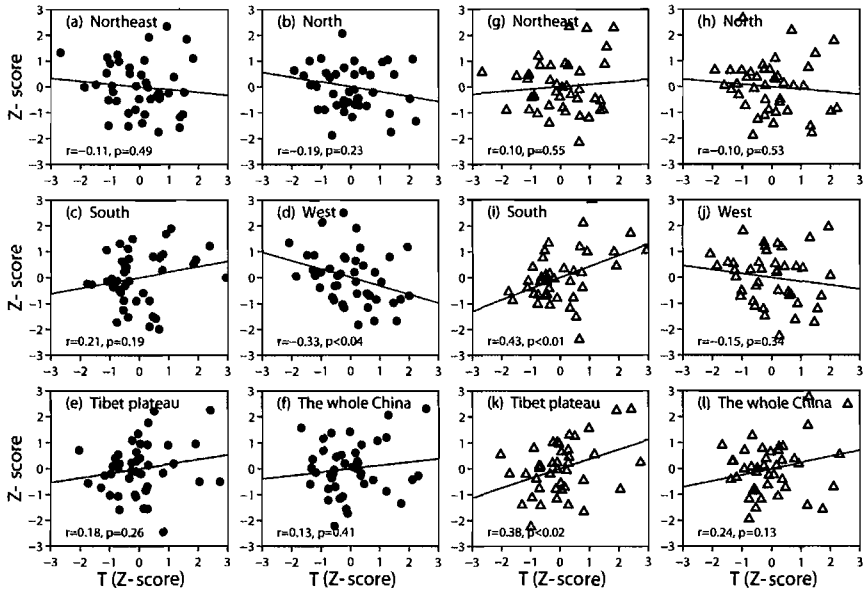

Figure 6.8 The impacts of annual mean temperature variation on soil moisture (circle) and actual ET (triangle) in different regions of China. The solid lines are the regression lines between temperature and each of soil moisture and ET respectively.

The sensitivity of soil moisture and ET to the variation of precipitation

The results indicate that annual soil moisture and actual ET are positively and linearly correlated with precipitation in all regions (Figure 6.9), reflecting the fact that soils will tend to become saturated and actual ET will likely equal potential ET when water is sufficient. For example, an increase of 1 cm in annual precipitation will increase

soil moisture by 0.12 mm ($r=0.92$, $p<0.01$), and annual actual ET by 0.88 mm ($r=0.99$, $p<0.01$) in west China. However, because of the spatiotemporal heterogeneity of annual precipitation, the strength of such a linear and positive relationship between two hydrologic variables and the variation of annual precipitation varied from one region to another. For example, the statistics suggest that annual actual ET was more sensitive to the variation of annual precipitation in west, north and northeast China ($r>0.90$, $p<0.01$) (Figure 6.9a, b & d) than that in south China ($r=0.69$, $p<0.01$) (Figure 6.9c) and in the Tibetan Plateau of China ($r=0.72$, $p<0.01$) (Figure 6.9e), indicating that water was comparatively more limiting in north, northeast and west China than in south China and in the Tibetan Plateau of China. For example, as stated before, annual precipitation showed an increase in south China (Figure 6.7c) over the study period but did not show an increase in north, northeast and west China (Figure 6.7a, b & d). Over China as a whole, annual soil moisture and actual ET were both positively correlated with the variation of precipitation ($r=0.82$, $p<0.01$) (Figure 6.9f).

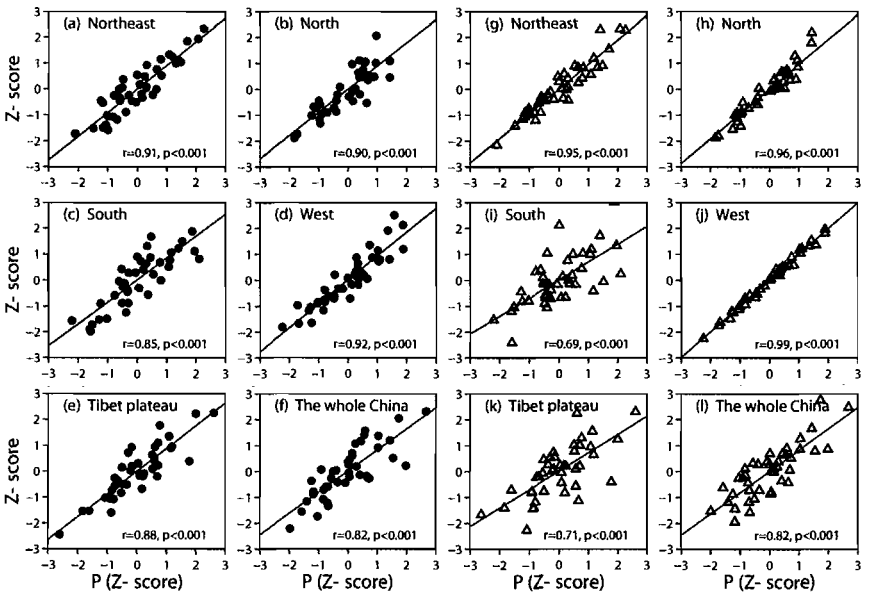

Figure 6.9 The impacts of annual precipitation variation on soil moisture (circle) and actual ET (triangle) in different regions of China and in the whole China. The solid and dashed lines are the regression lines between precipitation and each of soil moisture and ET respectively.

The sensitivity of soil moisture and ET to increase in CO_2 concentration

To analyze the effects of changes in atmospheric CO_2 concentration on soil moisture and actual ET in China, we designed three experiments with different CO_2 concentrations: (i) the reference experiment in which atmospheric CO_2 concentrations increased from 315.20 ppm in 1961 to 374.45 ppm in 2002; (ii) a low CO_2 experiment in which atmospheric CO_2 concentration was held constant at 300.82 ppm, the value of the atmospheric CO_2 concentration in 1930; and (iii) a high CO_2 experiment in which atmospheric CO_2 concentration was held constant at 520.00 ppm, the projected value of the atmospheric CO_2 concentration in 2050. In all three experiments, the input climate data used to run LH were the observed data that from 1961 to 2002.

Figure 6.10 shows the impacts of changes in atmospheric CO_2 concentration on actual ET and soil moisture in China under three experiments. Compared to the reference experiment, the low CO_2 experiment increases annual actual ET while the high CO_2 experiment decreases it in all five regions (Figure 6.10a, b, c, d, e & f), indicating that a higher CO_2 concentration is likely to induce the stomatal closure of plants thus decreasing actual ET by reducing plant transpiration. For example, annual plant transpiration in south China decreases on an average by 32.7 mm under the high CO_2 concentration experiment while it increases on an average by 10.8 mm under the low CO_2 concentration experiment. As a result, annual actual ET in south China decreases on an average by 31.2 mm under the high CO_2 concentration experiment while it increases on an average by 10.3 mm under the low CO_2 concentration experiment (Figure 6.10c). However, the impacts of both the low and high CO_2 experiments on actual ET are more discernible in northeast and south China (Figure 6.10a & c) than in the north, west and the Tibetan Plateau of China (Figure 6.10b, d & e), partially because precipitation is relatively higher in the former areas than in the later (Figure 6.5d).

The impacts of shifts in atmospheric CO_2 concentration on actual ET eventually affect the state of soil moisture at the land surface. For example, annual soil moisture increases on an average by 3.4 mm in northeast China (Figure 6.10g) and by 3.1 mm in south China (Figure 6.10i) as a result of higher CO_2 concentration-induced decrease in

actual ET. Because the impacts of shifts in atmospheric CO_2 concentration on actual ET are more discernible in south and northeast China than in west, north and the Tibetan Plateau of China, the resulting changes in soil moisture under both the low and high CO_2 experiments in relation to the reference experiments are also more remarkable in areas where water is less limiting such as in south China (Figure 6.10i) than in areas where water is more limiting such as in west China (Figure 6.10j).

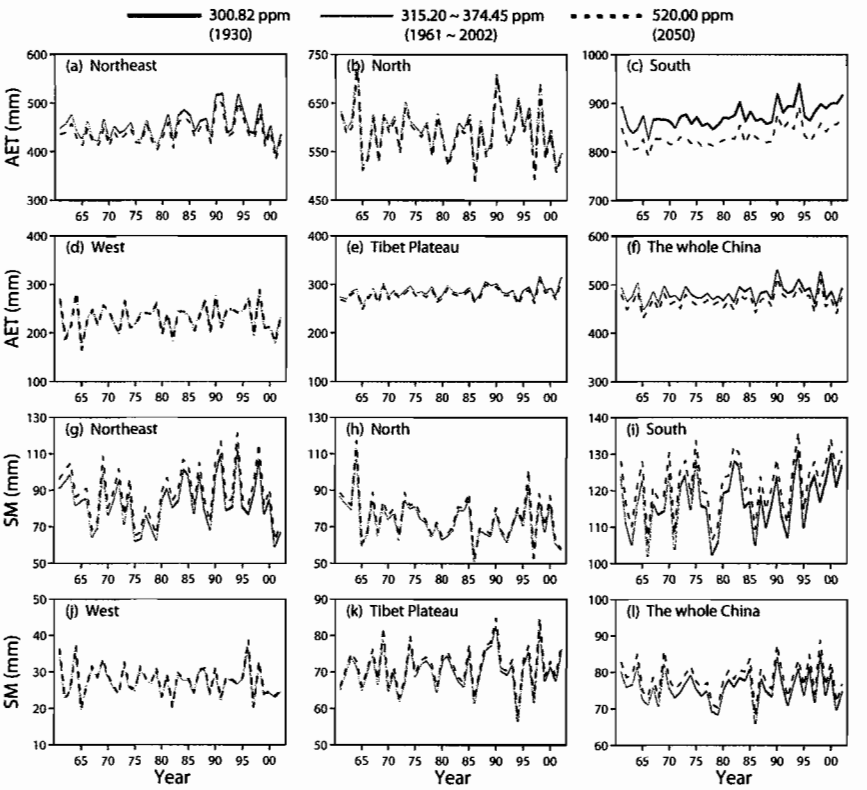

Figure 6.10 The impacts of shifts in atmospheric CO_2 concentration on actual ET and soil moisture in different regions of China under three experiments.

Conclusion

This study developed a stand-alone regional water-balance model (LH) based on the LPJ-DGVM, and used it to examine how the historical climate and atmospheric CO_2 variations influenced soil moisture and actual ET in China. The results indicate that:

(1) By specifying vegetation as an input variable and by incorporating satellite-based foliar vegetation cover data for specified vegetation, the LH model can accurately simulate terrestrial soil moisture and actual ET at the regional to global scales. Therefore, it is not only a useful tool for studying the hydrologic cycle at the land surface but also expands the application of LPJ dynamic global vegetation model.

(2) The model results show that annual soil moisture in the top 50 cm layer of soil has the highest value (about 117 mm) in south China and the lowest value (about 28.3 mm) in west China. Similar to soil moisture, annual ET was over 800 mm in south China, about 600 mm higher than annual ET in west China (less than 200 mm). Over China as a whole, both soil moisture and ET tended to decrease from the southeast to the northwest China, a pattern that highly depends on the spatial variation of temperature and precipitation in China. Temporally, soil moisture showed a decrease in north China but an increase in south China over the years 1961-2002. In contrast, annual actual ET showed an increase in both south China and the Tibetan Plateau of China.

(3) Temperature increase tended to decrease annual soil moisture in west China and increase annual actual ET in both south China and the Tibetan Plateau of China over the years 1961-2002. Unlike the temperature, annual soil moisture and actual ET were positively and linearly correlated with the variation of precipitation in all five regions over the years 1961-2002. However, the strength of such positive relationship was stronger in west, north and northeast China than that in south China and the Tibetan Plateau of China, largely because water is comparatively more limiting in west, north and northeast China than in south China and in the Tibetan Plateau.

(4) An increase in atmospheric CO_2 concentrations tends to decrease actual ET and in turn increase soil moisture. However, the impacts of changes in atmospheric CO_2 concentration are more discernible in south and northeast China where precipitation is higher than in north, west and the Tibetan Plateau of China where precipitation is low.

CHAPTER VII

CONCLUSION

The literature synthesis presented in Chapter II indicated that vegetation models have progressed from static to dynamic and to current coupled multi-objective models. However, the accuracy of model results is subject to various limitations, including the structure, assumption and parameterization of a model, the data used to run a model and to evaluate model results, the potential weakness of map comparison approaches for model evaluation, and the scaling issues in model simulation. To address these limitations, the potential strategies include (1) the development of structural and coupled dynamic vegetation models that can include as many of the factors as possible that have important roles in vegetation's structure and function, and in the cycling of carbon, nitrogen and water in terrestrial vegetation, (2) the improvement of model input and validation data, and (3) the promotion of the approaches for model evaluation and for analyzing the sensitivity and uncertainty of model results.

Through a sequence of experiments, Chapter III confirmed that the accuracy assessment of model results is sensitive to input climate data, to the selection of observed validation data, and to the choice of map comparison approaches. These sensitivities can result from the difference in vegetation tolerances of different types to climate change, the variation of monthly-mean climatologies of different length, the temporal mismatches between the data used to run a model and that used to evaluate model results, and the strength or weakness of different comparison approaches used to compare simulated and observed vegetation. Therefore, in model-based research, researcher must consider these particular factors that may lead to the uncertainty of model results. For example, the results of Chapter III indicated that the use of a 30-year monthly-mean climatology from the years immediately preceding the time that the observed data are recorded produces

the best simulation by BIOME4 of the current vegetation for Asia. The results of this study can help model users in designing experimental protocols for simulating vegetation.

As mentioned above, existing approaches for comparing or evaluating model results have their own strength and weakness. A correct comparison or evaluation requires that the weakness of selected approach be minimized. Chapter IV developed the OI index for quantifying the agreement between two simulation results. Two model simulations could be similar in most grid cells but distinct from each other in just a few, producing outliers that could unduly affect the agreement analysis of two model results if the correlation coefficient is used for such an analysis, owing to the well-known sensitivity of the correlation coefficient to outliers and influential data. In contrast, chapter IV demonstrated that the OI index is more resistant to outliers and influential data. As a result, it can in some cases quantify the agreement between two simulation results more robustly than the correlation coefficient. In addition, the results of this study indicated that the OI index provides researchers with multiple and flexible ways to compare two simulations results.

NPP is a key component in soil-vegetation-atmosphere systems and affects the cycling of carbon, water and nutrients between the biosphere and the atmosphere. Because the rates of photosynthesis and respiration of plants are sensitive to changes in environmental conditions, climate change can trigger changes in terrestrial NPP. Therefore, the climate sensitivity of terrestrial NPP has implications for understanding various feedbacks in soil-vegetation-atmosphere systems. Chapter V modified an empirical model to analyze the effects of historical climate variation on terrestrial NPP in China. The results of this study indicated that the sensitivity of terrestrial NPP in China to the historical climate variation differed from one region to another because of the spatial heterogeneity of prevailing climate conditions and human activities among different regions. In more detail, the results of this study revealed that the variability of NPP in the north-west arid zone and in the Tibetan Plateau frigid zone of China was mainly correlated with climatic variation. In contrast, climatic variation and human activities jointly controlled the NPP dynamics in the east monsoon zone of China.

Soil moisture and actual evapotranspiration (ET) are two other key components of soil-vegetation-atmosphere systems and influence many important processes linking the biosphere and the atmosphere. Dynamic vegetation models of high sophistication have illustrated their general ability to simulate various mechanisms, such as water balance, in soil-vegetation-atmosphere systems. However, they still may not correctly simulate vegetation at the regional scale because of their inadequacy in incorporating important factors controlling terrestrial vegetation, and so simulations of the surface water balance will be only as good as the vegetation simulations. Also, the results from such applications should also be sensitive to the direct and indirect effects of CO_2 in order to correctly simulate the relative importance of climate and atmospheric composition on hydrological processes. To address these issues, Chapter VI developed the LH model that used prescribed (as opposed to simulated) vegetation and CO_2 (along with the usual soils and climate data). This model was developed by modifying LPJ dynamic global vegetation model, and was applied as a case study for China. The evaluation of the LH model using observed data sets demonstrated that LH can accurately simulate soil moisture, actual ET and surface runoff at the land surface. The results of this study also indicated that the spatial pattern of soil moisture and actual ET in China decreases spatially from the southeast to the northwest China, a pattern that matches the spatial pattern of temperature and precipitation change in China. In depth, the study shows that the impacts of temperature on soil moisture and actual ET are confined to annul precipitation. In areas where annual precipitation is less than 500 mm, the effects of changes in annual temperature on soil moisture and actual ET are negligible. Increase in atmospheric CO_2 concentration tends to decrease actual ET by inducing stomatal closure, thus increasing soil moisture.

APPENDIX A

THE ALGEBRA OF THE OPPOSITE AND IDENTITY (OI) INDEX

Assume that a and b refer to two sets of time-series simulations. Let vector $a_{i,j}$ and $b_{i,j}$ $(i = 1,2,\ldots,m;\ j = 1,2\ldots,n)$ be the simulated anomalies of an ecological variable in grid cell i at time-step j, where m and n are the total numbers of grid cells and time-steps respectively. Let $c_{i,j}$ be the vector sum of $a_{i,j}$ and $b_{i,j}$, and $\alpha_{i,j}$ be the acute angle between the vector sum $c_{i,j}$ and the identity axis. Thus, the magnitude of $c_{i,j}$ and the acute angle $\alpha_{i,j}$ are calculated through the following equations:

$$\left|c_{i,j}\right| = \sqrt{\left|a_{i,j}\right|^2 + \left|b_{i,j}\right|^2} \quad i = 1,2,\ldots,m;\ j = 1,2,\ldots,n \tag{1}$$

$$\alpha_{i,j} = \begin{cases} \beta_{i,j} - 45.0 & \text{if } a_{i,j}b_{i,j} > 0 \ \&\ \left|a_{i,j}\right| > \left|b_{i,j}\right| \\ 45.0 - \beta_{i,j} & \text{if } a_{i,j}b_{i,j} > 0 \ \&\ \left|a_{i,j}\right| \le \left|b_{i,j}\right| \\ \beta_{i,j} + 45.0 & \text{if } a_{i,j}b_{i,j} < 0 \ \&\ \left|a_{i,j}\right| < \left|b_{i,j}\right| \\ 135.0 - \beta_{i,j} & \text{if } a_{i,j}b_{i,j} < 0 \ \&\ \left|a_{i,j}\right| \ge \left|b_{i,j}\right| \\ 45.0 & \text{if } \left|a_{i,j}\right| = 0 \ \&\ \left|b_{i,j}\right| \ne 0 \quad or \quad \left|a_{i,j}\right| \ne 0 \ \&\ \left|b_{i,j}\right| = 0 \\ 0.0 & \text{if } \left|a_{i,j}\right| = 0 \ \&\ \left|b_{i,j}\right| = 0 \end{cases} \quad \begin{array}{l} i = 1,2,\ldots,m \\ j = 1,2,\ldots,n \end{array} \tag{2}$$

where $\beta_{i,j} = \cos^{-1}(\left|b_{i,j}\right| / \left|c_{i,j}\right|)$, and $\left|a_{i,j}\right|$ and $\left|b_{i,j}\right|$ are the magnitudes of vector $a_{i,j}$ and $b_{i,j}$ respectively. The "if expression" in equation 2 suggests that the calculation of $\alpha_{i,j}$ depends on both the directions and magnitudes of vector $a_{i,j}$ and $b_{i,j}$.

Given that all resultant vectors $c_{i,j}$ $(i = 1,2,\ldots,m;\ j = 1,2,\ldots,n)$ start from the same tail (the origin in the Cartesian plane) with the direction determined by the acute angle $\alpha_{i,j}$, we can put them in a transformed coordinate plane for further analysis (see an example in Figure 1 below).

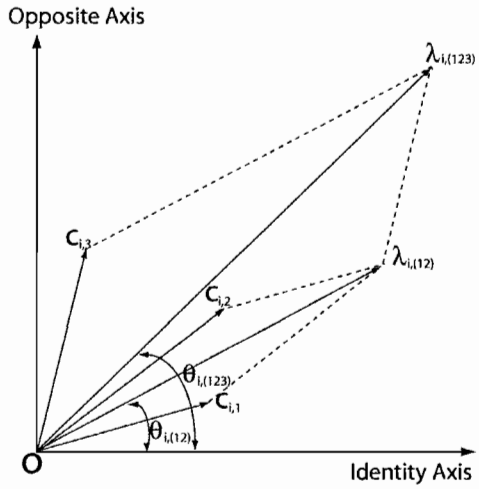

Figure A.1 An example: using a transformed coordinate plane for integrating three resultant vectors $c_{i,j}$ $(j=1,2,3)$ in grid cell i. $c_{i,j}$ is the vector sum of $a_{i,j}$ and $b_{i,j}$ $(j=1,2,3)$. $a_{i,j}$ and $b_{i,j}$ represents the simulated anomalies of an ecological variable in the grid cell i and at time-step j respectively. $\lambda_{i,(12)}$ is the vector sum of $c_{i,1}$ and $c_{i,2}$, and $\theta_{i,(12)}$ is the acute angle between the vector sum $\lambda_{i,(12)}$ and the identity axis. $\lambda_{i,(123)}$ is the vector sum of $c_{i,1}$, $c_{i,2}$ and $c_{i,3}$, and $\theta_{i,(123)}$ is the acute angle between the vector sum $\lambda_{i,(123)}$ and the identity axis.

Let vector λ_i be the vector sum of all vectors $c_{i,j}$ $(j=1,2,\ldots,n)$ in grid cell i and θ_i be the angle between the vector sum λ_i and the identity axis. By the Pythagorean Theorem, the magnitude of λ_i and θ_i are expressed by the following equations:

$$|\lambda_i| = \sqrt{(\sum_{j=1}^{n}|c_{i,j}|\cos\alpha_{i,j})^2 + (\sum_{j=1}^{n}|c_{i,j}|\sin\alpha_{i,j})^2} \quad i=1,2,\ldots,m \tag{3}$$

$$\theta_i = \tan^{-1}(\sum_{j=1}^{n}|c_{i,j}|\sin\alpha_{i,j} / \sum_{j=1}^{n}|c_{i,j}|\cos\alpha_{i,j}) \quad i=1,2,\ldots,m \tag{4}$$

In theory, the size of θ_i reflects the integrated difference between two sets of simulated anomalies in grid cell i and at all time. Thus, the opposite and identity (OI) index of two simulations results in grid cell i and at all time is defined as:

$$OI_i = 1-\theta_i/90.0° \quad i=1,2,\ldots,m \tag{5}$$

To analyze the overall agreement between two simulation results, let vector λ be the vector sum of all vectors $c_{i,j}$ $(i = 1,2,\ldots,m;\ j = 1,2,\ldots,n)$ and θ be the angle between the vector sum λ and the identity axis. According to the Pythagorean Theorem again, the magnitude of λ and the acute angle θ are expressed as:

$$|\lambda| = \sqrt{(\sum_{i=1}^{m}\sum_{j=1}^{n}|c_{i,j}|\cos\alpha_{i,j})^2 + (\sum_{i=1}^{m}\sum_{j=1}^{n}|c_{i,j}|\sin\alpha_{i,j})^2} \tag{6}$$

$$\theta = \tan^{-1}(\sum_{i=1}^{m}\sum_{j=1}^{n}|c_{i,j}|\sin\alpha_{i,j} / \sum_{i=1}^{m}\sum_{j=1}^{n}|c_{i,j}|\cos\alpha_{i,j}) \tag{7}$$

Similarly, the size of θ reflects the overall difference between two sets of simulated anomalies in the whole study area or in a given biome (when m represents the number of grid cells for a given biome) and at all time. Thus, the overall OI (OOI) index of two simulation results is defined as:

$$OOI = 1 - \theta / 90.0° \tag{8}$$

The equation 6 and 7 can be transformed into the following expressions by keeping the time-step j variable:

$$|\lambda_j| = \sqrt{(\sum_{i=1}^{m}|c_{i,j}|\cos\alpha_{i,j})^2 + (\sum_{i=1}^{m}|c_{i,j}|\sin\alpha_{i,j})^2} \quad j = 1,2,\ldots,n \tag{9}$$

$$\theta_j = \tan^{-1}(\sum_{i=1}^{m}|c_{i,j}|\sin\alpha_{i,j} / \sum_{i=1}^{m}|c_{i,j}|\cos\alpha_{i,j}) \quad j = 1,2,\ldots,n \tag{10}$$

where λ_j is the vector sum of all vectors $c_{i,j}$ $(i = 1,2,\ldots,m)$ at time j , θ_j refers to the angle between the vector sum λ_j and the identity axis. The size of θ_j reflects the difference between two sets of simulated anomalies at time-step j. Correspondingly, the OI index of two simulation results at time-step j is defined as:

$$OI_j = 1 - \theta_j / 90.0° \qquad j = 1,2,\ldots,n \tag{11}$$

FORTRAN90 subroutine for calculating the OI index at a grid cell and at all time for equation 5

```
Subroutine OI_index(N,X,Y,OI,R)
  ! the meanings of input,output and local variables::
  ! n--the number of data points (or time-steps) in each of compared datasets
  ! x--input datasets x or simulated time-series values from one model
  ! y--input datasets y or simulated time-series values from another model or observation
  ! OI-the opposite and identity index
  ! R--Pearson correlation coefficient
  ! xl--the length of the vector sum based on dataset x
  ! yl--the lenght of the vector sum based on dataset y
  ! xmean--the mean of dataset x
  ! ymean--the mean of dataset y
  ! dev1--the deviation of each individual value in dataset x from xmean
  ! dev2--the deviation of each individual value in dataset y from ymean
  ! angle--the acute anagle between the final vector sum and the defined identity axis
  ! magnitude--the length of the vector sum of two compared anomalies
  ! degree--the acute anagle between the vector sum of two compared anomlies and the
  ! defined identity axis
Implicit none
  ! input variables
  integer,intent(in)                  :: n
  real*4,intent(in),dimension(n)   :: x,y
  ! output variables
  real*4,intent(out)                  :: OI,R
  ! local variables
  integer                             :: i,j,m,yr,status
  real*4,allocatable,dimension(:):: degree,magnitude,dev1,dev2
  real*4                              :: xmean,ymean,xl,yl,angle
  ! local variables used to calculate Pearson's coefficient
  real,dimension(n)                   :: xdevydev,Sxdev,Sydev
  real                                :: Sxdevydev,SSxdev,SSydev

  allocate(degree(n),stat=status);    allocate(magnitude(n),stat=status)
  allocate(dev1(n),stat=status);      allocate(dev2(n),stat=status)
  xmean=sum(x)/(n*1.0);    ymean=sum(y)/(n*1.0)

  ! Calculating the acute angel between two compared anomlies
  do yr=1,n
    dev1(yr)=(X(yr)-xmean)
    dev2(yr)=(Y(yr)-ymean)
    magnitude(yr)=sqrt(dev1(yr)**2+dev2(yr)**2)

    if  (dev2(yr).ne.0.0.and.dev1(yr).ne.0.0) then
     if    (dev1(yr)*dev2(yr).gt.0.0 .and. abs(dev1(yr)).gt.abs(dev2(yr))) then
       degree(yr)=acosd(abs(dev2(yr))/magnitude(yr))-45.0
     elseif(dev1(yr)*dev2(yr).gt.0.0 .and. abs(dev1(yr)).le.abs(dev2(yr))) then
       degree(yr)=45.0-acosd(abs(dev2(yr))/magnitude(yr))
     elseif(dev1(yr)*dev2(yr).lt.0.0 .and. abs(dev1(yr)).lt.abs(dev2(yr))) then
       degree(yr)=acosd(abs(dev2(yr))/magnitude(yr))+45.0
     elseif(dev1(yr)*dev2(yr).lt.0.0 .and. abs(dev1(yr)).ge.abs(dev2(yr))) then
```

```
          degree(yr)=135.0-acosd(abs(dev2(yr))/magnitude(yr))
        endif
      elseif(dev2(yr).eq.0.0.and.dev1(yr).eq.0.0) then
        degree(yr)=0.0
      else
        degree(yr)=45.0
      endif
    enddo

    ! Calculating the mangitude of the final vector sum from two compared datasets X and Y
    xl=0.0;yl=0.0
    do i=1,n
      xl=cosd(degree(i))*magnitude(i)+xl
      yl=sind(degree(i))*magnitude(i)+yl
    enddo

    ! Calculating the acuate angle between the final vector sum and the defined identity axis
    If(xl.eq.0 .and. yl.ne.0 ) then
      angle=90
    elseif(xl.ne.0 .and.yl.eq.0) then
      angle=0
    elseif(xl.ne.0. .and.yl.ne.0) then
      angle=atand(yl/xl)
    endif
    ! Calcualting the OI index
    OI=1-angle/90.0

    ! Calculate Pearson's correlation coefficient (r)
    Sxdevydev=0.0; SSxdev=0.0; SSydev=0.0
    do i=1,n
      xdevydev(i)  = dev1(i)*dev2(i)
      Sxdevydev   = Sxdevydev+xdevydev(i)
      Sxdev(i)     = dev1(i)**2
      Sydev(i)     = dev2(i)**2
      SSxdev       = SSxdev+Sxdev(i)
      SSydev       = SSydev+Sydev(i)
    enddo
    r=Sxdevydev/sqrt(SSxdev*SSydev)

    deallocate(degree,stat=status)
    deallocate(magnitude,stat=status)
    deallocate(dev1,stat=status)
    deallocate(dev2,stat=status)
end subroutine OI_index
```

Note: To calculate the overall OI index for a given biome or plant functional type (see equation 8 in S1), the user need to modify the dimesion of relatvant vriables from one to two. Please feel free to contact the author by gtang1@uoregon.edu for any question, comment and requirement.

APPENDIX B

COMPARISON BETWEEN THE OI INDEX AND THE CORRELATION COEFFICIENT

The basic concepts underlying the OI index and the Pearson correlation coefficient are somewhat similar, because both are based on the means of two datasets and the deviation of each value in the two datasets from these means. Taking the OOI index (see equation 2) as an example, let $a_{i,j}$ and $b_{i,j}$ be the deviations of $A_{i,j}$ and $B_{i,j}$ from the means of datasets A and B, respectively. Let point P (Figure 2) be a random sample of the points ($a_{i,j}$, $b_{i,j}$) derived from datasets A and B. The coordinates of P are OL=$a_{i,j}$ and LP=$b_{i,j}$. Let the perpendicular distance PM be denoted by $d_{i,j}$, and the acute angle between OP and the line $b_{i,j} = a_{i,j}$ be denoted by $\alpha_{i,j}$. Thus, it is seen that (Jackson, 1924):

$$d_{i,j} = \frac{(b_{i,j} - a_{i,j})}{\sqrt{2}} \tag{12}$$

Because of the fact that: $OP = \sqrt{a_{i,j}^2 + b_{i,j}^2} = |c_{i,j}|$, where $|c_{i,j}|$ is the magnitude of vector $c_{i,j}$, which is the vector sum of $a_{i,j}$ and $b_{i,j}$; $PM = |c_{i,j}| * \sin\alpha_{i,j} = d_{i,j}$ and $OM = |c_{i,j}| * \cos\alpha_{i,j} = \sqrt{OP^2 - d_{i,j}^2} = \sqrt{a_{i,j}^2 + b_{i,j}^2 - d_{i,j}^2}$. Thus, the equation 8 can be transformed into the following expression:

$$OOI = 1 - \tan^{-1}\left(\sum_{i=1}^{m}\sum_{j=1}^{n} d_{i,j} \Big/ \sum_{i=1}^{m}\sum_{j=1}^{n}\sqrt{a_{i,j}^2 + b_{i,j}^2 - d_{i,j}^2}\right)/90.0° \tag{13}$$

By introducing equation 12, the equation 13 can be further transformed into:

$$OOI = 1 - \tan^{-1}\left(\sum_{i=1}^{m}\sum_{j=1}^{n}(b_{i,j} - a_{i,j}) \Big/ \sum_{i=1}^{m}\sum_{j=1}^{n}(b_{i,j} + a_{i,j})\right)/90.0° \tag{14}$$

According to Jackson (1924), the correlation (r) is mathematically expressed as:

$$r = \begin{cases} 1-(\sum_{i=1}^{m}\sum_{j=1}^{n}(b_{i,j}-a_{i,j})^2/(2m*n)) & a_{i,j}b_{i,j} \geq 0 \\ -1+(\sum_{i=1}^{m}\sum_{j=1}^{n}(b_{i,j}+a_{i,j})^2/(2m*n)) & a_{i,j}b_{i,j} < 0 \end{cases} \quad (15)$$

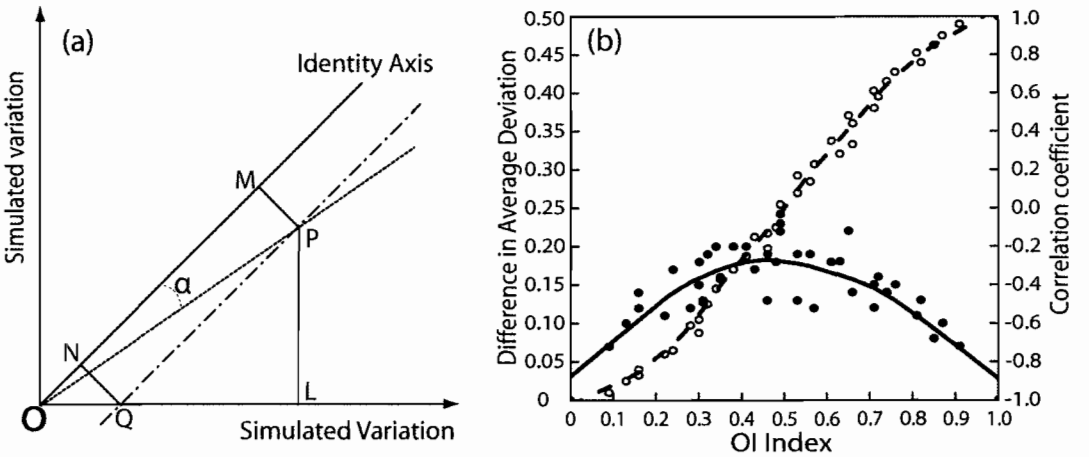

Figure B.1 (a): For any point P, the OI index depends on the measure of the acute angle α and the correlation is associated with the perpendicular distance PM. (b): the relationship (as shown by the dashed line) between the OI index and the correlation, and the relationship (as shown by the solid black curve) between the OI index and the difference in the averaged deviations of two compared datasets from their corresponding means. Each data point in (b) is based on two sets of data points that are randomly created with values between 0 and 1. The number of data points in each dataset is 16.

APPENDIX C

SELECTED NPP INVENTORY DATA FOR DETERMINING THE ε_{max} IN EACH BIOME

Table C.1 Description of selected NPP inventory data for determining the ε_{max} in each of biomes

Biome types	Data sources	Location	Data description	ε_{max}
Tropical forest	Zheng et al., (2003)	Asia	NPP for multi-biomes	0.67
Temperate forest	Zheng et al., (2003)	Asia	NPP for multi-biomes	0.56
Boreal forest	Zheng et al., (2003)	Asia	NPP for multi-biomes	0.82
Temperate herbaceous	Togtohyn & Ojima, (1996)	Mongolia	NPP grassland for 1982-1990	
		China	NPP grassland for 1980-1989	0.46
	Xiao & Ojima, (1996)	China	NPP grassland for 1981-1990	
	Xiao & Ojima, (1999)			
Tropical herbaceous	Pandey & Singh, (1997)	India	NPP grassland for 1986-1989	0.64

Data sources:

Pandey, C.B. & Singh, J.S. (1997) NPP Grassland: Vindhyan, India, 1986-1989. Data set. Available on-line [http://www.daac.ornl.gov] from Oak Ridge National Laboratory Distributed Active Archive Center, Oak Ridge, Tennessee, U.S.A.

Togtohyn, C. & Ojima, D. (1996) NPP Grassland: Tumentsogt, Mongolia, 1982-1990. Data set. Available on-line [http://www.daac.ornl.gov] from Oak Ridge National Laboratory Distributed Active Archive Center, Oak Ridge, Tennessee, U.S.A.

Xiao, X.M. & Ojima, D. (1999) NPP Grassland: Tumugi, China, 1981-1990. Data set. Available on-line [http://www.daac.ornl.gov] from Oak Ridge National Laboratory Distributed Active Archive Center, Oak Ridge, Tennessee, U.S.A.

Xiao, X.M., Chen, D., Peng, Y.M., Cui, X.Y. & Ojima, D.S. (1996) Observation and modeling of plant biomass of meadow steppe in Tumugi, Xingan league, Inner Mongolia, China. *Plant Ecology*, 127, 191-201.

Zheng, D.L., Prince, S.D. & Wright, R. (2003) Terrestrial net primary production estimates for 0.5 degree grid cells from field observations-a contribution to global biogeochemical modeling. *Global Change Biology,* 9, 46-64.

APPENDIX D

THE LOW AND HIGH TEMPERATURE LIMITS FOR CO_2 UPTAKE AND THE OPTIMUM PHOTOSYNTHETICAL TEMPERATURE

Table D.1 The temperature limits for CO_2 uptake and the temperature optimum for photosynthesis

PFTs simulated by LPJ	T_{low} (°C)	T_{opt1} (°C)	T_{opt2} (°C)	T_{high} (°C)
Tropical broad-leaved evergreen woody (TrBE)	2.0	25.0	30.0	55.0
Tropical broad-leaved raingreen woody (TrBR)	2.0	25.0	30.0	55.0
Temperate needle-leaved evergreen woody (TeNE)	-4.0	20.0	30.0	42.0
Temperate broad-leaved evergreen woody (TeBE)	-4.0	20.0	30.0	42.0
Temperate broad-leaved summergreen woody (TeBS)	-4.0	20.0	25.0	38.0
Boreal needle-leaved evergreen woody (BoNE)	-4.0	15.0	25.0	38.0
Boreal needle-leaved summergreen woody (BoNS)	-4.0	15.0	25.0	38.0
Boreal broad-leaved summergreen woody (BoBS)	-4.0	15.0	25.0	38.0
Temperate herbaceous (TeH)	-4.0	10.0	30.0	45.0
Tropical herbaceous (TrH)	6.0	20.0	45.0	55.0

Data source: Sitch, S., Smith, B., Prentice, I.C., Arneth, A., Bondeau, A., Cramer, W., Kaplan, J.O., Levis, S., Lucht, W., Sykes, M.T., Thonicke, K. & Venevsky, S. (2003) Evaluation of ecosystem dynamics, plant geography and terrestrial carbon cycling in the LPJ Dynamic Global Vegetation Model. *Global Change Biology*, 9, 161-185.

BIBLIOGRAPHY

Chapter I

Brogaard, S., Runnstrom, M., and Seaquist, J. W., 2005, Primary production of Inner Mongolia, China, between 1982 and 1999 estimated by a satellite data-driven light use efficiency model. *Global and Planetary Change*, 45, 313-332.

Gao, G., D. Chen, C.Y. Xu, and E. Simelton. 2007. Trend of estimated actual evapotranspiration over China during 1960-2002. *Journal of Geophysical Research-Atmospheres* **112**:doi:10.1029/2006JD008010.

Kaplan JO, Prentice IC, Buchmann N. 2002. The stable carbon isotope composition of the terrestrial biosphere: Modeling at scales from the leaf to the globe. *Global Biogeochemical Cycles* 16: 1060.

Mitchell TD, Carter TR, Jones PD, Hulme M, New M. 2004. A comprehensive set of high-resolution grids of monthly climate for Europe and the globe: the observed record (1901–2000) and 16 scenarios (2001–2100). Tyndall Working Paper 55, 25pp, Tyndall Centre, UEA, Norwich, UK.

Potter, C. S., and Klooster, S. A.. 1999. Detecting a terrestrial biosphere sink for carbon dioxide: Interannual ecosystem modeling for the mid-1980s. *Climatic Change* 42: 489-503.

Sitch, S., Smith, B., Prentice, I. C., Arneth, A., Bondeau, A., Cramer, W., Kaplan, J. O., Levis, S., Lucht, W., Sykes, M. T., Thonicke, K., and Venevsky, S.. 2003. Evaluation of ecosystem dynamics, plant geography and terrestrial carbon cycling in the LPJ Dynamic Global Vegetation Model. *Global Change Biology* 9: 161-185.

Tang, G. 2008. A new metric for evaluating the correspondence of spatial patterns in vegetation models. *Global Ecology and Biogeography* 17:465-478.

Zhao, M., and Zhou, G. S., 2006, Estimating net primary productivity of Chinese pine forests based on forest inventory data. *Forestry*, 79, 231-239.

Chapter II

Adams, R.M., B.A. McCarl, and L.O. Mearns. 2003. The effects of spatial scale of climate scenarios on economic assessments: An example from US agriculture. *Climatic Change* **60**:131-148.

Araujo, M.B., and A. Guisan. 2006. Five (or so) challenges for species distribution modelling. *Journal of Biogeography* **33**:1677-1688.

Arora, V.K., and G.J. Boer. 2005. A parameterization of leaf phenology for the terrestrial ecosystem component of climate models. *Global Change Biology* **11**:39-59.

Arora, V.K., and G.J. Boer. 2006. Simulating competition and coexistence between plant functional types in a dynamic vegetation model. *Earth Interactions* **10**:1-30.

Bachelet, D., R.P. Neilson, J.M. Lenihan, and R.J. Drapek. 2001. Climate change effects on vegetation distribution and carbon budget in the United States. *Ecosystems* **4**:164-185.

Barrett, D.J., I.E. Galbally, and R.D. Graetz. 2001. Quantifying uncertainty in estimates of C emissions from above-ground biomass due to historic land-use change to cropping in Australia. *Global Change Biology* 7: 883-902.

Berthelot, M., P. Friedlingstein, P. Ciais, J.L. Dufresne, and P. Monfray. 2005. How uncertainties in future climate change predictions translate into future terrestrial carbon fluxes. *Global Change Biology* **11**: 959-970.

Bolliger, J., F. Kienast, and H. Bugmann. 2000. Comparing models for tree distributions: concept, structures, and behavior. *Ecological Modelling* **134**:89-102.

Bond-Lamberty, B., S.T. Gower, D.E. Ahl, and P.E. Thornton. 2005. Reimplementation of the Biome-BGC model to simulate successional change. *Tree Physiology* **25**:413-424.

Box, E.O. 1981. Macroclimate and Plant Forms: an Introduction to Predictive Modeling in Phytogeography. Dr W Junk Publishers, The Hague.

Burke, I.C., W.K. Lauenroth, and W.J. Parton. 1997. Regional and temporal variation in net primary production and nitrogen mineralization in grasslands. *Ecology* **78**:1330-1340.

Calef, M.P., A.D. McGuire, H.E. Epstein, T.S. Rupp, and H.H. Shugart. 2005. Analysis of vegetation distribution in Interior Alaska and sensitivity to climate change using a logistic regression approach. *Journal of Biogeography* **32**:863-878.

Camill, P. 2000. How much do local factors matter for predicting transient ecosystem dynamics? Suggestions from permafrost formation in boreal peatlands. *Global Change Biology* **6**: 169-182.

Campbell, J.B. 2002. Accuracy assessment. In: Introduction to Remote Sensing (3rd Ed.), pp. 383-406. The Guilford Press. New York. London

Cao, M.K., G.R. Yu, J.Y. Liu, and K.R. Li. 2005. Multi-scale observation and cross-scale mechanistic modeling on terrestrial ecosystem carbon cycle. *Science in China Series D-Earth Sciences* 48:17-32.

Chen, H., H.Q. Tian, M.L. Liu, J. Melillo, S.F. Pan, and C. Zhang. 2006. Effect of land-cover change on terrestrial carbon dynamics in the southern United States. *Journal of Environmental Quality* **354**:1533-1547.

Congalton, R.G. 1991. A review of assessing the accuracy of classifications of remotely sensed data. *Remote Sensing of Environment* **37**:35-46.

Congalton, R.G., and K. Green. 1999. Assessing the accuracy of remotely sensed data: Principles and practices. Boca Raton: CRC press.

Cowling, S.A., and Y. Shin. 2006. Simulated ecosystem threshold responses to co-varying temperature, precipitation and atmospheric CO_2 within a region of Amazonia. *Global Ecology and Biogeography* **15**:553-566.

Cramer, W. 2002. Biome models. Volume 2, the Earth system: biological and ecological dimensional of global environmental change, pp 166-171. In: Encyclopedia of Global Environmental Change. Edited by Mooney, H.A. and Canadell, J.G., John Wiley & Sons, Ltd, Chichester, 2002

Cramer, W., A. Bondeau, S. Schaphoff, W. Lucht, B. Smith, and S. Sitch. 2004. Tropical forests and the global carbon cycle: impacts of atmospheric carbon dioxide, climate change and rate of deforestation. *Philosophical Transactions of the Royal Society of London Series B-Biological Sciences* **359**:331-343.

Dale, V.H., and H.M. Rauscher. 1994. Assessing Impacts of Climate-Change on Forests - the State of Biological Modeling. *Climatic Change* **28**:65-90.

Daly, C., D. Bachelet, J.M. Lenihan, R.P. Neilson, W.J. Parton, and D. Ojima. 2000. Dynamic simulation of tree-grass interactions for global change studies. *Ecological Applications* **10**:449-469.

Fielding, A.H., and J.F. Bell. 1997. A review of methods for the assessment of prediction errors in conservation presence/absence models. *Environmental Conservation* **24**:38-49.

Foley, J.A., S. Levis, M.H. Costa, W. Cramer, and D. Pollard. 2000. Incorporating dynamic vegetation cover within global climate models. *Ecological Applications* **10**:1620-1632.

Foody, G.M. 1992. On the compensation for chance agreement in image classification accuracy assessment. *Photogrammetric Engineering and Remote Sensing* **58**:1459-1460.

Foody, G.M. 2002. Status of land cover classification accuracy assessment. *Remote Sensing of Environment* **80**:185-201.

Forest, C.E., P.H. Stone, A.P. Sokolov, R.A. Myles, and M.D. Webster. 2002. Quantifying uncertainties in climate system properties with the use of recent climate observations. *Science* **295**:113-117.

Gifford, R.M. 1992. Implications of the Globally Increasing Atmospheric CO_2 Concentration and Temperature for the Australian Terrestrial Carbon Budget - Integration Using a Simple-Model. *Australian Journal of Botany* **40**:527-543.

Gifford, R.M. 2003. Plant respiration in productivity models: conceptualisation, representation and issues for global terrestrial carbon-cycle research. Functional Plant Biology **30**:171-186.

Gordon, W.S., J.S. Famiglietti, N.L. Fowler, T.G.F. Kittel, K.A. Hibbard. 2004. Validation of simulated runoff from six terrestrial ecosystem models: Results from VEMAP. *Ecological Applications* **14**:527-545.

Grieb, T.M., R.J.M. Hudson, N. Shang, R.C. Spear, S.A. Gherini, and R.A. Goldstein. 1999. Examination of model uncertainty and parameter interaction in a global carbon cycling model (GLOCO). *Environment International* **25**:787-803.

Hagen, A. 2003. Fuzzy set approach to assessing similarity of categorical maps. *International Journal of Geographical Information Science* **17**:235-249.

Halldin, S., H. Bergstrom, D. Gustafsson, L. Dahlgren, P. Hjelm, L.-C. Lundin, P.-E. Mellander, T. Nord, P.-E. Jansson, J. Seibert, M. Stähli, A. Szilágyi Kishné, and A.-S. Smedman. 1999. Continuous long-term measurements of soil-plant-atmosphere variables at an agricultural site. *Agricultural and Forest Meteorology* **98**:75-102.

Hallgren, W.S., and A.J. Pitman. 2000. The uncertainty in simulations by a Global Biome Model (BIOMES to alternative parameter values. *Global Change Biology* **6**:483-495.

Hanson, P.J., S.D. Wullschleger, R.J. Norby, T.J. Tschaplinski, and C.A. Gunderson. 2005. Importance of changing CO_2, temperature, precipitation, and ozone on carbon and water cycles of an upland-oak forest: incorporating experimental results into model simulations. *Global Change Biology* **11**:1402-1423.

Haxeltine, A., and I.C. Prentice. 1996. BIOME3: An equilibrium terrestrial biosphere model based on ecophysiolical constraints, resource availability, and competition among plant functional types. *Global Biogeochemical Cycles* **10**:693-709

Hickler, T., B. Smith, M.T. Sykes, M.B. Davis, S. Sugita, and K. Walker. 2004. Using a generalized vegetation model to simulate vegetation dynamics in northeastern USA. *Ecology* **85**:519-530.

Higgins, S.I., J.S. Clark, R. Nathan, T. Hovestadt, F. Schurr, J.M.V. Fragoso, M.R. Aguiar, E. Ribbens, and S. Lavorel. 2003. Forecasting plant migration rates: managing uncertainty for risk assessment. *Journal of Ecology* **91**:341-347.

Higgins, P.A.T., and M. Vellinga. 2004. Ecosystem responses to abrupt climate change: Teleconnections, scale and the hydrological cycle. *Climatic Change* **64**:127-142.

Hinzman, L.D., N.D. Bettez, W.R. Bolton, F.S. Chapin, M.B. Dyurgerov, C.L. Fastie, B. Griffith, R.D. Hollister, A. Hope, H.P. Huntington, A.M. Jensen, G.J. Jia, T. Jorgenson, D.L. Kane, D.R. Klein, G. Kofinas, A.H. Lynch, A.H. Lloyd, A. D. McGuire, F.E. Nelson, W.C. Oechel, T.E. Osterkamp, C.H. Racine, V. E. Romanovsky, R. S. Stone, D.A. Stow, M. Sturm, C.E. Tweedie, G.L. Vourlitis, M.D. Walker, D.A. Walker, P.J. Webber, J.M. Welker, K.S. Winker, and K. Yoshikawa1. 2005. Evidence and implications of recent climate change in northern Alaska and other arctic regions. *Climatic Change* **72**:251-298.

Holdridge, L.R., 1947. Determination of world plant formations from simple climate data. *Science* **105**:367-368.

Hollister, R.D., P.J. Webber, and C. Bay. 2005. Plant response to temperature in Northern Alaska: Implications for predicting vegetation change. *Ecology* ***86***:1562-1570.

Homann, P.S., R.B. McKane, and P. Sollins. 2000. Belowground processes in forest-ecosystem biogeochemical simulation models. *Forest Ecology and Management* **138**:3-18.

House, J.I., I.C. Prentice, N. Rammankutty, R.A. Houghton, and M. Heimann. 2003. Reconciling apparent inconsistencies in estimates of terrestrial CO_2 sources and sinks. *Tellus Series B-Chemical and Physical Meteorology* **55**:345-363.

Huntley, B., P.M. Berry, W. Cramer, and A.P. McDonald. 1995. Modelling present and potential future ranges of some European higher plants using climate response surfaces. *Journal of Biogeography* **22**:967-1001.

IPCC. 2001. Climate Change 2001: Impacts, Adaptation, and Vulnerability. Contribution of Working Group II to the Third Assessment Report of the Intergovernmental Panel on Climate Change. Cambridge University Press, 2001

Ito, A., and T. Oikawa. 2002. A simulation model of the carbon cycle in land ecosystems .Sim-CYCLE: a description based on dry-matter production theory and plot-scale validation. *Ecological Modelling* **151**:143-176

Jackson, S.T., and J.T. Overpeck. 2000. Responses of plant populations and communities to environmental changes of the late Quaternary. *Paleobiology* **26**:194-220.

Jones, R.N. 2000. Managing uncertainty in climate change projections - Issues for impact assessment - An editorial comment. *Climatic Change* **45**:403-419.

Kaplan, J.O., N.H. Bigelow, C.I. Prentice, S.P. Harrsison, P.J. Bartlein, T.R. Christensen, W. Cramer, N.V. Matveyeva, A.D. McGuire, D.F. Murray, V.Y. Razzhivin, B. Smith, D.A. Walker, P.M. Anderson, A.A. Andreev, L.B. Brubaker, M.E. Edwards, and A.V. Lozhkin. 2003. Climate change and Arctic ecosystems II: Modeling, paleodat-model comparisons, and future projections. *Journal of Geophysical Research* 108:8171.

Kaplan, J.O., I.C. Prentice, and N. Buchmann. 2002. The stable carbon isotope composition of the terrestrial biosphere: Modeling at scales from the leaf to the globe. *Global Biogeochemical Cycles* **16**:1060.

Katz, R.W. 2002. Techniques for estimating uncertainty in climate change scenarios and impact studies. *Climate Research* **20**:167-185.

Kickert, R.N., G. Tonella, G. Simonov, and S.V. Krupa. 1999. Predictive modeling of effects under global change. *Environmental Pollution* **100**:87-132.

King, A.W., W.M. Post, and S.D. Wullschlegeret. 1997. The potential response of terrestrial carbon storage to changes in climate and atmospheric CO_2. *Climatic Change* **35**:199-227.

Kirilenko, A.P., and A.M. Solomon. 1998. Modeling dynamic vegetation response to rapid climate change using bioclimatic classification. *Climatic Change* **38**:15-49.

Kittel, T.G.F., N.A. Rosenbloom, J.A. Royle, C. Daly, W.P. Gibson, H.H. Fisher, P. Thornton, D.N. Yates, S. Aulenbach, C. Kaufman, R. McKeown, D. Bachelet, and D.S. Schimel. 2004. VEMAP phase 2 bioclimatic database. I. Gridded historical (20th century) climate for modeling ecosystem dynamics across the conterminous USA. *Climate Research* **27**:151-170.

Knorr, W., and M. Heimann. 2001. Uncertainties in global terrestrial biosphere modeling, part II: Global constraints for a process-based vegetation model. *Global Biogeochemical Cycles* **15**:227-246.

Knorr, W., and M. Heimann. 2001. Uncertainties in global terrestrial biosphere modeling 1. A comprehensive sensitivity analysis with a new photosynthesis and energy balance scheme. *Global Biogeochemical Cycles* **15**:207-225.

Koca, D., B. Smith, and M.T. Sykes. 2006. Modelling regional climate change effects on potential natural ecosystems in Sweden. *Climatic Change* 78:381-406.

Lenihan, J.M., and R.P. Neilson. 1993. A Rule-Based Vegetation Formation Model for Canada. *Journal of Biogeography* **20**:615-628.

Lenton, T.M., and C. Huntingford. 2003. Global terrestrial carbon storage and uncertainties in its temperature sensitivity examined with a simple model. *Global Change Biology* **9**:1333-1352.

Liu, J.X., S.G. Liu, and T.R. Loveland. 2006. Temporal evolution of carbon budgets of the Appalachian forests in the US from 1972 to 2000. *Forest Ecology and Management* **222**:191-201.

Loehle, C., and D. LeBlanc. 1996. Model-based assessments of climate change effects on forests: A critical review. *Ecological Modelling* **90**:1-31.

Lundin, L.C., S. Halldin, A. Lindroth, E. Cienciala, A. Grelle, P. Hjelm, E. Kellner, A. Lundberg, M. Mölder, A.-S. Morén, T. Nord, J. Seibert, and M. Stähli. 1999. Continuous long-term measurements of soil-plant-atmosphere variables at a forest site. *Agricultural and Forest Meteorology* **98**:53-73.

Matthews, H.D., M. Eby, A.J. Weaver, and B.J. Hawkins. 2005. Primary productivity control of simulated carbon cycle-climate feedbacks. *Geophysical Research Letters* 32:10.1029/2005GL022941

Meir, P., P. Cox, and J. Grace. 2006. The influence of terrestrial ecosystems on climate. *Trends in Ecology & Evolution* **21**:254-260.

Mitchell, S.W., and F. Csillag. 2001. Assessing the stability and uncertainty of predicted vegetation growth under climatic variability: northern mixed grass prairie. *Ecological Modelling* **139**:101-121.

Moorcroft, P.R., G.C. Hurtt, and S.W. Pacala. 2001. A method for scaling vegetation dynamics: The ecosystem demography model (ED). *Ecological Monographs* **71**:557-585.

Murphy, A.H., and E.S. Epstein. 1989. Skill scores and correlation coefficients in model verification. *Monthly Weather Review* **117**:572-581.

Neilson, R.P. 1993. Transient Ecotone Response to Climatic-Change - Some Conceptual and Modeling Approaches. *Ecological Applications* **3**:385-395.

Neilson, R.P., G.A. King, and G. Koerper. 1992. Toward a Rule-Based Biome Model. *Landscape Ecology* **7**:27-43.

Neilson, R.P., L.F. Pitelka, F. Louis, A.M. Solomon, R. Nathan, G.F. Midgley, J.M. Fragoso, H. Lischke, and K. Thompson. 2005. Forecasting regional to global plant migration in response to climate change. *Bioscience* **55**:749-759.

Overpeck, J.T., P.J. Bartlein, and W.III. Thompson. 1991. Potential Magnitude of Future Vegetation Change in Eastern North-America - Comparisons with the Past. *Science* **254**:692-695.

Pan, Y., A.D. McGuire, D.W. Kicklighter, and J.M. Melillo. 1996. The importance of climate and soils for estimates of net primary production: A sensitivity analysis with the terrestrial ecosystem model. *Global Change Biology* **2**:5-23.

Peng, C.H. 2000. From static biogeographical model to dynamic global vegetation model: a global perspective on modelling vegetation dynamics. *Ecological Modelling* **135**:33-54.

Peters, D. 2002. Plant species dominance at a grassland-shrubland ecotone: an individual-based gap dynamics model of herbaceous and woody species. *Ecological Modelling* **152**: 5-32.

Pontius, R.G. 2000. Quantification error versus location error in comparison of categorical maps. *Photogrammetric Engineering and Remote Sensing* **66**:1011-1016.

Pontius, R.G., and L.C. Schneider. 2001. Land-cover change model validation by an ROC method for the Ipswich watershed, Massachusetts, USA. *Agriculture, Ecosystems and Environment* **85**:239-248.

Prentice, I.C., W. Cramer, S.P. Harrison, R. Leemans, R.A. Monserud, and A.M. Solomon. 1992. A global biome model based on plant physiology and dominance, soil properties and climate. *Journal of Biogeography* **19**:117–134.

Prentice, I.C., J. Guiot, B. Huntley, D. Jolly, and R. Cheddadi. 1996. Reconstructing biomes from palaeoecological data: A general method and its application to European pollen data at 0 and 6 ka. *Climate Dynamics* **12**:185-194.

Prentice, I.C., and A.M. Solomon. 1990. Vegetation models and global change. In. Bradley, R.S. .Ed., Global changes of the past, UCAR/Office for Interdisciplinary Earth Studies Boudler, Colorado, CO, pp. 365-383.

Radtke, P.J., T.E. Burk, and P.V. Bolstad. 2001. Estimates of the distributions of forest ecosystem model inputs for deciduous forests of eastern North America. *Tree Physiology* **21**:505-512.

Running, S.W., R.R. Nemani, D.L. Peterson, L.E. Band, D.F. Potts, L.L. Pierce, and M.A. Spanner. 1989. Mapping Regional Forest Evapotranspiration and Photosynthesis by Coupling Satellite Data with Ecosystem Simulation. *Ecology* **70**:1090-1101.

Scheffer, M., M. Holmgren, V. Brovkin, and M. Claussen. 2005. Synergy between small- and large-scale feedbacks of vegetation on the water cycle. *Global Change Biology* **11**:1003-1012.

Schulz, K., A. Jarvis, K. Beven, and H. Soegaard. 2001. The predictive uncertainty of land surface fluxes in response to increasing ambient carbon dioxide. *Journal of Climate* **14**:2551-2562.

Schumacher, S., H. Bugmann, and D.J. Mladenoff. 2004. Improving the formulation of tree growth and succession in a spatially explicit landscape model. *Ecological Modelling* **180**:175-194.

Shafer, S., P. Bartlein, and Robert S. Thompson. 2001. Potential changes in the distributions of western North America tree and shrub taxa under future climate scenarios. *Ecosystems* **4**:200-215.

Siegel, E., H. Dowlatabadi, and M.J. Small. 1995. A probabilistic model of ecosystem prevalence. *Journal of Biogeography* **22**:875-879.

Sitch, S., B. Smith, I.C. Prentice, A. Arneth, A. Bondeau, W. Cramer, J.O. Kaplan, S. Levis, W. Lucht, M.T. Sykes, K. Thonicke, and S. Venevsky. 2003. Evaluation of ecosystem dynamics, plant geography and terrestrial carbon cycling in the LPJ dynamic vegetation model. *Global Change Biology* **9**:161-185.

Smith, T.M., and H.H. Shugart. 1993. The Potential Response of Global Terrestrial Carbon Storage to a Climate-Change. *Water Air and Soil Pollution* **70**: 629-642.

Steffen, W.L., W. Cramer, M. Plochl, and H. Bugmann. 1996. Global vegetation models: Incorporating transient changes to structure and composition. *Journal of Vegetation Science* **7**:321-328.

Storch, H.V., and F.W. Zwiers. 1999. Forecast quality evaluation. In: Statistical analysis in climate research. Cambridge University Press. The Edinburgh Building, Cambridge CB2 2RU, UK.

Stott, P.A., and J.A. Kettleborough. 2002. Origins and estimates of uncertainty in predictions of twenty-first century temperature rise. *Nature* **416**:723-726.

Taylor, K.E. 2001. Summarizing multiple aspects of model performance in a single diagram. *Journal of Geographical Research* **106**:7183-7192.

Tian, H., C.A.S. Hall, and Y. Qi. 1998. Modeling primary productivity of the terrestrial biosphere in changing environments: Toward a dynamic biosphere model. *Critical Reviews in Plant Sciences* **17**:541-557.

Turner, D.P., R. Dodson, and D. Marks. 1996. Comparison of alternative spatial resolutions in the application of a spatially distributed biogeochemical model over complex terrain. *Ecological Modelling* **90**:53-67.

Thonicke, K., S. Venevsky, S. Sitch, and W. Cramer. 2001. The role of fire disturbance for global vegetation dynamics: coupling fire into a Dynamic Global Vegetation Model. *Global Ecology and Biogeography* **10**: 661-677.

Vellinga, M., and R.A. Wood. 2002. Global climatic impacts of a collapse of the Atlantic thermohaline circulation. *Climatic Change* **54**:251-267.

Walker, B.H. 1994. Landscape to Regional-Scale Responses of Terrestrial Ecosystems to Global Change. *Ambio* **23**: 67-73.

Webster, M.D., and A.P. Sokolov. 2000. A methodology for quantifying uncertainty in climate projections. *Climatic Change* **46**:417-446.

Woodward, F.I., and M.R. Lomas. 2004. Vegetation dynamics - simulating responses to climatic change. *Biological Reviews* **79**: 643-670.

Wythers, K.R., P.B. Reich, M.G. Tjoelker, and P.B. Bolstad. 2005. Foliar respiration acclimation to temperature and temperature variable Q.10 alter ecosystem carbon balance. *Global Change Biology* **11**:435-449.

Zaehle, S., S. Sitch, B. Smith, and F. Hatterman. 2005. Effects of parameter uncertainties on the modeling of terrestrial biosphere dynamics. *Global Biogeochemical Cycles* **19**: doi:10.1029/2004GB002395.

Zhang, X.Y., M.A. Friedl, C.B. Schaaf, A.H. Strahler, J.C.F. Hodges, F. Gao, B.C. Reed, and A. Huete. 2003. Monitoring vegetation phenology using MODIS. *Remote Sensing of Environment* **84**:471-475.

Chapter III

Allen M, Raper S, Mitchell J (2001) Climate change-Uncertainty in the IPCC's third assessment report. *Science*, 293, 430-433.

Barrett DJ, Galbally IE, Graetz RD (2001) Quantifying uncertainty in estimates of C emissions from aboveground biomass due to historic land-use change to cropping in Australia. *Global Change Biology*, 7, 883-902.

Bigelow NH, Brubaker LB, Edwards ME *et al.* (2003) Climate change and Arctic ecosystems I, Vegetation changes north of 55°N between the last glacial maximum, mid-Holocene and present. *Journal of Geophysical Research*, 108, 8170.

Bolliger J, Kienast F, Bugmann H (2000) Comparing models for tree distributions: concept, structures, and behavior. *Ecological Modelling*, 134, 89-102.

Campbell JB (2002) Accuracy assessment. In: *Introduction to Remote Sensing (3rd Ed.)*, pp. 383-406. The Guilford Press. New York. London

Cohen J (1960) A coefficient of agreement for nominal scales. *Educational and Psychological Measurement*, 20, 37-46.

Congalton RG (1991) A review of assessing the accuracy of classifications of remotely sensed data. *Remote Sensing of Environment*, 37, 35-46.

Congalton RG, Green K (1999) *Assessing the accuracy of remotely sensed data: Principles and practices*. Boca Raton: CRC press.

Costanza R (1989) Model goodness of fit: A multiple resolution procedure. *Ecological Modelling*, 47, 199-215.

DeFries R, Hansen M, Townshend JRG *et al.* (1998) Global land cover classifications at 8km spatial resolution: The use of training data derived from Landsat imagery in decision tree classifiers. *International Journal of Remote Sensing*, 19, 3141-3168.

DeFries R, Hansen M, Townshend JRG *et al.* (2000) A new global 1km data set of percent tree cover derived from remote sensing. *Global Change Biology*, 6, 247-254.

Diffenbaugh NS, Sloan LC, Snyder MA *et al.* (2003) Vegetation sensitivity to global anthropogenic carbon dioxide emissions in a topographically complex region. *Global Biogeochemical Cycles*, 17, 1067.

Eidenshink JC, Faundeen JL (1994) The 1km AVHRR global land dataset-1st stages in implementation. *International Journal of Remote Sensing*, 15, 3443-3462.

Fielding AH, Bell JF (1997) A review of methods for the assessment of prediction errors in conservation presence/absence models. *Environmental Conservation*, 24, 38-49.

Foley JA, Prentice IC, Ramankutty N *et al.* (1996) An integrated biosphere model of land surface processes, terrestrial carbon balance, and vegetation dynamics. *Global Biogeochemical Cycles*, 10, 603-628.

Food and Agriculture Organization (1995) Digital soil map of the world and derived soil properties. Food and Agriculture Organization, Rome.

Foody GM (1992) On the compensation for chance agreement in image classification accuracy assessment. *Photogrammetric Engineering and Remote Sensing*, 58, 1459-1460.

Foody GM (2002) Status of land cover classification accuracy assessment. *Remote Sensing of Environment*, 80, 185-201.

Gould W (2000) Remote sensing of vegetation, plant species richness, and regional biodiversity hotspots. *Ecological Applications*, 10, 1861-1870.

Hagen A (2003) Fuzzy set approach to assessing similarity of categorical maps. *International Journal of Geographical Information Science,* 17, 235-249.

Hagen-Zanker A, Straatman B, Uljee I (2005) Further developments of a fuzzy set map comparison approach. *International Journal of Geographical Information Science,* 19, 769-785.

Hansen M, Defries R, Townshend JRG *et al.* (2000) Global land cover classification at 1km spatial resolution using a classification tree approach. *International Journal of Remote Sensing*, 21, 1331-1364.

Harrison SP, Prentice IC (2003) Climate and CO_2 controls on global vegetation distribution at the last glacial maximum: analysis based on palaeovegetation data, biome modelling and palaeoclimate simulations. *Global Change Biology*, 9, 983-1004.

Haxeltine A, Prentice IC (1996) BIOME3: An equilibrium biosphere model based on ecophysiological constraints, resource availability and competition among plant functional types. *Global Biogeochemical Cycles*, 10, 693–709.

Holman JO (2004) *Quantitative comparison of categorical maps with applications for the analysis of global environmental data.* A dissertation: Presented to the Department of Geography and the Graduate School of the University of Oregon.

Kaplan JO, Bigelow NH, Prentice IC *et al.* (2003) Climate change and Arctic ecosystems II: Modeling, paleodat-model comparisons, and future projections. *Journal of Geophysical Research*, 108, 8171.

Kaplan JO, Prentice IC, Buchmann N (2002) The stable carbon isotope composition of the terrestrial biosphere: Modeling at scales from the leaf to the globe. *Global Biogeochemical Cycles*, 16, 1060.

Kickert RN, Tonella G, Simonov A *et al.* (1999) Predictive modeling of effects under global change. *Environmental Pollution*, 100, 87-132.

Kicklighter DW, Bruno M, Donges S *et al.* (1995) A first-order analysis of the potential role of CO_2 fertilizaiton to affect the global carbon budget: a comparison of four terrestrial biosphere models. *Tellus*, 51B, 343-366.

Landis JR, Koch GG (1977) Application of hierarchical Kappa-type statistics in assessment of majority agreement among multiple observers. *Biometrics*, 33, 363-374.

Loveland TR, Reed BC, Brown JF *et al.* (2000) Development of a global land cover characteristics database and IGBP DISCover from 1-km AVHRR data. *International Journal of Remote Sensing*, 21, 1303-1313.

Luoto M, Poyry J, Heikkinen RK *et al.* (2005) Uncertainty of bioclimate envelope models based on the geographical distribution of species. *Global Ecology and Biogeography*, 14, 575-584.

Ma Z, Redmond RL (1994) Tau coefficients for accuracy assessment of classification of remote sensing data. *Photogrammetric Engineering and Remote Sensing*, 61, 435-439.

Melillo JM, McGuire AD, Kicklighter DW *et al.* (1993) Global climate change and terrestrial net primary production. *Nature,* 363, 234–240.

Mitchell TD, Carter TR, Jones PD, Hulme M, New M (2004) A comprehensive set of high-resolution grids of monthly climate for Europe and the globe: the observed record (1901–2000) and 16 scenarios (2001–2100). Tyndall Working Paper 55, 25pp, Tyndall Centre, UEA, Norwich, UK.

Monserud RA, Leemans R (1992) Comparing global vegetation maps with the Kappa statistic. *Ecological Modelling*, 62, 275-293.

New M, Hulme M, Jones PD (1999) New representing twentieth-century space–time climate variability. Part I: development of a 1961–90 mean monthly terrestrial climatology. *Journal of Climate*, 12, 829–856.

New M, Hulme M, Jones PD (2000) Representing twentieth century space-time climate variability. Part 2: development of 1901-96 monthly grids of terrestrial surface climate. *Journal of Climate*, 13, 2217-2238.

Parton WJ, Schimel DS, Cole CV *et al.* (1987) Analysis of factors controlling soil organic matter levels in Great Plains grasslands. *Soil Science Society of America Journal,* 51, 1173-1179.

Pontius RG (2000) Quantification error versus location error in comparison of categorical maps. *Photogrammetric Engineering and Remote Sensing*, 66, 1011-1016.

Pontius RG, Schneider LC (2001) Land-cover change model validation by an ROC method for the Ipswich watershed, Massachusetts, USA. *Agriculture, Ecosystems and Environment*, 85, 239-248.

Prentice IC, Cramer W, Harrison SP *et al.* (1992) A global biome model based on plant physiology and dominance, soil properties and climate. *Journal of Biogeography*, 19, 117–134.

Prentice IC, Sykes MT, Cramer W (1993) A simulation model for the transient effects of climate change on forest landscapes. *Ecological Modelling*, 65, 51–70.

Ramankutty N, Foley JA (1999) Estimating historical changes in global land cover: croplands from 1700 to 1992. *Global Biogeochemical Cycles*, 13, 997-1027.

Roy PS, Joshi PK (2002) Forest cover assessment in northeast India - the potential of temporal wide swath satellite sensor data (IRS-1C WiFS). *International Journal of Remote Sensing*, 23, 4881-4896.

Running SW, Coughlan JC (1988) A general model of forest ecosystem processes for regional applications, I. Hydrologic balance, canopy gas exchange and primary production processes. *Ecological Modelling*, 42, 125-154.

Sitch S, Smith B, Prentice IC *et al.* (2003) Evaluation of ecosystem dynamics, plant geography and terrestrial carbon cycling in the LPJ Dynamic Global Vegetation Model. *Global Change Biology*, 9, 161-185.

Song MH, Zhou CP, Ouyang H. (2005) Simulated distribution of vegetation types in response to climate change on the Tibetan Plateau. *Journal of Vegetation Science*, 16, 341-350.

Turner DP, Koerper G, Gucinski H *et al.* (1993) Monitoring global change-comparison of forest cover estimates using remote-sensing and inventory approaches. *Environmental Monitoring and Assessment*, 26, 295-305.

White A, Cannell MGR *et al.* (2000) CO_2 stabilization, climate change and the terrestrial carbon sink. *Global Change Biology*, 6, 817-833.

Woodward FI, Lomas MR (2004) Simulating vegetation processes along the Kalahari transect. *Global Change Biology*, 10, 383-392.

Chapter IV

Allen, M., Raper, S. & Mitchell, J. (2001) Climate change: uncertainty in the IPCC's Third Assessment Report. *Science*, 293, 430-433.

Barrett, D.J., Galbally, I.E. & Graetz, R.D. (2001) Quantifying uncertainty in estimates of C emissions from above-ground biomass due to historic land-use change to cropping in Australia. *Global Change Biology,* 7, 883-902.

Belsley, F.J.M., Kuh, E. & Welsch, R.E. (1980) Regression diagnostics: identifying influential data and sources of collinearity. Wiley, New York.

Bishop, J.K.B. & Rossow, W.B. (1991) Spatial and temporal variability of global surface solar irradiance. *Journal of Geophysical Research*, 96, 16839-16858.

Bolliger, J., Kienast, F. & Bugmann, H. (2000) Comparing models for tree distributions: concept, structures, and behavior. *Ecological Modelling*, 134, 89-102.

Congalton, R.G. (1991) A review of assessing the accuracy of classifications of remotely sensed data. *Remote Sensing of Environment*, 37, 35-46.

Congalton, R.G. & Green, K. (1999) *Assessing the accuracy of remotely sensed data: Principles and practices*. Boca Raton: CRC press.

Cowling, S.A. & Shin, Y. (2006) Simulated ecosystem threshold responses to co-varying temperature, precipitation and atmospheric CO_2 within a region of Amazonia. *Global Ecology and Biogeography,* 15, 553-566.

Cramer, W., Kicklighter, D.W., Bondeau, A., Iii, B.M., Churkina, G., Nemry, B., Ruimy, A., Schloss, A.L. & The Participants of The Potsdam NPP Model Intercomparison. (1999) Comparing global models of terrestrial net primary productivity (NPP): overview and key results. *Global Change Biology*, 5, 1-15.

Fang, J.Y., Piao, S.L., Field, C.B., Pan, Y., Guo, Q.H., Zhou, L., Peng, C.H., & Tao, S. (2003) Increasing net primary production in China from 1982 to 1999. *Frontiers in Ecology and the Environment*, 1, 293-297.

Fielding, A.H. & Bell, J.F. (1997) A review of methods for the assessment of prediction errors in conservation presence/absence models. *Environmental Conservation*, 24, 38-49.

Food and Agriculture Organization. (1995) *Digital soil map of the world and derived soil properties*. Food and Agriculture Organization, Rome.

Foody, G.M. (1992) On the compensation for chance agreement in image classification accuracy assessment. *Photogrammetric Engineering and Remote Sensing*, 58, 1459-1460.

Foody, G.M. (2002) Status of land cover classification accuracy assessment. *Remote Sensing of Environment*, 80, 185-201.

Gerten, D., Schaphoff, S., Haberlandt, U., Lucht, W. & Sitch, S. (2004) Terrestrial vegetation and water balance - hydrological evaluation of a dynamic global vegetation model. *Journal of Hydrology,* 286, 249-270.

Gordon, W.S., Famiglietti, J.S., Fowler, N.L., Kittel, T.G.F. & Hibbard, K.A. (2004) Validation of simulated runoff from six terrestrial ecosystem models: Results from VEMAP. *Ecological Applications,* 14, 527-545.

Hagen, A. (2003) Fuzzy set approach to assessing similarity of categorical maps. *International Journal of Geographical Information Science,* 17, 235-249.

Hagen-Zanker, A., Straatman, B. & Uljee, I. (2005) Further developments of a fuzzy set map comparison approach. *International Journal of Geographical Information Science,* 19, 769-785.

Jackson D. (1924) The algebra of correlation. *Mathematical monthly*, 8, 110-121.

Keeling, C.D., Guenther, P.R., Emanuele, G. III., Bollenbacher, A. & Moss, D.J. (2002) *Scripps reference gas calibration system for carbon dioxide-in-nitrogen and carbon dioxide-in-air standards: revision of 1999 (with Addendum).* SIO Reference Series No. 01-11

Kickert, R.N., Tonella, G., Simonov, A. & Krupa, S.V. (1999) Predictive modeling of effects under global change. *Environmental Pollution*, 100, 87-132.

Kicklighter, D.W., Bondeau, A., Schloss, A.L., Kaduk, J., Mcguire, A.D. & The participants of the Potsdam NPP model intercomparison. (1999) Comparing global models of terrestrial net primary productivity (NPP): global pattern and differentiation by major biomes. *Global Change Biology*, 5, 16-24.

Kicklighter, D.W., Bruno, M., Dönges, S., Esser, G., Heimann, M., Helfrich, J., Ift, F., Joos, F., Kaduk, J., Kohlmaier, G.H., McGuire, A.D., Melillo, J.M., Meyer, R., Moore, B. III., Nadler, A., Prentice, I.C., Sauf, W., Schloss, A.L., Sitch, S., Wittenberg, U. & Wurth, G. (1995) A first-order analysis of the potential role of CO_2 fertilization to affect the global carbon budget: a comparison of four terrestrial biosphere models. *Tellus*, 51B, 343-366.

Knorr, W. & Heimann, M. (2001) Uncertainties in global terrestrial biosphere modeling 1. A comprehensive sensitivity analysis with a new photosynthesis and energy balance scheme. *Global Biogeochemical Cycles*, 15, 207-225.

Luoto, M., Pöyry, J., Heikkinen, R.K. & Saarinen, K. (2005) Uncertainty of bioclimate envelope models based on the geographical distribution of species. *Global Ecology and Biogeography*, 14, 575-584.

Ma, Z. & Redmond, R.L. (1994) Tau coefficients for accuracy assessment of classification of remote sensing data. *Photogrammetric Engineering and Remote Sensing*, 61, 435-439.

Mitchell, T.D. & Jones, P.D. (2005) An improved method of constructing a database of monthly climate observations and associated high-resolution grids. *International Journal of Climatology*, 25, 693-712.

Murphy, A.H. & Epstein, E.S. (1989) Skill scores and correlation coefficients in model verification. *Monthly Weather Review*, 117, 572-581

Murphy, A.H. (1988) Skill Scores based on the mean square error and their relationships to the correlation coefficient. *Monthly Weather Review*, 116, 2417-2424

New, M., Hulme, M. & Jones, P.D. (2000) Representing twentieth century space-time climate variability. Part 2: development of 1901-96 monthly grids of terrestrial surface climate. *Journal of Climate*, 13, 2217-2238.

Ni, J., Zhang, X.S. & Scurlock, J.M.O. (2001) Synthesis and analysis of biomass and net primary productivity in Chinese forests. *Annals of Forest Science*, 58, 351-384.

Piao, S.L., Fang, J.Y., Zhou, L.M., Guo, Q.H., Henderson, M., Ji, W., Li, Y. & Tao, S. (2003) Interannual variations of monthly and seasonal normalized difference vegetation index (NDVI) in China from 1982 to 1999. *Journal of Geophysical Research-Atmospheres*, 108, doi: 10.1029/2002JD002848.

Pinzon, J. (2002) *Using HHT to successfully uncouple seasonal and interannual components in remotely sensed data.* SCI 2002. Conference Proceedings Jul 14-18. Orlando, Florida.

Pontius, R.G. & Schneider, L.C. (2001) Land-cover change model validation by an ROC method for the Ipswich watershed, Massachusetts, USA. *Agriculture, Ecosystems and Environment*, **85**, 239-248.

Pontius, R.G. (2000) Quantification error versus location error in comparison of categorical maps. *Photogrammetric Engineering and Remote Sensing*, **66**, 1011-1016.

Potter, C.S. & Klooster, S.A. (1999) Detecting a terrestrial biosphere sink for carbon dioxide: Interannual ecosystem modeling for the mid-1980s. *Climatic Change,* 42, 489-503.

Potter, C.S., Klooster, S.A. & Brooks, V. (1999) Interannual variability in terrestrial net primary production: Exploration of trends and controls on regional to global scales. *Ecosystems,* 2, 36-48.

Potts, J.M., Folland, C.K., Jolliffe, I.T. & Sexton, D. (1996) Revised "LEPS" scores for assessing climate model simulations and long-range forecasts. *Journal of Climate*, 9, 34-53.

Sitch, S., Smith, B., Prentice, I.C., Arneth, A., Bondeau, A., Cramer, W., Kaplan, J.O., Levis, S., Lucht, W., Sykes, M.T., Thonicke, K. & Venevsky, S. (2003) Evaluation of ecosystem dynamics, plant geography and terrestrial carbon cycling in the LPJ Dynamic Global Vegetation Model. *Global Change Biology*, 9, 161-185.

Storch, H.V. & Zwiers, F.W. (1999) *Forecast quality evaluation.* In: Statistical analysis in climate research. Cambridge University Press., Cambridge.

Taylor, K.E. (2001) Summarizing multiple aspects of model performance in a single diagram. *Journal of Geophysical Research*, 106, 7183-7192.

Tucker, C., Pinzon, J., Brown, M., Slayback, D., Pak, E., Mahoney, R., Vermote, E. & El Saleous, N. (2005) An extended AVHRR 8-km NDVI dataset compatible with MODIS and SPOT vegetation NDVI data. *International Journal of Remote Sensing*, 26, 4485-4498.

Chapter V

Bishop, J. K. B., and Rossow, W. B., 1991, Spatial and temporal variability of global surface solar irradiance. *Journal of Geophysical Research*, 96, 16839-16858.

Brogaard, S., Runnstrom, M., and Seaquist, J. W., 2005, Primary production of Inner Mongolia, China, between 1982 and 1999 estimated by a satellite data-driven light use efficiency model. *Global and Planetary Change*, 45, 313-332.

Cao, M. K., Prince, S. D., Li, K. R., Tao, B., Small, J., and Shao, X. M., 2003, Response of terrestrial carbon uptake to climate interannual variability in China. *Global Change Biology*, 9, 536-546.

Cao, M. K., Prince, S. D., Small, J., and Goetz, S. J., 2004, Remotely sensed interannual variations and trends in terrestrial net primary productivity 1981-2000. *Ecosystems*, 7, 233-242.

Chen, Z. M., Babiker, I. S., Chen, Z. X., Komaki, K., Mohamed, M. A. A, and Kato, K., 2004, Estimation of interannual variation in productivity of global vegetation using NDVI data. *International Journal of Remote Sensing*, 25, 3139-3159.

Clein, J. S., McGuire, A. D., Zhang, X., Kicklighter, D. W., Melillo, J. M., Wofsy, S. C., Jarvis, P. G., and Massheder, J. M., 2002, Historical and projected carbon balance of mature black spruce ecosystems across North America: the role of carbon-nitrogen interactions. *Plant and Soil*, 242, 15-32.

Cleveland, W. S., 1979, Robust locally weighted regression and smoothing scatter plots. *Journal of the American Statistical Association*, 74, 829-839.

Cramer, W., Bondeau, A., Woodward, F. I., Prentice, I. C., Betts, R. A., Brovkin, V., Cox, P. M., Fisher, V., Foley, J., Friend, A. D., Kucharik, C., Lomas, M. R., Ramankutty, N., Sitch, S., Smith, B., White, A., and Young-Molling, C., 2001, Global response of terrestrial ecosystem structure and function to CO_2 and climate change: results from six dynamic global vegetation models. *Global Change Biology*, 7, 357-373.

Cramer, W., Kicklighter, D. W., Bondeau, A., Iii, B. M., Churkina, G., Nemry, B., Ruimy, A., Schloss, A. L., and The Participants of The Potsdam NPP Model Intercomparison, 1999, Comparing global models of terrestrial net primary productivity (NPP): overview and key results. *Global Change Biology*, 5, 1-15.

Daly, C., Bachelet, D., Lenihan, J. M., Neilson, R. P., and Parton, W., 2000, Dynamic simulation of tree-grass interactions for global change studies. *Ecological Applications*, 10, 449-469.

Dawson, T. P., North, P. R. J, Plummer, S. E., and Curran, P. J., 2003, Forest ecosystem chlorophyll content: implications for remotely sensed estimates of net primary productivity. *International Journal of Remote Sensing*, 24, 611-617.

Ding, T. S., Yuan, H. W., Geng, S., Lin, Y. S., and Lee, P. F., 2005, Energy flux, body size and density in relation to bird species richness along an elevational gradient in Taiwan. *Global Ecology and Biogeography*, 14, 299-306.

Fang, J. Y., Piao, S. L., Field, C. B., Pan, Y., Guo, Q. H., Zhou, L., Peng, C. H., and Tao, S., 2003, Increasing net primary production in China from 1982 to 1999. *Frontiers in Ecology and the Environment*, 1, 293-297.

Food and Agriculture Organization, 1995, Digital soil map of the world and derived soil properties. Food and Agriculture Organization, Rome.

Gao, Z. Q., Liu, J. Y., Cao, M. K., Li, K., and Tao, B., 2005, Impacts of land-use and climate changes on ecosystem productivity and carbon cycle in the cropping-grazing transitional zone in China. Science in China Series D-Earth Sciences 48, 1479-1491.

Jenkins, J. C., Birdsey, R. A., and Pan, Y. D., 2001, Biomass and NPP estimation for the mid-Atlantic region (USA) using plot-level forest inventory data. *Ecological Applications*, 11, 1174-1193.

Jenkins, J. C., Kicklighter, D. W., Ollinger, S. V., Aber, J. D., and Melillo, J. M., 1999, Sources of variability in net primary production predictions at a regional scale: A comparison using PnET-II and TEM 4.0 in northeastern US forests. *Ecosystems*, 2, 555-570.

Jiang, H., Apps, M. J., Zhang, Y., Peng, C., and Woodard, P. M., 1999, Modelling the spatial pattern of net primary productivity in Chinese forests. *Ecological Modelling*, 122, 275-288.

Kaplan, J. O., Prentice, I. C., and Buchmann, N., 2002, The stable carbon isotope composition of the terrestrial biosphere: Modeling at scales from the leaf to the globe. *Global Biogeochemical Cycles*, 16, 1060, doi:10.1029/2001GB001403.

Keeling, C. D., Guenther, P. R., Emanuele, III. G., Bollenbacher, A., and Moss, D. J., 2002, Scripps Reference Gas Calibration System for Carbon Dioxide-in-Nitrogen and Carbon Dioxide-in-Air Standards: Revision of 1999 (with Addendum). SIO Reference Series No. 01-11

Kicklighter, D. W., Bruno, M., Donges, S., Esser, G., Heimann, M., Helfrich, J., Ift, F., Joos, F., Kaduk, J., Kohlmaier, G. H., McGuire, A. D., Melillo, J. M., Meyer, R., Moore, B. III., Nadler, A., Prentice, I. C., Sauf, W., Schloss, A. L., Sitch, S., Wittenberg, U., and Wurth, G., 1995, A first-order analysis of the potential role of CO_2 fertilization to affect the global carbon budget: a comparison of four terrestrial biosphere models. *Tellus*, 51B, 343-366.

Kimball, J. S., Keyser, A. R., Running, S. W., and Saatchi, S. S., 2000, Regional assessment of boreal forest productivity using an ecological process model and remote sensing parameter maps. *Tree Physiology*, 20, 761-775.

Lu, J. H., and Ji, J. J., 2006, A simulation and mechanism analysis of long-term variations at land surface over arid/semi-arid area in north China. *Journal of Geophysical Research-Atmospheres*, 111, D09306, doi:10.1029/2005JD006252.

Lucht, W., Prentice, I. C., Myneni, R. B., Sitch, S., Friedlingstein, P., Cramer, W., Bousquet, P., Buermann, W., and Smith, B., 2002, Climatic control of the high-latitude vegetation greening trend and Pinatubo effect. *Science*, 296, 1687-1689.

Luo, T. X., Li, W. H., and Zhu, H. Z., 2002, Estimated biomass and productivity of natural vegetation on the Tibetan Plateau. *Ecological Applications*, 12, 980-997.

Markon, C. J., and Peterson, K. M., 2002, The utility of estimating net primary productivity over Alaska using baseline AVHRR data. *International Journal of Remote Sensing*, 23, 4571-4596.

Mitchell, T. D., and Jones, P. D., 2005, An improved method of constructing a database of monthly climate observations and associated high-resolution grids. *International Journal of Climatology*, 25, 693-712.

Nabuurs, G.J., Schelhaas, M., Mohren, G., and Field, C.B., 2003, Temporal evolution of the European forest sector carbon sink from 1950 to 1999. *Global Change Biology*, 9, 152-160.

New, M., Hulme, M., and Jones, P.D., 2000, Representing twentieth century space-time climate variability. Part 2: development of 1901-96 monthly grids of terrestrial surface climate. *Journal of Climate*, 13, 2217-2238.

Ni, J., Zhang, X. S., and Scurlock, J. M. O., 2001, Synthesis and analysis of biomass and net primary productivity in Chinese forests. *Annals of Forest Science*, 58, 351-384.

Ni, J., 2000, Net primary production, carbon storage and climate change in Chinese biomes. *Nordic Journal of Botany*, 20, 415-426.

Ni, J., 2004, Estimating net primary productivity of grasslands from field biomass measurements in temperate northern China. *Plant Ecology*, 174, 217-234.

Ni, J., 2004, Forest productivity of the Altay and Tianshan Mountains in the dryland, northwestern China. *Forest Ecology and Management*, 202, 13-22.

Parton, W. J., Schimel, D. S., Cole, C. V., and Ojima, D. S., 1987, Analysis of factors controlling soil organic matter levels in Great Plains grasslands. *Soil Science Society of America Journal*, 51, 1173-1179.

Piao, S. L., Fang, J. Y., and He, J. S., 2006, Variations in vegetation net primary production in the Qinghai-Xizang Plateau, China, from 1982 to 1999. *Climatic Change*, 74, 253-267.

Piao, S. L., Fang, J. Y., Zhou, L. M., Guo, Q. H., Henderson, M., Ji, W., Li, Y., and Tao, S., 2003, Interannual variations of monthly and seasonal normalized difference vegetation index (NDVI) in China from 1982 to 1999. *Journal of Geophysical Research-Atmospheres*, 108, 4401, doi:10.1029/2002JD002848.

Piao, S. L., Fang. J. Y., Zhou, L. M., Zhu, B., Tan, K., and Tao, S., 2005, Changes in vegetation net primary productivity from 1982 to 1999 in China. *Global Biogeochemical Cycles*, 19, 1-16.

Pinzon, J., 2002, Using HHT to successfully uncouple seasonal and interannual components in remotely sensed data. SCI 2002. Conference Proceedings Jul 14-18. Orlando, Florida.

Potter, C. S., Davidson, E. A., Klooster, S. A., Nepstad, D. C., Negreiros, G. H. D., and Brooks, V., 1998, Regional application of an ecosystem production model for studies of biogeochemistry in Brazilian Amazonia. *Global Change Biology*, 4, 315-333.

Potter, C. S., Klooster, S., and Vanessa, B., 1999, Interannual variability in terrestrial net primary production: Exploration of trends and controls on regional to global scales. *Ecosystems*, 2, 36-48.

Potter, C. S., and Klooster, S. A., 1999, Detecting a terrestrial biosphere sink for carbon dioxide: Interannual ecosystem modeling for the mid-1980s. *Climatic Change*, 42, 489-503.

Prentice, I. C., Heimann, M., and Sitch, S., 2000, The carbon balance of the terrestrial biosphere: Ecosystem models and atmospheric observations. *Ecological Applications*, 10, 1553-1573.

Raich, J. W., Rastetter, E. B., Melillo, J. M., Kicklighter, D. W., Steudler, P. A., and Peterson, B. J., 1991, Potential Net Primary Productivity in South-America - Application of a Global-Model. *Ecological Applications*, 1, 399-429.

Ramankutty, N., and Foley, J. A., 1999, Estimating historical changes in global land cover: croplands from 1700 to 1992. *Global Biogeochemical Cycles*, 13, 997-1027.

Running, S. W., and Coughlan, J. C., 1988, A general model of forest ecosystem processes for regional applications, I. Hydrologic balance, canopy gas exchange and primary production processes. *Ecological Modelling*, 42, 125-154.

Schellnhuber, H. J., Cramer, W., Nakicenovic, N., Wigley, T., and Yohe, G., (eds.) 2006, Avoiding dangerous climate change. Cambridge University Press, Cambridge, UK, 392pp.

Schloss, A., Kicklighter, D. W., Kaduk, J., Wittenberg, U., and The participants of the Potsdam NPP model intercomparison, 1999, Comparing global models of terrestrial net primary productivity (NPP): comparison of NPP to climate and the Normalized Difference Vegetation Index (NDVI). *Global Change Biology*, 5, 25-34.

Sitch, S., Smith, B., Prentice, I. C., Arneth, A., Bondeau, A., Cramer, W., Kaplan, J. O., Levis, S., Lucht, W., Sykes, M. T., Thonicke, K., and Venevsky, S., 2003, Evaluation of ecosystem dynamics, plant geography and terrestrial carbon cycling in the LPJ Dynamic Global Vegetation Model. *Global Change Biology*, 9, 161-185.

Tucker, C., Pinzon, J., Brown, M., Slayback, D., Pak, E., Mahoney, R., Vermote, E., and El Saleous, N., 2005, An extended AVHRR 8-km NDVI dataset compatible with MODIS and SPOT vegetation NDVI data. *International Journal of Remote Sensing*, 26, 4485-4498.

Wang, H. Q., Hall, C. A. S., Scatena, F. N., Fetcher, N., and Wu, W., 2003, Modeling the spatial and temporal variability in climate and primary productivity across the Luquillo Mountains, Puerto Rico. *Forest Ecology and Management*, 179, 69-94.

Xiao, X., and Ojima, D., 1996, NPP Grassland: Xilingol, China, 1980-1989. Data set. Available on-line [http://www.daac.ornl.gov] from Oak Ridge National Laboratory Distributed Active Archive Centre, Oak Ridge, Tennessee, U.S.A.

Xiao, X., and Ojima, D., 1999, NPP Grassland: Tumugi, China, 1981-1990. Data set. Available on-line [http://www.daac.ornl.gov] from Oak Ridge National Laboratory Distributed Active Archive Centre, Oak Ridge, Tennessee, U.S.A.

Zhao, M., and Zhou, G. S., 2006, Estimating net primary productivity of Chinese pine forests based on forest inventory data. *Forestry*, 79, 231-239.

Zheng, D. L., Prince, S. D., and Wright, R., 2003, Terrestrial net primary production estimates for 0.5 degree grid cells from field observations-a contribution to global biogeochemical modeling. *Global Change Biology*, 9, 46-64.

Chapter VI

Arora, V. 2002. The use of the aridity index to assess climate change effect on annual runoff. *Journal of Hydrology* **265**:164-177.

Arora, V. and G. Boer. 2001. Effects of simulated climate change on the hydrology of major river basins. *Journal of Geophysical Research-Atmospheres* **106**:3335-3348.

Arora, V. and G. Boer. 2006. The temporal variability of soil moisture and surface hydrological quantities in a climate model. *Journal of Climate* **19**: 5875-5888.

Bowen, I.S. 1926. The ratio of heat losses by conduction and by evapotranspiration from any water surface. *Physical Review* **27**:779-787.

Brabson BB, Lister DH, Jones PD, Palutikof JP. 2005. Soil moisture and predicted spells of extreme temperatures in Britain. *Journal of Geophysical Research* **110**:D05104.

Bronstert, A. and E. Plate. 1997. Modelling of runoff generation and soil moisture dynamics for hillslopes and micro-catchments. *Journal of Hydrology* **198**:177-195.

Burns, D., J. Klaus, and M.R. McHale. 2007. Recent climate trends and implications for water resources in the Catskill Mountain region, New York, USA. *Journal of Hydrology* **336**:155-170.

Chattopadhyay, N. and M. Hulme. 1997. Evaporation and potential evapotranspiration in India under conditions of recent and future climate change. *Agricultural and Forest Meteorology* **87**:55-73.

Chiew, F. and T. McMahon. 2002. Modelling the impacts of climate change on Australian streamflow. *Hydrological Processes* **16**:1235-1245.

Choudhury, B. and N. DiGirolamo. 1998. A biophysical process-based estimate of global land surface evaporation using satellite and ancillary data - I. Model description and comparison with observations. *Journal of Hydrology* **205**:164-185.

Claessens, L., C. Hopkinson, E. Rastetter and J. Vallino. 2006. Effect of historical changes in land use and climate on the water budget of an urbanizing watershed. *Water Resources Research* **42**: doi:10.1029/2005WR004131.

Dyer, J. 2003. A comparison of moisture scalars and water budget methods to assess vegetation-site relationships. *Physical Geography* **23**:245-258.

Dyer, J. 2004. A water budget approach to predicting tree species growth and abundance, utilizing paleoclimatology sources. *Climate Research* **28**:1-10.

Edraki, M., H. So, and E.A. Gardner. 2004. Water balance of Swamp Mahogany and Rhodes grass irrigated with treated sewage effluent. *Agricultural Water Management* **67**: 157-171.

Eitzinger, J., M. Trnka, J. Hösch, Z. Žalud and M. Dubrovský. 2004. Comparison of CERES, WOFOST and SWAP models in simulating soil water content during growing season under different soil conditions. *Ecological Modelling* **171**:223-246.

Engstrom, R., A. Hope, H. Kwon, Y. Harazono, M. Mano, and W. Oechel. 2006. Modeling evapotranspiration in Arctic coastal plain ecosystems using a modified BIOME-BGC model. *Journal of Geophysical Research Biogeosciences* **111**: doi:10.1029/2005JG000102.

Evans, S. and M. Trevisan. 1995. A soil water-balance bucket model for paleoclimatic purposes.1. model structure and validation. *Ecological Modelling* **82**:109-129.

Federer, C., C. Vörösmarty, and B. Fekete. 1996. Intercomparison of methods for calculating potential evaporation in regional and global water balance models. *Water Resources Research* **32**:2315-2321.

Federer, C.A. 1982. Transpirational supply and demand: plat, soil, and atmospheric effects evaluated by simulation. *Water Resource Research* **18**:355-362.

Fekete, B.M., Vörösmarty, C.J., Grabs, W., 2002. High-resolution fields of global runoff fields of observed river discharge and simulated water balances. *Global Biogeochemical Cycles* **16**: DOI:10.1029/1999gb001254.

Food and Agriculture Organization. 1995. Digital soil map of the world and derived soil properties. Food and Agriculture Organization, Rome.

Gao, G., D. Chen, C.Y. Xu, and E. Simelton. 2007. Trend of estimated actual evapotranspiration over China during 1960-2002. *Journal of Geophysical Research-Atmospheres* **112**:doi:10.1029/2006JD008010.

German, E.R.. 2000. Regional evaluation of evapotranspiration in the Everglades: U.S. Geological Survey Investigations Report 00-4217, 48p.

Gerten, D., Schaphoff, S., Haberlandt, U., Lucht, W. & Sitch, S. 2004. Terrestrial vegetation and water balance - hydrological evaluation of a dynamic global vegetation model. *Journal of Hydrology* **286**:249-270.

Glenn, E.P, A.R. Huete, P.L. Nagler, K.K. Hirschboeck, and P. Brown. 2007. Integrating remote sensing and ground methods to estimate evapotranspiration. *Critical Reviews in Plant Sciences* **26**:139-168.

Gordon, W. and J. Famiglietti. 2004. Response of the water balance to climate change in the United States over the 20th and 21st centuries: Results from the VEMAP Phase 2 model intercomparisons. *Global Biogeochemical Cycles* **18**: doi:10.1029/2003GB002098.

Guo, J., X. Liang, and L.R. Leung. 2004. Impacts of different precipitation data sources on water budgets. *Journal of Hydrology* **298**:311-334.

Hailemarian, K. 1999. Impact of climate change on the water resources of Awash River Basin, Ethiopia. *Climate Research* **12**:91-96.

Hamlet, A., P. Mote, M.P. Clark. 2007. Twentieth-century trends in runoff, evapotranspiration, and soil moisture in the western United States. *Journal of Climate* **20**: 1468-1486.

Hansen, M. C., R. S. DeFries and J. R. G. Townshend and R. Sohlberg. 2000. Global land cover classification at 1km spatial resolution using a classification tree approach. *International Journal of Remote Sensing* **21**:1331-1364.

Hansen, M., R.S. DeFries, J.R.G. Townshend, M. Carroll, C. Dimiceli, and R.A. Sohlberg. 2003. Global Percent Tree Cover at a Spatial Resolution of 500 Meters: First Results of the MODIS Vegetation Continuous Fields Algorithm. *Earth Interactions* **7**:1-15.

Haxeltine A, Prentice IC. 1996. BIOME3: An equilibrium biosphere model based on ecophysiological constraints, resource availability and competition among plant functional types. *Global Biogeochemical Cycles* **10**:693–709.

Hirschi, M., S. Seneviratne, S. Hagemann, and C. Scha¨r. 2007. Analysis of seasonal terrestrial water storage variations in regional climate simulations over Europe. *Journal of Geophysical Research-Atmospheres* **112**: doi:10.1029/2006JD008338.

Hollinger, Steven E., and Scott A. Isard 1994. A soil moisture climatology of Illinois. *Journal of Climate* 7:822-833.

Huang, J., van den Dool, H.M., Georgakakos, K.P. 1996. Analysis of model-calculated soil moisture over the United States, 1931-1993, and applications of to long-range temperature forcasts. *Journal of Climate* 9:1350-1362.

Huntington, T. 2003. Climate warming could reduce runoff significantly in New England, USA. *Agricultural and Forest Meteorology* **117**:193-201.

Kaplan JO, Prentice IC, Buchmann N. 2002. The stable carbon isotope composition of the terrestrial biosphere: Modeling at scales from the leaf to the globe. *Global Biogeochemical Cycles* **16**:1060.

Kergoat, L. 1998. A model for hydrological equilibrium of leaf area index on a global scale. *Journal of Hydrology* **213**:268-286.

Kergoat, L., S. Lafont, H. Douville, B. Berthelot, G. Dedieu, S. Planton, and J.F. Royer. 2002. Impact of doubled CO2 on global-scale leaf area index and evapotranspiration: Conflicting stomatal conductance and LAI responses. *Journal of Geophysical Research-Atmospheres* **107**:doi:10.1029/2001JD001245.

Kosugi, Y. and M. Katsuyama. 2007. Evapotranspiration over a Japanese cypress forest. II. Comparison of the eddy covariance and water budget methods. *Journal of Hydrology* **334**:305-311.

Kosugi, Y., S. Takanashi, H. Tanaka, S. Ohkubo, M. Tani, M. Yano, and T. Katayama. 2007. evapotranspiration over a Japanese cypress forest. I. Eddy covariance fluxes and surface conductance characteristics for 3 years. *Journal of Hydrology* **337**:269-283.

Leipprand, A. and D. Gerten. 2006. Global effects of doubled atmospheric CO_2 content on evapotranspiration, soil moisture and runoff under potential natural vegetation. *Hydrological Sciences Journal-Journal Des Sciences* 51:171-185.

Liang, X., D. P. Lettenmaier, E. F. Wood and S. J. Burges.1994. A Simple hydrologically Based Model of Land Surface Water and Energy Fluxes for GSMs. *Journal of Geophysical Research* **99**:415-14,428.

Lookingbill, T. and D. Urban. 2004. An empirical approach towards improved spatial estimates of soil moisture for vegetation analysis. *Landscape Ecology* **19**:417-433.

Loveland TR, Reed BC, Brown JF, D.O. Ohlen, Z. Zhu, L. Yang, and J.W. Merchant. 2000. Development of a global land cover characteristics database and IGBP DISCover from 1-km AVHRR data. *International Journal of Remote Sensing* **21**: 1303-1313.

Lu, J., G. Sun, S.G. McNulty, and D.M. Amatya. 2003. Modeling actual evapotranspiration from forested watersheds across the Southeastern United States. *Journal of the American Water Resources Association* **39**:887-896.

Manabe S, Delworth T. 1990. The temporal variability of soil wetness and its impact on climate. *Climatic Change* **16**:185-192

Metcalfe, R. and J. Buttle. 1999. Semi-distributed water balance dynamics in a small boreal forest basin. *Journal of Hydrology* **226**:66-87.

Miller, G.R., D.D. Baldocchi, B.E. Law, and T. Meyers. 2007. An analysis of soil moisture dynamics using multi-year data from a network of micrometeorological observation sites. *Advances in Water Resources* **30**:1065-1081.

Mitchell T.D. and P.D. Jones. 2005. An improved method of constructing a database of monthly climate observations and associated high-resolution grids. International *Journal of Climatology* **25**:693-712.

Mohseni O, Stefan HG. 1998. A monthly streamflow model. *Water Resources Research* **34**:1287–1298.

Morrill, C. 2004. The influence of Asian summer monsoon variability on the water balance of a Tibetan lake. *Journal of Paleolimnology* **32**:273-286.

Murphy, S. and G. Lodge. 2004. Surface soil water dynamics in pastures in northern New South Wales. 1. Use of electrical resistance sensors. *Australian Journal of Experimental Agriculture* **44**:273-281.

New M, Hulme M, Jones PD. 1999. New representing twentieth-century space–time climate variability. Part I: development of a 1961–90 mean monthly terrestrial climatology. *Journal of Climate* **12**:829–856.

New M, Hulme M, Jones PD. 2000. Representing twentieth century space-time climate variability. Part 2: development of 1901-96 monthly grids of terrestrial surface climate. *Journal of Climate* **13**:2217-2238.

Nishida, K., R.R. Nemani, J.M. Glassy, and S.W. Running. 2003. Development of an evapotranspiration index from aqua/MODIS for monitoring surface moisture status. *IEEE Transactions on Geosciences and Remote Sensing* **41**:493-501.

Pope, D.V., M. Gallani, R. Rowntree, and A. Stratton. 2000. The impact of new physical parameterizations in the Hadley Centre climate model: HadAM3. *Climate Dynamic* **16**:123– 146.

Prentice, i.c., Sykes, M.T., Cramer, W. 1993. A simulation model for the transient effects of climate change on forest landscapes. *Ecological Modelling* **64**:51-70.

Ramankutty N, Foley JA. 1999. Estimating historical changes in global land cover: croplands from 1700 to 1992. *Global Biogeochemical Cycles* **13**:997-1027.

Robock, Alan, Konstantin Y. Vinnikov, Govindarajalu Srinivasan, Jared K. Entin, Steven E. Hollinger, Nina A. Speranskaya, Suxia Liu, and A. Namkhai. 2000: The Global Soil Moisture Data Bank. *Bulletin American Meteorology Society* 81:1281-1299.

Rodell, M., J.S. Famiglietti, J. Chen, S.I. Seneviratne, P. Viterbo, S. Holl, and C.R. Wilson. 2004. Basin scale estimates of evapotranspiration using GRACE and other observations. *Geophysical Research Letters* **31**:doi:10.1029/2004GL020873.

Running, S.W., Baldocchi, D.D., Turner, D.P., Gower, S.T., Bakwin, P.S., Hibbard, K.A. 1999. A global terrestrial monitoring network integrating tower fluxes, flask sampling, ecosystem modeling and EOS data. *Remote Sensing of Environment* **70**: 108–127.

Schlesinger M.E., and S. Malyshev. 2001. Changes in Near-Surface Temperature and sea level for the Post-SRES CO2-Stabilization Scenarios. *Integrated Assessment* **2**:95-110

Scurlock, J. M. O., G. P. Asner, and S. T. Gower. 2001. Worldwide Historical Estimates and Bibliography of Leaf Area Index, 1932-2000. ORNL Technical Memorandum TM-2001/268, Oak Ridge National Laboratory, Oak Ridge, Tennessee, U.S.A

Shukla J, Mintz Y. 1982. Influence of land-surface evapotranspiration on earth's climate. *Science* **215**:1498–1501

Sitch, S., Smith, B., Prentice, I.C., Arneth, A., Bondeau, A., Cramer, W., Kaplan, J.O., Levis, S., Lucht, W., Sykes, M.T., Thonicke, K. & Venevsky, S. 2003. Evaluation of ecosystem dynamics, plant geography and terrestrial carbon cycling in the LPJ Dynamic Global Vegetation Model. *Global Change Biology* **9:**161-185.

Song, J., M.L. Wesely, M.A. LeMone, and R.L. Grossman. 2000. Estimating watershed evapotranspiration with PASS. Part II: Moisture budgets during drydown periods. *Journal of Hydrometeorology* **1:** 462-473.

Tao, F., M. Yokozawa, Y. Hayashi, E. Lin. 2003. Future climate change, the agricultural water cycle, and. agricultural production in China. *Agriculture Ecosystems and Environment* **95**:203-215.

Tao, F., M. Yokozawa, Y. Hayashi and E. LIN. 2005. A perspective on water resources in China: Interactions between climate change and soil degradation. *Climatic Change* **68**:169-197.

Tateishi R. and C.H. Ahn. (1996) Mapping evapotranspiration and water balance for global land surface. *Journal of Photogrammetry and Remote Sensing* **51**: 209-215.

Thomas, A. 2000. Climatic changes in yield index and soil water deficit trends in China. *Agricultural and Forest Meteorology* **102**:71-81.

Thornthwaite CW. 1948. An approach toward a rational classification of climate. *Geographical Review* **38**: 55–89.

Thornthwaite CW and J.R. Mather. 1955. The water balance. *Publications in Climatology* **8**:1-104.

Wever, L.A, L.B. Flanagan, and P.J. Carlson. 2002. Seasonal and interannual variation in evapotranspiration, energy balance and surface conductance in a northern temperate grassland. *Agricultural and Forest Meteorology* **112**: 31-49.

Wilson, D., A. Western, and R.B. Grayson. 2004. Identifying and quantifying sources of variability in temporal and spatial soil moisture observations. *Water Resources Research* **40**:doi:10.1029/2003WR002306.